INNATE IMMUNE MECHANISM OF PLATELET-NEUTROPHIL AGGREGATION DEPENDENT VASO-OCCLUSION IN SICKLE CELL DISEASE

by

Maritza Ann (Jimenez) Montanez

B.S. in Biomedical Engineering, Robert Morris University, 2013

Submitted to the Graduate Faculty of

Swanson School of Engineering in partial fulfillment

of the requirements for the degree of

PhD in Bioengineering

University of Pittsburgh

2018

UNIVERSITY OF PITTSBURGH

SWANSON SCHOOL OF ENGINEERING

This dissertation was presented

by

Maritza Ann (Jimenez) Montanez

It was defended on

December 5, 2017

and approved by

Sanjeev Shroff, PhD, Distinguished Professor, Gerald E. McGinnis Chair of the Bioengineering Department, and Department of Medicine

Marina Kameneva, PhD, Professor, Departments of Surgery and Bioengineering, McGowan Institute for Regenerative Medicine

Gregory Kato, MD, Professor of Medicine, Vascular Medicine Institute

Dissertation Director: Prithu Sundd, PhD Assistant Professor, Department of Medicine and Bioengineering, Vascular Medicine Institute

INNATE IMMUNE MECHANISM OF PLATELET-NEUTROPHIL AGGREGATION DEPENDENT VASO-OCCLUSION IN SICKLE CELL DISEASE

Maritza Ann Montanez, PhD

University of Pittsburgh, 2018

Sickle Cell Disease (SCD) is an autosomal-recessive–genetic-disorder that affects 100,000 in the U.S. and millions worldwide. Sickle cell anemia, the most common form of SCD results from a single nucleotide polymorphism in the β-globin gene that causes the hemoglobin to polymerize under deoxygenated conditions. Hemoglobin polymerization leads to sickling of erythrocytes, exposure of adhesion molecules on the erythrocyte membrane, and hemolysis. Hemolysis releases erythrocyte derived danger-associated molecular pattern molecules (DAMPs) that activate leukocytes, platelets and endothelium and enable interactions with sickle erythrocytes and promote vaso-occlusion (VOC). VOC is the predominant pathophysiology responsible for acute systemic vaso-occlusive crisis, the leading cause of emergency medical care among SCD patients. VOC is also believed to contribute to progression of other morbidities such as pulmonary hypertension, stroke, and acute chest syndrome, however, the cellular, molecular and biophysical mechanisms that enable VOC in SCD patients remain incompletely understood.

To determine the mechanisms that promote VOC in SCD patients, we developed quantitative microfluidic fluorescence microscopy (qMFM), a novel fluorescence imaging approach that utilizes PDMS-based microfluidic devices to visualize single-cell interactions in SCD human blood. Using qMFM, neutrophils were observed to roll, arrest and capture freely flowing platelets leading to formation of large platelet-neutrophil aggregates that occluded microfluidic flow channels. Quantitative analysis revealed that platelet-neutrophil interactions in SCD patient blood were not only more numerous but also significantly longer in duration than

those in control blood. These platelet-neutrophil interactions were enabled by platelet P-selectin and GPIbα binding to neutrophil PSGL-1 and Mac-1, respectively and were abolished following blockade of these interactions. qMFM revealed for the first time that platelets in SCD blood form P-selectin expressing “hair-like” membrane tethers that promote platelet-neutrophil interactions by shielding the bonds from the hydrodynamic shear forces of blood. Hair-like tethers act like a ‘lasso’ that allows circulating platelets to interact more efficiently with neutrophils within the vasculature. Inhibition of platelet TLR4 or NLRP3 inflammasome dependent signaling abolished “hair-like” platelet tethers and attenuated platelet-neutrophil aggregation in SCD human blood. This study highlights the potential of therapeutic inhibition of platelet P-selectin or NLRP3 inflammasome pathway in preventing VOC in SCD patients.

TABLE OF CONTENTS

LIST OF TABLES

LIST OF FIGURES

PREFACE

Throughout my doctoral work in the Sundd lab there were many people both in and outside of the lab who have helped me reach this day and aided in my development as a researcher.

Dr. Prithu Sundd has been an amazing advisor throughout the four plus years I have been at Pitt. His mentorship has helped me become an independent researcher and has aided in my development. The knowledge and skills I have gained in his lab have been invaluable and will help me in the next stages of my career. As he began his lab he took a chance and chose me as his first graduate student and for that I am forever grateful.

My committee members, Dr. Sanjeev Shroff, Dr. Marina Kameneva, and Dr. Gregory Kato have each played an essential role throughout my dissertation and development. With their help and guidance, I have not only become a more well-rounded researcher but a better person.

The friendships that I have developed with my fellow Sundd lab members have been great and have helped those crazy research days become more bearable. Maggie, Tomasz, Ravi and Egemen, our group has been small throughout the way and I could not have asked for a better lab group. Maggie, our friendship has been special, and you have become a role model for me as I've gone through my graduate studies. You have been there since the very first day and have blazed a path on your way to becoming a professor while showing me what I could become as I move forward with my career as a postdoctoral scholar and beyond.

Last but not least my family who I dedicate this dissertation to. Without each and everyone one of you I probably wouldn't be here right now. My parents, Ann and Ish, have made me into the person I am today and have taught me that I can achieve anything I put my mind to, no matter how crazy it may seem in the beginning. You have been the steady hand as I've gone through this

journey and taught me the value of perseverance even in the face of insurmountable odds. My sister and brother, Maria and JJ, you both have provided me with the support and relief from the daily grind. You guys put a smile on my face and I hope that one day you too will achieve your goals in life. Lastly my husband, Anthony, who has been there pretty much from the beginning. Your support and understanding have meant the world to me and have made the many ups and downs of research bearable. From the long nights of analysis and late meetings and conferences, to the conversations about whether or not I got blood that day, you have been there without complaint. There are no words to describe how much you have meant to me through this journey and I can't wait to see what the future holds. I know I can achieve anything with you by my side.

ABBREVIATIONS

ACS	Acute Chest Syndrome
ADP	Adenosine di-phosphate
ASC	Apoptosis-Associated Speck-like Protein. Part of the NLRP3 inflammasome complex.
Caspase-1	Part of the NLRP3 inflammasome complex. Activation leads to the cleavage of IL1β
CXCR1	Chemokine Receptor 1. Member of the GPCR family. Expressed on neutrophils and binds to IL-8 on endothelial cells leading to neutrophil activation.
CXCR2	Chemokine Receptor 2. Member of the GPCR family. Expressed on neutrophils and binds to IL-8 on endothelial cells leading to neutrophil activation.
DAMP	Damage-associated molecular pattern
EC	Endothelial Cells
EV	Extracellular Vesicles
FOV	Field of view
GPIbα	Glycoprotein Ibα. Expressed on platelets. Can bind to neutrophil Mac-1.
HbF	Fetal hemoglobin
HbS	Sickle Hemoglobin
HCAEC	Human coronary artery cells
HMVEC-L	Human lung microvascular endothelial cells

ICAM-1	Intercellular Adhesion Molecule 1. Expressed on endothelial cells. Ligand for neutrophil Mac-1 and LFA-1 assisting in neutrophil arrest and crawling.
IL-8	Interleukin – 8 (CXCL8). Expressed on activated endothelial cells. Binds to neutrophil CXCR1/2. Leads to neutrophil activation.
IL1β	Interleukin-1β. Proinflammatory cytokine
LFA-1	Lymphocyte function-associated antigen-1. β2 Integrin Expressed on neutrophils. Binds to endothelial ICAM-1 leading to neutrophil arrest and crawling.
LPS	Lipopolysaccharide, gram negative bacteria
Mac-1	β2 Integrin Expressed on neutrophils. Binds to endothelial ICAM-1 leading to neutrophil arrest and crawling. Binds to platelet GPIbα
MP	Microparticles
Mitotempo	Scavenger of mitochondrial reactive oxygen species
mROS	Mitochondrial reactive oxygen species
NLRP3	Nucleotide-binding domain, leucine-rich-containing family, pyrin domain-containing-3. Part of NLRP3 inflammasome complex.
NO	Nitric Oxide
PAMP	Pattern-associated molecular patterns
qDF	Quantitative Dynamic Footprinting Microscopy
qMFM	Quantitative Microfluidic Fluorescence Microscopy
P-selectin	Member of selectin family. Expressed on platelets and endothelial cells. Binds to its ligand, PSGL1.

PSGL-1	P-selectin glycoprotein ligand-1. Expressed on neutrophils. Binds to P-selectin.
RBC	Red Blood cell (Erythrocyte)
ROS	Reactive oxygen Species
sRBC	Sickle Red Blood Cells
SCD	Sickle Cell Disease
SCA	Sickle Cell Anemia. Most common form of SCD.
Tak242	Restorvid. Small molecule inhibitor of toll like receptor 4 (TLR4)
TLR4	Toll Like Receptor-4
YVAD-CHO	Caspase-1 Inhibitor

1.0 INTRODUCTION

1.1 SICKLE CELL DISEASE

1.1.1 Background

Sickle Cell Disease (SCD) is an autosomal recessive genetic disorder that affects 100,000 in the U.S. and millions worldwide (5-8). As shown in Figure 1, the global distribution of SCD is primarily centered in Sub-Saharan Africa (regions marked in red and dark red). SCD was first described in 1910 by James B. Herrick who noticed “thin elongated sickle shaped cells” in a blood smear of a patient of African Descent(3, 9). It was not until 40 years later that Linus Pauling attributed the disease to the hemoglobin within erythrocytes (red blood cells, RBC) (3, 9). SCD results from a single point mutation (β^S allele) in the sixth codon of the beta globin gene, where polar hydrophilic glutamic acid is substituted for non-polar hydrophobic valine(6, 9). The aberrant hemoglobin is commonly referred to as sickle hemoglobin (HbS)(9). Hemoglobin S is one of the most common hemoglobin mutation worldwide(4, 10).

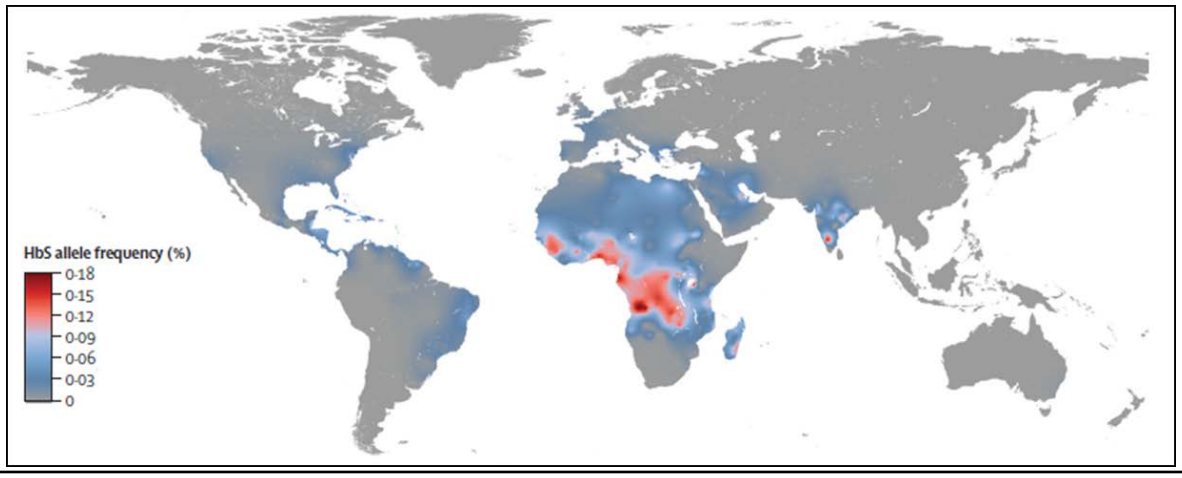

Figure 1: *Global distribution of Sickle Cell Disease.* Map displays the prevalence of the sickle hemoglobin (HbS) allele globally. Areas of red depict the highest prevalence while areas in grey have the lowest prevalence. Figure adapted with permission from Lancet from reference (4).

There are several forms of Sickle Cell Disease with varying levels of severity including Sickle Cell Anemia and HbS beta Thalassemia. Sickle Cell Anemia (HbSS) is the most severe and common form of SCD and occurs when a child is homozygous for the β^S allele. Sickle cell β0 thalassemia (S/β^0) occurs when a child is heterozygous for β^S and β^0 allele. Sickle Cell trait (HbAS) occurs when a child is heterozygous for the β^S allele. Most trait patients are known to be asymptomatic(4). A recent study estimated that in 2010 around 300,000 babies were born with Sickle Cell Anemia (HbSS), while over 5 million babies were born with Sickle Trait (HbAS)(4). Although Sickle Cell Disease is widespread, there is no cure for the disease and the median lifespan of SCD patients is 48 years in women and 42 years in men (6)**.** In 2013, over 175,000 deaths were associated with SCD and SCD related morbidities(11).

1.1.2 Vaso-occlusive Pathophysiology in SCD

1.1.2.1 Polymerization

Under normal circumstances the RBCs ability to deform is key to the flow of blood throughout the body and allows RBCs to easily pass through narrow vessels and capillaries to transport oxygen and other molecules throughout the body. In SCD patients, the RBCs deformability is greatly impaired under all conditions but especially under deoxygenated conditions. When the RBC reaches deoxygenated conditions, the sickle hemoglobin (HbS) polymerize forming long rigid fibers within the RBC leading to rigidity, distortion and damage to the membrane and cytoskeleton of the RBC. Although polymerization is reversible under oxygenated conditions, it causes irreversible damage to the RBC membrane due to repeated sickling and unsickling cycles. This reversible process leads to irreversibly sickled cells (9), exposure of adhesion molecules on the RBC membrane (3, 9, 12) and hemolysis (3, 9). It has been shown that hemoglobin concentration can also greatly affect the level and speed of sickling within the RBC (6, 12). When hemoglobin levels increase there is increased polymerization within the RBC.

1.1.2.2 Hemolysis

As a result of chronic hemolysis due to the sickling and unsickling processes within the RBC, SCD patients are highly susceptible to anemia. Under normal conditions, the RBC lifespan is around 120 days but in SCD patients the average lifespan is less than 20 days. As a result, there is a significant increase in reticulocyte production, immature RBCs. Furthermore, hemolysis leads to the release of erythroid damage-associated molecular patterns (DAMPs) including cell free hemoglobin, heme, and ADP, among others into the plasma (2, 3, 12, 13). Hemoglobin release leads to a decrease in nitric oxide (NO) and an increase in reactive oxygen species (ROS) formation

promoting endothelial dysfunction, platelet activation and pulmonary hypertension(Figure 2) (2). During this process (Figure 2), hemoglobin can be oxidized leading to the release of free heme into the plasma(2, 3). Although both hemoglobin and heme can be scavenged by haptoglobin and hemopexin, respectively, these processes are overwhelmed in SCD due to the extensive hemolysis. As a result, free heme activates sterile inflammation via TLR4 activation(3). The proinflammatory environment that exists as a result of hemolysis gets further enhanced during vaso-occlusive crisis.(3, 12, 14). Furthermore a chronic inflammatory state can lead to increased leukocyte activation and numbers (7) and a procoagulant state via increased tissue factor expression(3, 15) which has also been shown to contribute and promote vaso-occlusive crisis and acute chest syndrome.

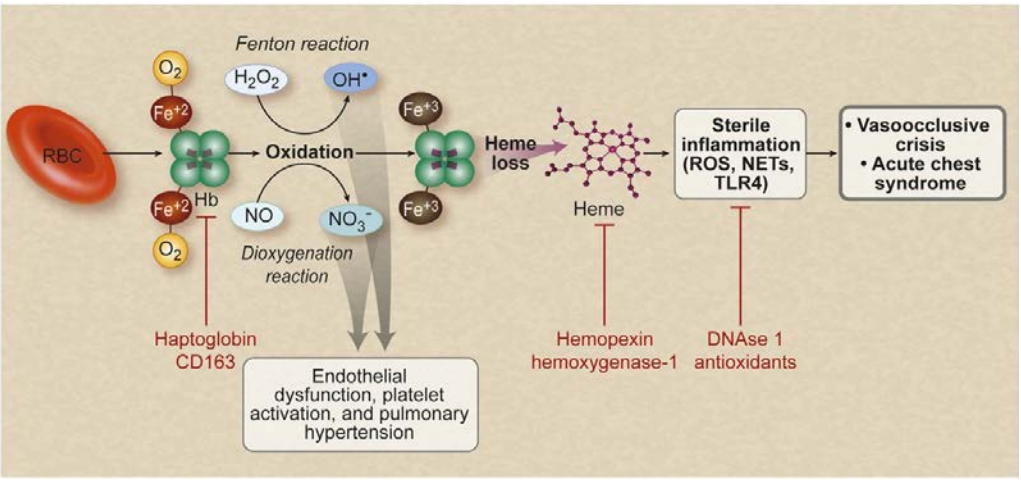

Figure 2: *RBC hemolysis leads to the release of cell free hemoglobin and heme.* Hemolysis of RBC leads to the release of cell free hemoglobin into the plasma. Hemoglobin gets oxidized promoting the release of Heme. Heme can then activate sterile inflammation via reactive oxygen species (ROS) formation, NET formation and TLR4 activation promoting vaso-occlusion and acute chest syndrome in SCD patients. Image adapted with permission from American Society of Hematology and Blood from Reference (2).

Vaso-occlusion (VOC), blockages in vessels by cellular aggregates, accounts for most of the morbidity and mortality faced by SCD patients(6, 9). It is the leading cause of emergency medical care in patients and leads to a global burden of almost $1 billion(16). VOC causes painful

crisis, bone marrow infarction, organ damage, pulmonary hypertension, ischemia reperfusion injury and stroke in SCD patients(3, 6, 7, 9, 12, 15, 17). Vaso-occlusion primarily manifests in patients with low levels of fetal hemoglobin (HbF), increased leukocyte count, increased sickle hemoglobin levels, and decreased hematocrit (6, 12). Although VOC affects millions of SCD patients the cellular, molecular and biophysical mechanisms that drive VOC remain unclear(17).

1.1.2.3 Current Paradigm

There have been several proposed models of the mechanisms of VOC throughout the years. The current paradigm suggests a role for not only sickle RBCs (sRBC), but also leukocytes, endothelium and platelets. As shown in Figure 3, which was adapted with permission from Blood, Frenette et al proposed that endothelial cells get activated as a result of triggers including inflammation, stress and hemolysis (3). Leukocytes are recruited to the site of insult through rolling followed by activation and arrest on the activated endothelium. sRBCs are then captured by the arrested neutrophils leading to blockage of the vessel by cellular aggregates (3). This study was one of the first to suggest a role for leukocytes in the onset of vaso-occlusion. It is important to note that this study was conducted in the cremaster microcirculation of BERK sickle mice and whether this paradigm translates to humans has yet to be elucidated.

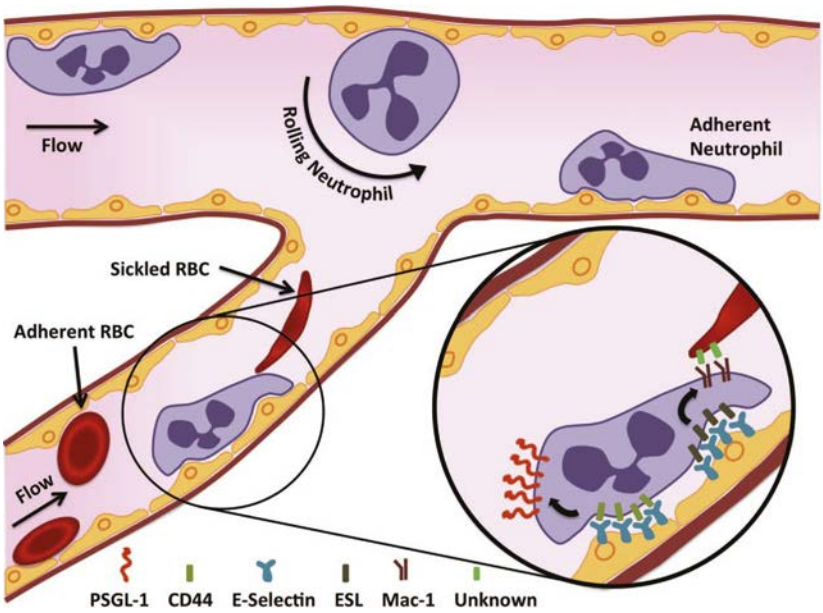

Figure 3: *Current paradigm for VOC in Sickle Cell Disease***.** The current paradigm suggests that VOC occurs as a result of the following events: 1) Endothelial cell activation, 2) recruitment and activation of neutrophils leading to arrest, 3) interactions of arrested neutrophils with RBC and sRBC, 4) blockage of the vessel by cellular aggregates leading to VOC. Image adapted with permission from American Society of Hematology and Blood from Reference (3).

1.1.3 Platelet-neutrophil Aggregation in SCD patients

High platelet and leukocyte counts are risk factors for VOC(18). Neutrophils are the most abundant leukocytes representing about 50-70% of all circulating leukocytes in human blood(19-21), while platelets in SCD patients are chronically activated with increased levels of P-selectin(3). Recent intravital studies have shown that platelet interactions with arrested neutrophils during acute inflammation results in the formation of neutrophil-platelet aggregates in both the systemic (22, 23) and pulmonary microcirculation of WT mice (22, 24). This phenomenon was further studied in TNF-α treated cremaster venules of transgenic SCD and WT mice, and was shown to be enabled by neutrophil Mac-1 binding to GPIbα on platelets (23) and P-selectin binding to platelet P-selectin glycoprotein ligand–1 (PSGL-1) on adherent neutrophils (22), respectively. Interestingly,

circulating neutrophil-platelet aggregates are significantly elevated in the blood of SCD patients who were not in crisis (25, 26).

During acute inflammation, neutrophils are the first to be recruited to the site of injury to help in the clearance of pathogens(27-29). As shown in Figure 4, neutrophils are recruited via a cascade that involves neutrophil rolling, arrest, and crawling along the endothelium prior to platelet and RBC capture(20). Endothelial cell activation is the first step of neutrophil recruitment. During activation, pre-stored P-selectin in Weibel Palade bodies get upregulated initiating neutrophil capture(17, 30, 31). As blood flows through the vessels, freely flowing platelets and RBCs primarily flow along the center line of the flow pushing neutrophils toward the blood vessel wall in what is known as the cell free layer, further potentiating neutrophil capture. Endothelial P-selectin is the primary initiator of neutrophil rolling in the post-capillary venules and prominently binds to neutrophil P-selectin glycoprotein ligand-1 (PSGL-1) leading to neutrophil rolling under wall shear stresses of 1-10 dynes/cm^2 (0.1 -10 Pa)(28). Studies have shown that post-capillary venules are the primary site of blood cell-endothelium interactions during inflammation (12, 32). Rapid association and dissociation of P-selectin and PSGL-1 bonds allow for smooth rolling(31). Previous studies have shown that neutrophils form tethers at the rear of the cell that help mediate neutrophil rolling by shielding the bonds of P-selectin and PSGL-1 from the hydrodynamic shear forces of blood(33). Eventually neutrophil tethers reach a crossover point where they can no longer retract into the cell and form into slings that are thrown to the front of the rolling neutrophil to further stabilize rolling along the endothelium(28, 33). These slings not only have patches of PSGL-1 but also express lymphocyte function antigen-1 (LFA-1) throughout the membrane (Figure 4A), a key contributor to neutrophil arrest and crawling(19, 28, 33).

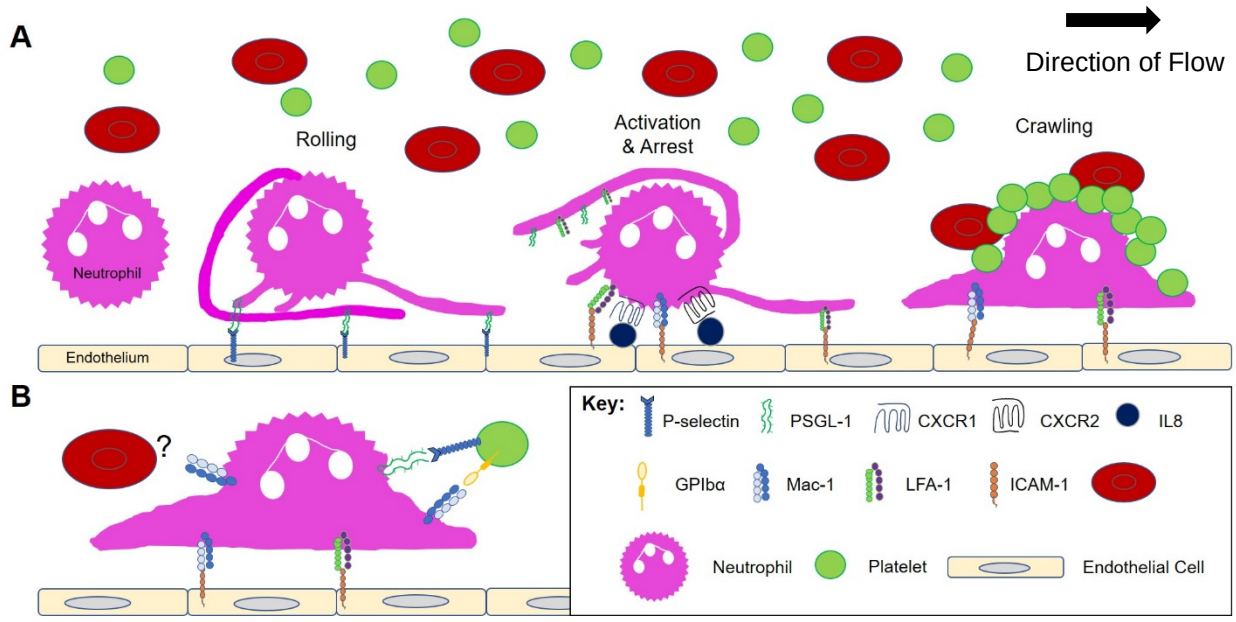

Figure 4: *Schematic of neutrophil-endothelium-platelet interactions.* (A) Neutrophils are recruited to a site of injury or infection via a cascade that involves neutrophil rolling, activation, arrest and crawling along the activated endothelium followed by capture of freely flowing RBCs and platelets. Neutrophil rolling is initiated by neutrophil PSGL-1 binding to endothelial P-selectin. Neutrophils then bind to the endothelial chemokine IL-8 via CXCR2/CXCR1 leading to neutrophil activation and arrest, which is mediated by the β2 integrins, Mac-1 and LFA-1, binding to ICAM-1 on the endothelium. Extended membrane extrusions are slings that promote neutrophil rolling on inflamed endothelium. (B) Neutrophil-platelet-RBC interactions. Neutrophils capture freely flowing platelets and RBC following arrest on the endothelium. Platelets express P-selectin and GPIbα which can bind to neutrophil PSGL-1 and Mac-1, respectively. RBC have the ability to bind to neutrophils by Mac-1. Arrow depicts direction of flow.

To transition from rolling to arrest, neutrophils must first be activated. Rolling increases a neutrophils exposure to the endothelial chemokine, interleukin-8 (IL-8 or CXCL8), which binds to neutrophil CXCR2 and CXCR1, leading to neutrophil activation and arrest(31). Neutrophil activation promotes conformational changes in the β2 integrins LFA-1 (CD11a:CD18) and Mac-1 (CD11b:CD18), increasing their ability to bind to their ligand, intercellular adhesion molecule-1 (ICAM-1) on endothelial cells. Neutrophil interactions between LFA-1 and Mac-1 to endothelial ICAM-1 allow for slow rolling and arrest, and is essential to maintain adhesion to the endothelium. Following arrest (Figure 4B), neutrophils have been shown to capture freely flowing platelets via interactions of neutrophil Mac-1 and PSGL-1 with platelet GPIbα and P-selectin, respectively(22,

23). Additionally, RBC can bind to neutrophil Mac-1 via an interaction that has yet to be fully determined(3).

1.1.4 Emerging role of platelet TLR4 and NLRP3 inflammasome in Inflammation

Recent studies in infectious diseases like dengue fever, have shown an emerging role for platelet activation by toll-like receptor 4 (TLR4), leading to nucleotide-binding domain, leucine-rich-containing family, pyrin domain-containing-3 (NLRP3) inflammasome complex formation and inflammation. These studies have identified that TLR4 and NLRP3-inflammasome dependent caspase-1 activation can promote the generation of IL-1β carrying extracellular vesicles (EVs) by platelets (34).

In Figure 5, NLRP3 inflammasome assembles in the cytosol after activation of TLR4 by damage-associated molecular patterns (DAMPs) and/or pathogen-associated molecular patterns (PAMPs) and serves as a scaffold to recruit apoptosis-associated speck-like protein containing a C-terminal caspase recruitment domain (ASC) and inactive pro-caspase-1(35). Once recruited, pro-caspase-1 is cleaved into active caspase-1 which then cleaves the pro-inflammatory cytokine pro-IL1β into its active form(35-37). IL1β can initiate the inflammatory cascade that leads to innate immune cell recruitment(21) and can propagate inflammation from one cell to another.

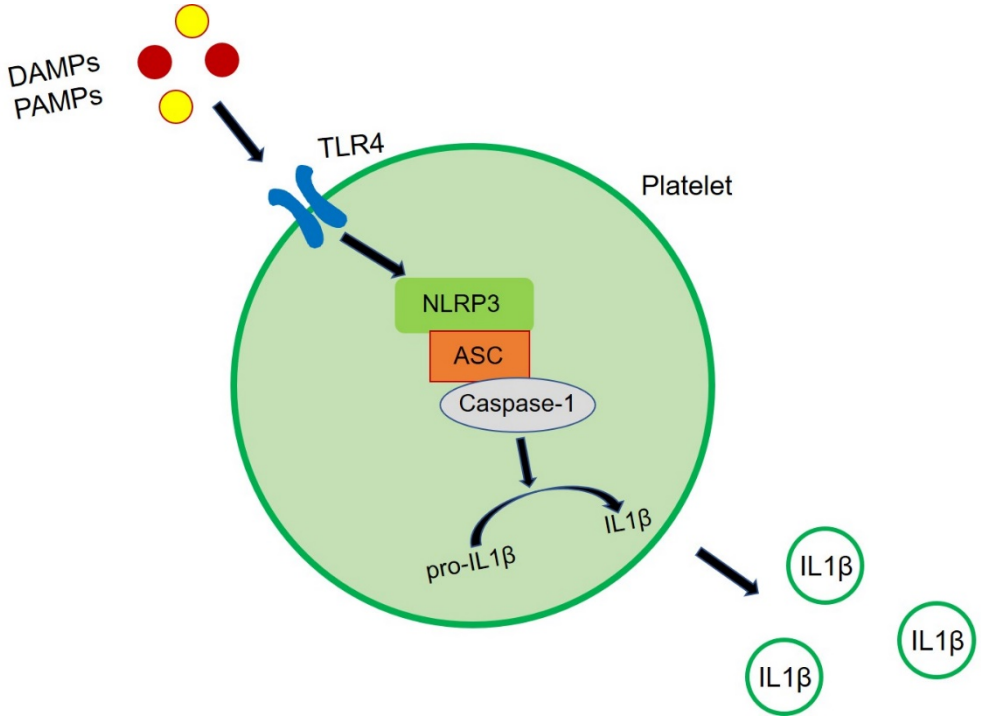

Figure 5: *NLRP3 inflammasome activation in platelets.* Platelet TLR4 gets activated by PAMPs and DAMPs that are released into the blood following hemolysis or infection, respectively. TLR4 activation promotes the formation of NLRP3-ASC-Caspase-1 inflammasome complex, which cleaves and activates Caspase-1. Active caspase-1 cleaves pro-IL1β into mature IL1β, which leads to the release of IL1β containing EVs.

Platelets are important in blood clotting initiation and are major inflammatory cells with key roles within the innate and adaptive immune response(29, 38). Unlike most blood cells, platelets do not have a nucleus, but they do have mitochondria. Due the lack of nuclei, platelets are unable to transcribe new mRNA but are able to translate a select group of preformed mRNA to new proteins(39, 40). This translation allows them to express, store and synthesize proinflammatory cytokines like IL1β, which promotes the body's inflammatory response(38). Following activation platelets have the ability to spice IL-1β pre-mRNA into mature IL-1β mRNA and then synthesize it(38). A recent study showed that lipopolysaccharide (LPS; PAMP) treated platelets released IL1β microparticles or what is now universally referred to as extracellular vesicles(40). Interestingly, platelet derived EVs are among the most abundant species of EVs in

SCD human blood and their numbers correlate with disease severity (15, 41) but the role of platelet EVs in SCD pathophysiology remains unknown.

1.1.5 Current Treatments

Until 2017, Hydroxyurea was the only FDA approved drug to treat VOC in SCD patients (9, 12, 29). Hydroxyurea treatments decrease the occurrence of VOC by increasing fetal hemoglobin (HbF) production which is resistant to sickling (3, 8, 9, 12, 29). It has also been shown to reduce sRBC adhesion. Unfortunately, not all patients are able to take hydroxyurea and many still get undesirable side effects leaving a major need for new therapeutic drugs to alleviate or prevent VOC(42).

Other treatments for SCD include chronic exchange transfusion, L-glutamine and hematopoietic stem cell transplantation. Chronic exchange transfusion is used primarily to treat patients who are anemic or have had a stroke, although over 90% of patients have received a transfusion at one point during their lifetime(43). Chronic exchange transfusions are effective at replacing rigid sRBC with normal RBC but there are many serious complications associated with the treatment including infection, hemolysis, iron overload and delayed hemolytic transfusion reaction(43). L-glutamine was recently approved by the FDA for treatment of SCD(44), but the long term effectiveness in SCD has yet to be determined. Initial studies showed a significant decrease in RBC adhesion following treatment with l-glutamine which led to a decrease in occurrence of VOC(44). Hematopoietic stem cell transplantation is the only curative treatment for SCD but finding an appropriate matching donor can be very difficult. Additionally, there are serious long-term complications which include infertility and graft versus host disease where the donor cells start to attack the recipient’s cells and organs.

1.1.6 Clinical Trials

Currently there are several drugs in clinical trial that are aiming to reduce or alleviate the effects of VOC in Sickle Cell Disease patients by targeting different cells and molecules. Two studies have shown promising results by inhibiting selectins (P-selectin and E-selectin). Rivipansel (GMI-1070) is a pan selectin inhibitor specifically targeting E-selectin which decreases leukocyte adhesion and rolling during VOC(3, 17, 29). During the phase 2 trial, Rivipansel treated SCD patients experienced a decrease in VOC time and hospital stays(45-47) leading to the progression of a Phase 3 clinical trial (3, 29, 46, 47) to further test the effectiveness in SCD patients. SelG1 is a humanized anti-P-selectin antibody that targets P-selectin and inhibits its interactions with PSGL1(29, 42, 47). SelG1 (crizanlizumab) was shown to decrease the rate of VOC in SCD patients in a recent phase 2 clinical trial (42).

Other studies have focused on leukocyte adhesion. Intravenous immunoglobulin (IVIG) has been shown to inhibit leukocyte activation and adhesion to endothelium as well as circulating RBC by inhibiting Mac-1 dependent interactions (3, 47, 48). IVIG is now in a Phase 2 trial to test its effectiveness at reversing acute VOC(29).

Tinzaparin is a low molecular weight heparin that inhibits P-selectin mediated adhesion and was shown to reduce the duration of VOC(3, 29). Prasugrel, a novel P2Y12 ADP receptor antagonist, inhibits ADP mediated platelet activation and aggregation(3). The drug showed promising results during Phase 1 and Phase 2 clinical trials with decreased platelet activation in SCD patients(29, 47). Unfortunately phase 3 clinical trials were terminated due to a lack in efficacy in reducing acute vaso-occlusive complications (49) but have opened the door to new drugs targeting platelet activation.

1.2 SUMMARY

Sickle Cell Disease is an autosomal recessive genetic disorder that affects 100,000 in the U.S. and millions worldwide. SCD results from a single point mutation in the β globin gene that causes the hemoglobin to polymerize under deoxygenated conditions. As a result of the polymerization the RBC sickles which exposes adhesion molecules on the RBC membrane and can lead to hemolysis. Hemolysis has been associated with a proinflammatory and procogulation state, both of which lead to vaso-occlusion. VOC is the primary cause of emergency medical care in SCD patients and leads to ischemia reperfusion injury, acute chest syndrome, stroke and pulmonary hypertension among others. Previous studies have shown in the cremaster of BERK sickle mice that neutrophils roll and arrest along the activated endothelium where they capture sickle RBC thus promoting vaso-occlusion. Neutrophils are the first responders to injury or infection and have the ability to interact with activated endothelium and platelets via a variety of mechanisms. Platelets in SCD patients are chronically activated and have been shown to release IL1β carrying EVs. Although VOC is the primary pathophysiology faced by SCD patients, the exact mechanisms of VOC in humans remains elusive. Furthermore, there are only two FDA approved drugs for SCD, HU and L-glutamine and there remains a need for a novel therapeutic approach to alleviate and reduce VOC more effectively.

1.3 HYPOTHESIS & AIMS OF STUDY

Sickle Cell Disease is a debilitating disease that affects millions worldwide. VOC is the major cause of the morbidity faced by SCD patients, yet the mechanisms remain unclear. The purpose of

this study is to determine the cellular, molecular and biophysical mechanisms that promote vaso-occlusion in Sickle Cell Disease patients.

1.3.1 Primary Hypothesis: *Vaso-occlusion in SCD patients is enabled by platelet nucleation on arrested neutrophils, and requires Mac-1-GPIbα and PSGL1-P-selectin mediated biophysical interactions between platelet hair-like tethers and arrested neutrophils.*

This hypothesis was tested using the following aims:

1.3.2 Aim 1: To develop a novel imaging approach that enables the study of vaso-occlusive events in SCD patient blood under vascular mimetic flow conditions.

Due to the limitations associated with imaging at single cell resolution in SCD patients, there is a great need for an *in vitro* approach that allows the study of whole human blood at a single cell resolution. Development of a new imaging setup utilizing fluorescence microscopy is crucial to allow the quantitative assessment of vaso-occlusion, unravel the mechanism of vaso-occlusion and test the efficacy of anti-adhesion drugs in preventing vaso-occlusive events in SCD patient blood.

1.3.3 Aim 2: To determine whether vaso-occlusive events in non-crisis (steady state) SCD patient blood involve P-selectin-PSGL-1 and Mac-1-GPIbα mediated platelet nucleation on arrested neutrophils.

The novel imaging approach developed in Aim 1 allows the study of the cellular and molecular mechanisms of vaso-occlusion. This technique will provide a way to determine whether platelet

nucleation on arrested neutrophils is significantly higher in non-crisis SCD blood than control human blood. Furthermore, it will allow us to explore the molecular mechanisms of vaso-occlusion by enabling us the ability to determine whether blocking P-selectin-PSGL-1 and Mac-1-GPIbα interactions in non-crisis SCD blood can reduce platelet nucleation on adhered neutrophils.

1.3.4 Aim 3: To test whether trace amounts of LPS is potent enough to selectively enhance platelet-neutrophil aggregation in SCD patient blood

As a result of hemolysis in SCD patients, DAMPs such as heme and hemoglobin are released into the blood leading to the activation of platelets, neutrophil and endothelial cells. Lipopolysaccharide from gram negative bacteria is a PAMP that has been shown to simulate an infection in the blood by activating the innate immune response. To test the hypersensitivity SCD patient blood to LPS, we need to determine a dose of LPS that can enhance platelet-neutrophil interactions in SCD but not control human blood. Once the dose is determined, we can test whether blocking platelet P-selectin or GPIbα and neutrophil PSGL-1 or Mac-1 can attenuate LPS induced platelet-neutrophil aggregation in SCD blood. Lastly, we want to test the specificity of LPS induced interactions by determining whether LPS induced platelet-neutrophil aggregation in SCD patient blood is TLR4 dependent.

1.3.5 Aim 4: To test whether platelet derived hair-like tethers enhance platelet-neutrophil interactions in non-crisis SCD human blood.

Preliminary studies revealed the presence of hair-like tethers on platelets in SCD patient blood. To establish a role for platelet tethers in SCD, we want to first determine whether tether formation by

platelets is higher in non-crisis SCD patient blood than control human blood. We then want to determine, whether tether formation by platelets enhances a platelets ability to interact with arrested neutrophils. Furthermore, the molecular mechanism that promotes tether formation by platelets remains elusive. To complete the study, we want to determine whether formation of platelet derived tethers is dependent on platelet NLRP3 inflammasome activation.

2.0 QUANTITATIVE MICROFLUIDIC FLUORESCENCE MICROSCOPY (QMFM) – A NOVEL IMAGING TECHNIQUE

Note: A majority of this chapter was previously published as: Jimenez MA, Tutuncuoglu E, Barge S, Novelli EM, Sundd P. Quantitative microfluidic fluorescence microscopy to study vaso-occlusion in sickle cell disease. Haematologica. 2015;100(10): e390-e393. doi:10.3324/haematol.2015.126631. Methods specific to lab protocols are described in Appendix A.

2.1 INTRODUCTION

Sickle Cell Anemia (SS), the most common form of SCD, leads to sickling of red blood cells (RBCs)(3). It is believed that sickle RBCs get trapped in blood vessels along with leukocytes and platelets to cause vaso-occlusion(3). Vaso-occlusive crisis is the primary reason for emergency medical care sought by Sickle Cell Disease (SCD) patients(5). Neutrophils are the most abundant leukocytes in human blood and their adhesion to the endothelium starts with rolling mediated by P-selectin on the endothelium binding to PSGL-1 on neutrophils(19). Interleukin-8 (IL-8) on the endothelium binds to CXCR2 on rolling neutrophils to activate β2-integrins Mac-1 and LFA-1 on neutrophils, which then bind to ICAM-1 on endothelium to enable arrest(19). Several studies have used polydimethylsiloxane (PDMS; Silicone) based microfluidic assays to extract invaluable insight into the mechanism of vaso-occlusion. However, these approaches were limited by the use of isolated SS-RBCs(50) or the inability to visualize cellular interactions at single cell

resolution(51) and distinguish different cell types that constitute the vaso-occlusive plug(52). *In vivo* imaging in transgenic SCD mice has identified molecular events that may promote vaso-occlusion(3, 23, 53), but the relevance of these mechanisms is not completely understood in humans. In this study we aim to develop a novel imaging approach to study vaso-occlusive events in whole human blood at a single cell resolution.

2.2 MATERIALS AND METHODS

2.2.1 Reagents

Recombinant human P-Selectin-Fc chimera (P-selectin) and recombinant human ICAM-1-Fc chimera (ICAM-1) were purchased from R&D Systems (Minneapolis, MN). Recombinant human CXCL8/interleukin-8 (IL-8) was purchased from Peprotech Inc. (Rocky Hill, NJ). Alexa Fluor-647 conjugated mouse anti-human CD16 mAb (clone 3G8, mouse IgG1), FITC conjugated mouse anti-human CD49b mAb (clone AK-7, mouse IgG1), FITC conjugated mouse anti-human CD66b (clone G10F5, mouse IgG1), function blocking purified NA/LE mouse anti-human CD11b mAb (clone ICFR44, mouse IgG1), mouse anti-human CD162 (clone KPL-1, mouse IgG1), PE-conjugated anti-human PECAM-1 (clone WM59, mouse IgG1) and isotype control mouse IgG1 were purchased from BD Biosciences (San Jose, CA). Function blocking anti human CD62P mAb (clone G1/G14, mouse IgG1), anti-human CD62E mAb (clone HAE-1f, mouse IgG1) were purchased from Ancell Corp. (Bayport, MN). Function blocking anti-human CD11a mAb (clone TS1/22, mouse IgG1) was purchased from Thermo Scientific™ (Rockford, IL). Human

fibronectin was purchased from Fisher Scientific, (Pittsburgh, PA). Recombinant human tumor necrosis factor-α (TNF-α) was purchased from Peprotech, Inc.

2.2.2 Blood collection

Blood samples were collected from 8 race-matched control and 10 SS patients in accordance with the guidelines set by the Institutional Review Board at the University of Pittsburgh. Informed written consent was obtained from all the participants in accordance with the Declaration of Helsinki. Non-smokers who were not on chronic blood transfusion or hydroxyurea therapy or were non-compliant to hydroxyurea were included in the study. Blood was drawn via venipuncture using a 21G needle into a 10-ml syringe filled with 20 U/ml of heparin or 25 U/ml hirudin. Fluorescent antibodies against human CD16 (3 μL) and CD49b (2.5 μL) were added to 500 μl of blood in a 1 ml Eppendorf tube to stain neutrophils and platelets in situ, respectively. CD49b is the α2 chain of the collagen receptor α2β1 on platelets and has been used to identify platelets in blood(54). CD16 has been used to identify human neutrophils which are defined as double positive for CD66b+ and CD16+(55). Based on this, Alexa Fluor 647 conjugated anti-human CD16 and FITC-conjugated anti-human CD49b antibodies to stain neutrophils and platelets, respectively, were added to the blood (3:500 CD16; 1:250 CD49b) in the inlet reservoir. Also, complete blood cell counts were conducted using Hemavet® HV950. All experiments were completed within 2 hours of blood draw and the blood sample was gently mixed on a blood rocker during the entire experiment.

2.2.3 Flow Cytometry

Heparinized blood was lysed with 1X RBC lysis buffer and cells were suspended in PBS without Ca2+ and Mg2+ + 1% BSA + 0.1% sodium azide, pH 7.4. The cell suspension was incubated with FITC-CD66b (1:100) and AlexaFluor647-CD16 (1:100) monoclonal antibodies or isotype matched control antibodies and analyzed on BD-Fortessa flow cytometer. Post-acquisition analysis was done using FlowJo software.

2.2.4 Quantitative Dynamic Footprinting (qDF)

qDF is an adaptation of total internal reflection fluorescence (TIRF) microscopy that allows visualization of the footprints of rolling and arresting neutrophils on a glass substrate coated with endothelial adhesion molecules(33, 56). A laser is incident through a high numerical aperture, high magnification, oil immersion objective at the glass-cell interface at an angle (70˚) greater than the critical angle, θc (64.33˚) = sin-1 (n_2/n_1), where $n_1 = 1.52$ and $n_2 = 1.37$ ($n_1 > n_2$) are the refractive index of glass and cell cytoplasm, respectively. The laser is completely reflected back into the objective but an evanescent wave (light blue box in Figure 7D) is established on the cell side of the coverslip. The intensity of the evanescent wave decreases with z-distance and becomes negligible within 200 nm above the coverslip (light blue box in Figure 7D). As a result, fluorescence is excited only in the cell membrane and cytosolic region that lies within 200 nm above the coverslip, while the remainder of the cell remains invisible.

2.2.5 Endothelial Cell Culture and Activation

A 12 mm^2 region on rectangular cover slips (Number 1.5, Fisher Scientific) was coated with 10 µg/ml of human fibronectin for 30 minutes at room temperature and 20,000 HMVECs-L or HCAECs in 50 µl culture medium (400,000 cells/ml) were allowed to adhere to the coated region. Cells were allowed to reach confluence at 37°C and 5% CO_2 in a CO_2 incubator for 5 days. Once confluent, cells were activated by overnight incubation with 100 ng/ml recombinant human TNF-α and used in microfluidic flow assays.

2.2.6 Preparation of adhesion molecule presenting substrates:

Coverslips were coated with a concentration of 2 µg/ml P-selectin, 10 µg/ml ICAM-1, and 10 µg/ml IL8 and stored in Casein until use in experiments. See Appendix A1.1 Preparation of adhesion molecule presenting substrates for further details on preparation of P-selectin, ICAM-1, and IL8 coated substrates.

2.2.7 Microfluidic flow device assembly

A PDMS based silicone chip with micro-channels engraved on its surface was gently placed on a glass coverslip coated with either a cocktail of P-selectin, ICAM-1, and IL-8 or cultured with TNF-α treated HMVECs-L or HCAECs and sealed together using vacuum (negative 30 kPa pressure; Figure 6B). Prior to blood perfusion, the endothelialized microfluidic devices were filled with a KREBS-HEPES buffer, pH 7.4 (NaCl, KCl, $MgSO_4$, $NaHCO_3$, KH_2PO_4, Hepes, Glucose and $CaCl_2$) to keep the endothelial monolayer viable. Microfluidic chips attached to adhesion

molecules was perfused with 1x PBS. The assembled device has an inlet, an outlet, a vacuum port connected to in-house vacuum supply and four identical micro-channels (30 µm high and 500 µm wide) with nearly identical flow rates and wall shear stresses (Figure 6). The wall shear stress was calibrated as a function of the differential pressure between the inlet and outlet reservoir. The differential pressure was set by placing the inlet reservoir next to the device while lowering the outlet reservoir to achieve the physiological wall shear stress (57) of 6 to 10 dyne cm^{-2}. See A1.3 Calibration of Wall Shear Stress in Microfluidic Device for the procedure to calibrate new device shear stress. Approximately 500 µL of anticoagulated blood was transferred to a 1.5 mL Eppendorf tube which served as an inlet reservoir while a 10-ml syringe filled with PBS served as the outlet reservoir. The inlet and outlet reservoirs were connected to the inlet and outlet ports of the device using PE10 (ID 0.28 mm, OD 0.61 mm) and TYGON (ID 0.8 mm, OD 2.4 mm) tubing, respectively.

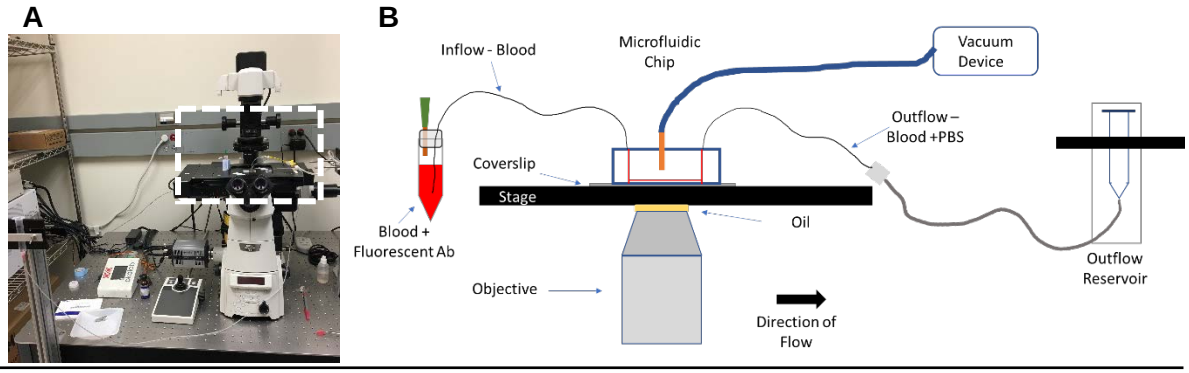

Figure 6: *Schematic of Microfluidic Setup.* (A) Nikon Eclipse-Ti inverted microscope with a TIRF photoactivation unit was used for the qMFM imaging setup. (B) Schematic depicting the area marked with the white dotted box in A. PDMS chip (blue rectangle) is connected to a glass coverslip (grey line) via vacuum. Blood with fluorescent antibodies is added to a 1.5mL Eppendorf and connected to the inlet of the PDMS chip (blue rectangle) and coverslip (grey thick line). Outlet reservoir is attached to the outlet port on the opposite end of the chip. Whole setup is placed on top of the stage with blood flowing from left to right. Wall shear stress is controlled by the height of the outlet reservoir with the stage level as 0. TIRF objective with oil is raised to the coverslip and imaging can occur.

2.2.8 qMFM data analysis guidelines

The following strategy was followed to record observations in adhesion molecule coated micro-channels.

Step-1: Neutrophils were allowed to roll, arrest and crawl for 2 min and observations were recorded in a field of view using qDF.

Step-2: After 2 min, the incident angle of the laser was reduced and the platelet-neutrophil interactions were observed in the same FOV for an additional 4 min.

Time series sequences of images were processed and analyzed using NIS-Elements Analysis Advanced Research software (Nikon). Image background was subtracted using the average intensity of a small region of the image background and platelets were identified using the spot detection algorithm available in NIS-Elements. The interacting platelets are marked with white circles shown. The spot-detection algorithm identifies only those platelets which slowdown to interact with arrested neutrophils and continues to track them until they detach and leave the FOV. Platelets are identified by defining a threshold based on the intensity and size of the bright spots. The final read-out is the number of interactions in a given observation period and the life-time of each interaction. Platelet-Neutrophil interactions were defined as following:

- A freely flowing platelet attaches to an arrested neutrophil → an interaction event.
- A freely flowing platelet aggregate attaches to an arrested neutrophil → an interaction event.
- A rolling neutrophil enters the FOV with a platelet attached to it → an interaction event.
- A platelet or an aggregate of platelets detaches from one neutrophil and attaches to another neutrophil → an interaction event.

2.2.9 Scanning Electron Microscopy

Blood was perfused through PDMS based microfluidic channels presenting P-selectin, ICAM-1, and IL-8. Neutrophils were allowed to roll, arrest and interact with freely flowing platelets prior to fixation under flow. Coverslips were processed as described in A1.9 Scanning Electron Microscopy.

2.2.10 Adhesion studies

Adhesion specificity was confirmed by either incubating the adhesion molecule or endothelial cells coated coverslips with function blocking antibodies against P-selectin (1:500) and E-selectin (1:500) for 10 min at 37˚C/5% CO_2 prior to their use in microfluidic assay. In some experiments, function blocking antibodies against Mac-1, LFA-1 and PSGL-1 were added to the blood (1:100) in the inlet reservoir followed by 10 min of incubation with mixing at room temperature prior to use in the microfluidic assay. Finally, the microfluidic device was placed on the heated stage set at 24˚ or 37˚C (Okolab, Ottaviano, Italy) of an inverted microscope and the blood was perfused through the micro-channels at a wall shear stress of 6 to 10 dyn cm^{-2}. Observations were made in the perfusion chambers (30 µm high and 500 µm wide).

2.2.11 Statistical Analysis

Mean number of platelet-neutrophil interactions under different conditions were compared using a student's t-test. Fourfold table analyses with Bonferroni χ^2-statistics were used to compare percentages between different groups. A p-value of less than 0.05 was used to determine

significance. Lifetimes of interactions under different conditions were compared as cumulative probability distributions using non-parametric Kruskal-Wallis H-test.

2.2.12 Microscope Set up

For the setup of the microscope and the equipment used for imaging See Appendix A1.8 Microscope Set up.

2.3 RESULTS

2.3.1 Working principle of qMFM.

A silicone chip with micro-channels engraved on its surface was gently placed on a glass coverslip (Figure 7A) coated with either a cocktail of P-selectin, ICAM-1, and IL-8 (Figure 7B) or cultured with TNF-α treated human coronary artery endothelial cells (HCAECs) or human lung micro-vascular endothelial cells (HMVECs-L) (Figure 7C) and vacuum-sealed. The assembled device had an inlet, an outlet and four identical perfusion chambers (30 µm high and 500 µm wide). Alexa Fluor 647 conjugated anti-human CD16 and FITC-conjugated anti-human CD49b antibodies were added to blood in the inlet reservoir to stain neutrophils and platelets, respectively. Finally, the microfluidic device was placed on the stage of the inverted microscope and the blood was perfused through the perfusion chambers at a wall shear stress of 6 dyne/cm^2 (See A1.3 Calibration of Wall Shear Stress in Microfluidic Device). Rolling, arrest and crawling of fluorescent neutrophils in human blood was visualized in the perfusion chambers using quantitative dynamic footprinting

(qDF)(33). In qDF, a laser is incident at the glass-cell interface at an angle greater than the critical angle. The laser is reflected back into the objective and an evanescent wave (Figure 7D - light blue box) is established on the cell side of the coverslip. The intensity of the evanescent wave becomes negligible greater than 200 nm above the coverslip. As a result, fluorescence is excited only in the cell membrane and cytosolic region that lies within 200 nm above the cover slip, while the remainder of the cell remains invisible. In order to observe platelets interacting with adhered neutrophils, the angle of the laser was reduced during imaging to increase the illumination zone from 200 nm to greater than 5 mm (Figure 7E - light blue box).

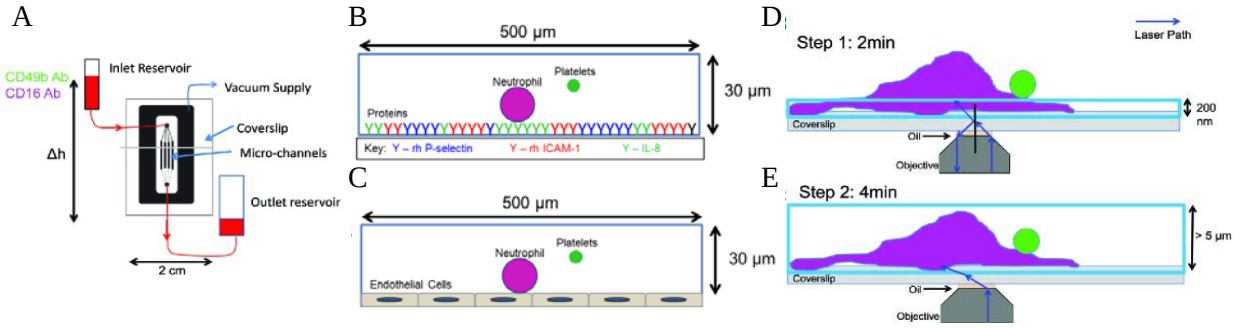

Figure 7:*The working principle of qMFM*. **(A)** Schematic of custom PDMS vacuum sealed microfluidic device. Δh is the difference in height between the inlet and the outlet reservoir. Cross-section of a micro-channel coated with **(B)** cocktail of P selectin, ICAM-1 and IL-8 and **(C)** cultured endothelial cells **(D)** Step 1 of qMFM - 200 nm evanescent wave (light blue box) which allows visualization of only the footprint of the neutrophil. **(E)** Step 2 of qMFM- illumination zone (light blue box) greater than 5 μm allowing visualization of the platelets nucleating on top of neutrophils. Neutrophil (violet) and platelet (green). Figure published in Jimenez, M *et al. Haematologica* 2015.

2.3.2 qMFM reproduces neutrophil rolling and arrest in SS patient blood.

Neutrophil rolling has been shown to be facilitated by ‘slings’, which are long membrane cell-autonomous structures extended at the front of rolling neutrophils (58). Although slings have been shown to exist on mouse neutrophils, the evidence to support their presence on human neutrophils

does not exist. When SS or control blood was perfused through P-selectin coated microfluidic channels, the majority of neutrophils were rolling (Figure 8A-B) and formed slings (Figure 8C) in SS and control blood. As SS and control blood was perfused through micro-channels coated with a cocktail of P-selectin, ICAM-1 and IL-8, neutrophils rolled and then quickly arrested (Figure 8D, E). Arrested neutrophils spread over time and crawl, which is similar to observations made in mice vasculature in vivo (22). Slings were also observed to exist on arrested neutrophils in SS (Figure 8E) as well as control subject blood (Figure 8F). Flow cytometry data also revealed in that 94% of CD16+ cells in human blood are neutrophils (Figure 8G), supporting its choice as a neutrophil marker.

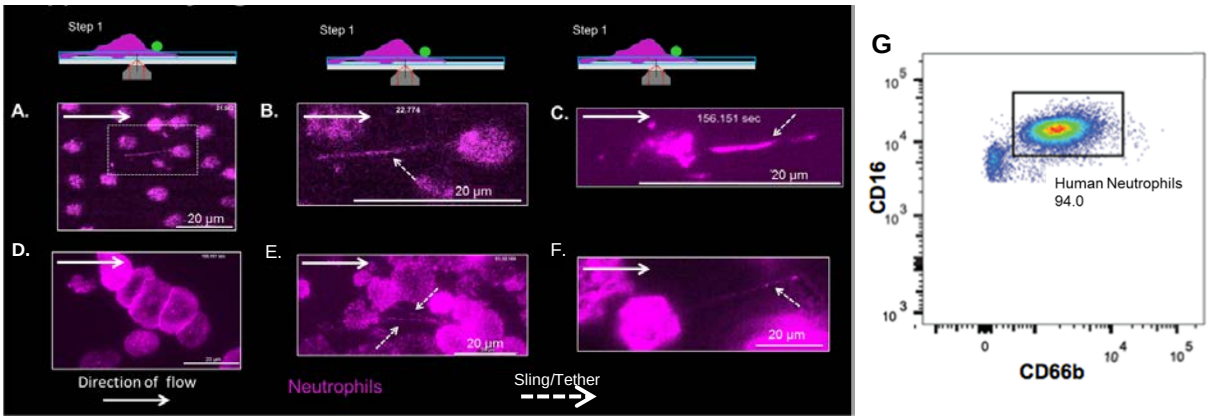

Figure 8: *qMFM reproduces rolling, arrest and sling formation by neutrophils in SS blood* (A) Neutrophils rolling on P-selectin coated substrate in SS patient blood. (B) Magnified view of the region marked with dotted box in A revealing the presence of slings in the rear of rolling neutrophils in SS blood and (C) in the front of a rolling neutrophil in control blood. (D) Neutrophils arrest on P-selectin, ICAM-1, and IL-8 coated substrate in SS patient blood. (E) Slings can be observed to connect adjacent arrested neutrophils in SS patient blood. (F) Sling exists on an arrested neutrophil in control human blood. Sling denoted by dotted line arrow. Wall shear stress 6 dyn cm^{-2}. Scale bars 20 µm. Neutrophils (violet). (G) Flow cytometry of human neutrophils stained for CD66b and CD16. Figure published as Jimenez, M *et al. Haematologica* 2015.

2.3.3 SS patients have enhanced neutrophil rolling and arrest.

This study found that the number of neutrophils that rolled in P-selectin coated micro-channels was fourfold higher in SS than control blood (Figure 9A, B). Similarly, the number of neutrophils that arrested on P selectin, ICAM-1 and IL-8 coated micro-channels was two to three-fold higher in SS than control blood (Figure 9C, D). This P-selectin dependent rolling was completely abolished by a function blocking antibody against P-selectin and PSGL-1, confirming the specificity of the molecular interactions (Figure 9E). Neutrophil arrest in control blood was completely abolished by a function blocking antibody against Mac-1, and partially by a function blocking antibody against LFA-1 (Figure 9E), suggesting that Mac-1 is the predominant β2-integrin mediating human neutrophil arrest.

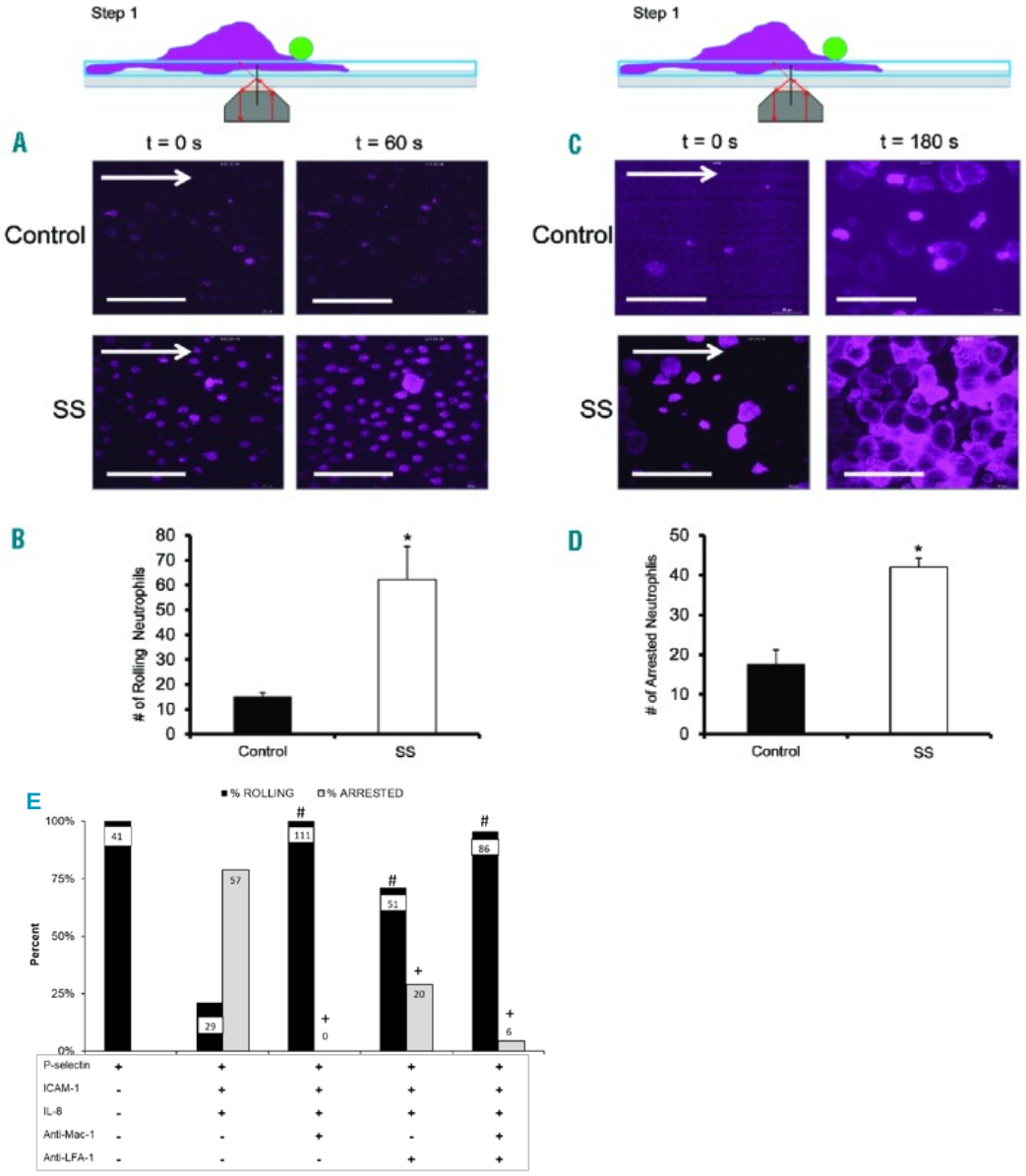

Figure 9: *More neutrophils roll and arrest in SS than in control blood.* qMFM step 1 imaging reveals (A) the accumulation of rolling neutrophils in control (top row) and SS blood (bottom row) over 60 s on a P-selectin coated substrate. (B) Number of rolling neutrophils during a 60s period on P-selectin coated substrate. qMFM also reveals the accumulation of (C) arrested neutrophils in control (top row) and SS blood (bottom row) over 180 s on a P-selectin, ICAM-1, and IL-8 coated substrate. (D) Number of arrested neutrophils during a 180s period. **P*<0.05 compared to control blood. N=3 SS N=3 control subjects. Error bars are SD. E) Verification of adhesion specificity. Percent rolling and arrested neutrophils. Numbers on bars represent total number of neutrophils. Fourfold table analysis with Bonferroni $\chi 2$-statistics was used to compare percentages between different groups. # $p<0.05$ for rolling when compared to untreated PIC. + $p<0.05$ for arrest when compared to untreated PIC. n=2 Wall shear stress 6 dyn/cm^2. Horizontal arrows denote direction of blood flow. Wall shear stress 6 dyn cm^{-2}. Scale bars 50 μm. Neutrophils (violet). Excitation laser 640 nm. Figure published in Jimenez, M *et al. Haematologica* 2015.

2.3.4 qMFM allows the visualization of neutrophil footprints and platelet-neutrophil interactions.

The capture of activated platelets by adherent neutrophils is believed to play a role in the onset of vaso-occlusion in the venules of SCD mice (23, 53). Using the two-step imaging strategy shown in Figure 7B-C, neutrophils were observed to arrest and then crawl on P-selectin, ICAM-1 and IL-8 coated microfluidic channels (Figure 10A) which enabled nucleation of platelets on top of crawling neutrophils (Figure 10B). The crawling of neutrophils followed by nucleation of platelets, is similar to observations reported in mice in vivo (22, 23, 53). We observed that platelet nucleation on arrested neutrophils in SS blood led to the formation of aggregates which partially occluded the microfluidic channels. As shown previously in SCD mice in vivo(53), RBCs were found to be trapped in these aggregates. qMFM allowed visualization of platelet-neutrophil interaction at single cell resolution (Figure 10C). The time-series of qMFM images were analyzed using the Nikon Elements spot detection algorithm to quantify the total number and lifetime of platelet-neutrophil interactions (Figure 10D). This methodology was used to evaluate the effect of different anticoagulants on the platelet-neutrophil interactions in control subject blood. We observed that the number (Figure 10E) and the lifetime (Figure 10F) of platelet-neutrophil interactions were comparable in heparin and hirudin anticoagulated control blood. Thus platelet-neutrophil interactions were independent of the choice of anticoagulant. The in vitro microfluidic approach also allows fixation of interacting cells under flow followed by scanning electron microscopy (See A1.9 Scanning Electron Microscopy for details on preparation and imaging). Figure 10G shows a scanning electron micrograph of a platelet interacting with an arrested neutrophil in control subject blood.

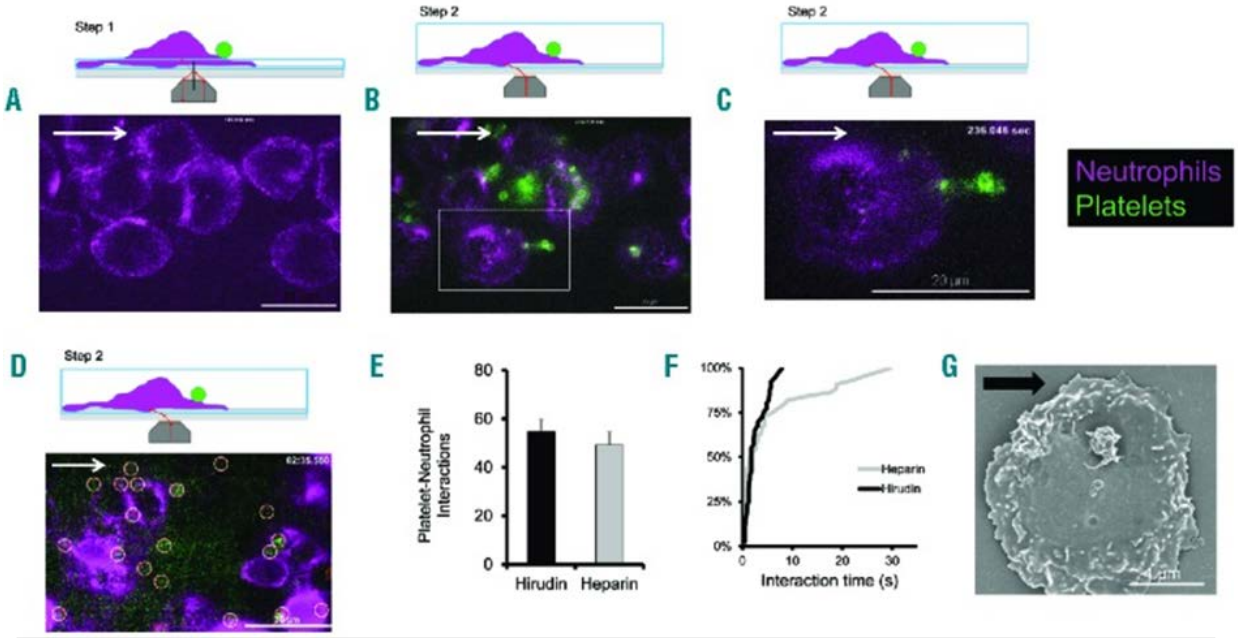

Figure 10: *qMFM provides the choice to visualize neutrophil footprints or platelet-neutrophil interactions.* (A) Imaging step 1 allows visualization of footprints of arrested neutrophils while (B) step 2 enables visualization of platelet-neutrophil interactions on P-selectin, ICAM-1 and IL-8 coated substrates in control human blood. (C) The region marked by a dashed box in B is magnified to reveal platelet-neutrophil interaction at single cell resolution. (D) White circles mark the platelets. (E) Comparison of total platelet-neutrophil interactions in hirudin vs. heparin anticoagulated control subject blood. Error bars are SE. (F) Cumulative probability distribution of the lifetime of platelet-neutrophil interactions in hirudin (n = 41 cells) vs. heparin (n = 44 cells) anticoagulated control human blood; n = 2 healthy control subjects with 4 FOV; (G) Scanning electron micrograph of platelet attached to an arrested neutrophil in control subject blood. Wall shear stress = 6 dyn cm^{-2}. Scale bars 20 μm. Horizontal arrows denote blood flow direction. Figure published in Jimenez, M *et al. Haematologica* 2015.

2.3.5 Neutrophils form slings which mediate rolling on endothelialized microchannels.

In order to establish that qMFM serves to visualize cellular interactions on cultured endothelium, blood from SS and control subjects was perfused through microfluidic micro-channels cultured with TNF-α activated HMVECsL or HCAECs and cellular interactions were recorded using step 2 of the imaging technique (Figure 7C). In some experiments (Figure 11A-C), cultured HMVECs-L were stained with a PE-conjugated antibody against endothelial PECAM-1 (green) to visualize the endothelial cell borders. Neutrophils in control blood were observed to roll and arrest on activated HMVECs-L (Figure 11A-C). Neutrophils in SS and control blood were also observed to

roll (Figure 11D), arrest (Figure 11E) and then capture freely flowing platelets on activated HCAECs (Figure 11F). The majority of neutrophils rolling on activated HCAECs were observed to form slings (Figure 11D). As shown in the Figure 11G, following arrest, neutrophils were also observed to crawl on activated HCAECs. In specificity studies neutrophil rolling and arrest on activated HCAECs in SS blood was not affected by blocking E-selectin, but was completely abolished by simultaneous blocking of P-selectin on HCAECs and Mac-1 on neutrophils (Figure 11H). Thus, neutrophil rolling on activated HCAECs is primarily mediated by P-selectin. See A1.4 Microfluidic Adhesion studies for further details on the methods.

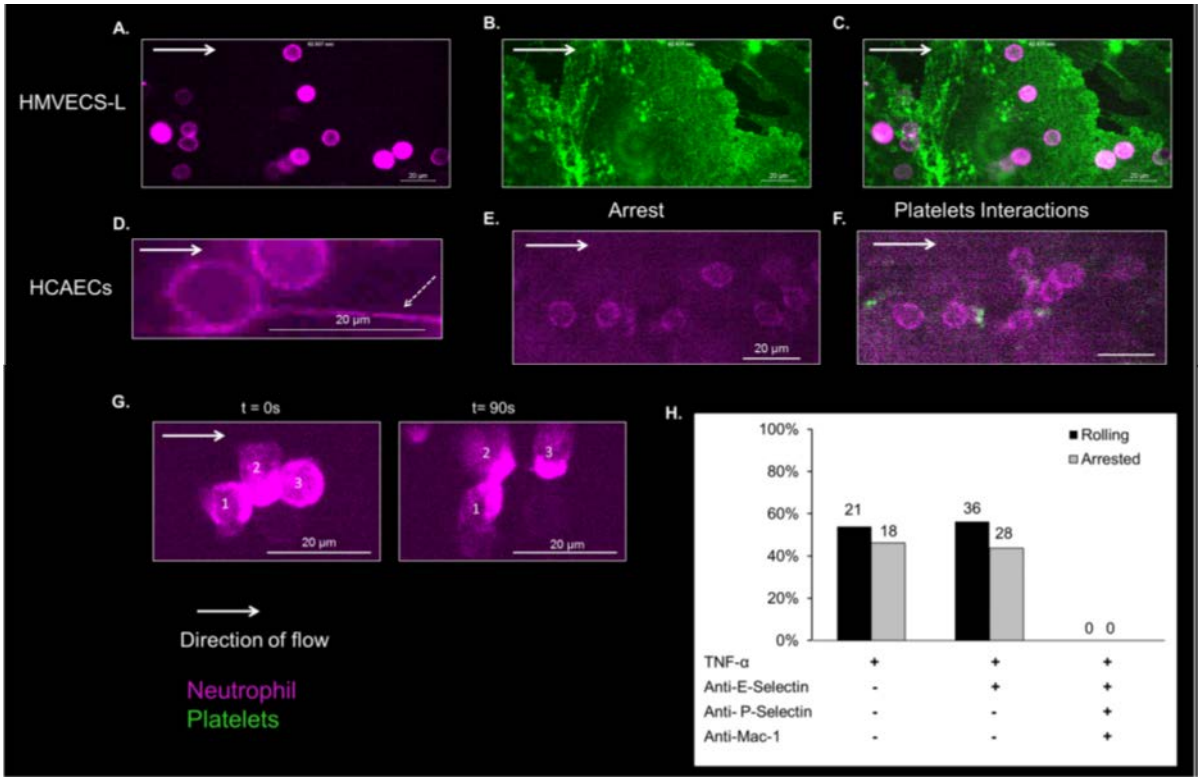

Figure 11: *Neutrophils form slings to mediate rolling on endothelialized microchannels.* qMFM reveals (A) rolling and (B) arresting neutrophils on TNFα treated HMVECs-L (green). (C) Overlay of A and B. (D) Sling (marked with dashed arrow) formation by rolling neutrophil on HCAECs in control human blood. (E) Neutrophil arrest on TNF-α activated HCAECs in SS patient blood. (F) Platelets (green) interacting with neutrophils (violet) that are arrested on TNF- α activated HCAECs in SS patient blood. (G) Neutrophils crawling on TNF-α activated HCAECs in control human blood at 0 s start to migrate away by 90 s. Numbers identify individual neutrophils. (H) Percent of arrested neutrophils on HCAECs following treatment with function blocking antibodies. Numbers on top of bars denote total number of neutrophils. N=3 experiments. Fourfold table analysis with Bonferroni $\chi 2$-statistics was used to compare percentages between different groups. Neutrophil (violet), platelet (green). Wall shear stress = 6 dyn cm-2. Scale bars 20 µm. Figure published in Jimenez, M *et al. Haematologica* 2015.

2.4 DISCUSSION

There are several advantages to using qMFM to study vaso-occlusion. Collection of large volumes of blood from SS patients can be challenging as these patients suffer from chronic anemia(5). The volumetric flow rate through the microfluidic device used in qMFM (Figure 7A) is 12 µl/min at a wall shear stress of 6 dyn/cm^2. Thus, qMFM allows for 4-minute-long experimental observations

using as little as 50-100 µl of anticoagulated blood. Also, the microfluidic chips are reusable, easy to fabricate and cost less than 10 cents per chip(33). On top of that, a two-step fluorescence microscopy approach (Figure 7B-C) provides a choice of studying either footprints of crawling neutrophils or platelet-neutrophil aggregation with a swift transition between the steps. This strategy of visualizing neutrophil footprints without platelets and RBCs in the background can be useful in determining the effect of anti-adhesion drugs on neutrophil rolling and arrest vs. neutrophil-platelet aggregation. In addition to scanning electron microscopy (SEM), the interacting cells fixed under flow can be stained with fluorescent antibodies against adhesion molecules or cytoskeletal proteins and be visualized using super-resolution fluorescence microscopic techniques like Structured-Illumination-Microscopy (SIM) or Stimulated Emission Depletion (STED) microscopy which are capable of visualizing cellular features at an unprecedented lateral resolution of 100 nm and 20 nm, respectively.

Although qMFM is a useful tool, there are a few limitations associated with this approach. The blood has a tendency to coagulate when coming in contact with silicone or glass. To avoid artifacts, microscopic observations in a single microfluidic chip should be limited to not more than six minutes. However, the low cost of microfluidic chips and their ability to be recycled circumvents this limitation. Anticoagulated blood tends to coagulate and separate into plasma and cell pellet when allowed to sit without any mixing. Pilot studies revealed that in order to eliminate artifacts, the anticoagulated blood needs to be mixed continuously and used in qMFM within 2 hours following blood collection thus allowing less time for data collection. qMFM requires in situ staining of blood cells by addition of fluorescent antibodies against lineage markers to blood. In order to visualize different blood cell types distinctly, it requires selection of fluorochromes with distinct excitation and emission spectra for each blood cell type so that cell types can be identified

based on the emission spectra. However, with the advent of commercially available multi-wavelength laser and LED sources as well as high sensitivity sCMOS cameras, video-rate sequential acquisition of at least four fluorochromes is easily achievable.

2.5 CONCLUSION

This study introduces quantitative microfluidic fluorescence microscopy (qMFM) which enables the visualization of cellular interactions in human blood flowing through silicone based microfluidic channels. qMFM reproduces the leukocyte-endothelium adhesion cascade, starting from rolling, transition to arrest followed by crawling and platelet capture by crawling leukocytes in human blood. Remarkably, qMFM reveals that leukocyte rolling and arrest is several fold higher in SS than in control human blood. qMFM also provides the first evidence to support the presence of slings in rolling and arresting human neutrophils. qMFM allows visualization of platelet-neutrophil interactions at single cell resolution and enables a numerical read-out of the vaso-occlusive events in the form of frequency and lifetime of interactions. This quantitative assessment renders qMFM a unique platform to study the molecular mechanisms of vaso-occlusion and test the efficacy of anti-adhesion drugs in preventing vaso-occlusion. In conclusion, qMFM serves as an in vitro imaging platform that can be used to elucidate the cellular, molecular and biophysical mechanisms of single cell adhesive events that potentiate vaso-occlusion in SS blood, in addition to evaluating the efficacy of a drug or treatment for individual patients.

3.0 VASO-OCCLUSION IN SICKLE CELL DISEASE IS MEDIATED BY NEUTROPHIL-PLATELET MICROEMBOLI

Note: A majority of this chapter was previously published as: Bennewitz MF†, Jimenez MA†, Vats R, Tutuncuoglu E, Jonassaint J, Kato GJ, Gladwin MT, Sundd P. Lung vaso-occlusion in sickle cell disease mediated by arteriolar neutrophil-platelet microemboli. Journal of Clinical Investigation-Insight. 2017 Jan 12;2(1):e89761. PubMed PMID: 28097236; PubMed Central PMCID: PMC5214368. †co-first author.

3.1 INTRODUCTION

Acute vaso-occlusive pain crisis is the predominant pathophysiology requiring emergency medical care by SCD patients (5). Repeated episodes of vaso-occlusive crisis contribute to morbidity and end organ damage in SCD patients, and there is a strong need for improved preventive strategies (3, 5). Acute vaso-occlusive crisis can involve the lung, bone marrow, and systemic blood vessels (5, 6). Systemic vaso-occlusive events have been characterized in transgenic mouse models of SCD and in the human retinal vasculature, and appear to be mediated by vaso-occlusive events in the postcapillary venules. While the lung is one of the most affected organs in SCD(59), the cellular, molecular, and biophysical mechanisms that contribute to pulmonary vaso-occlusion have not been characterized (5).

Intravital microscopic studies of the cremaster microcirculation of transgenic SCD mice have shown that systemic vaso-occlusion occurs primarily in the postcapillary venules, involving

Mac-1 (CD11b/CD18) dependent capture of sickle erythrocytes by adherent neutrophils (53). Recent studies of the TNF-α–treated cremaster venules in WT mice revealed that platelets can interact through P-selectin binding to PSGL-1 on adherent neutrophils (22). Additionally, neutrophil-platelet aggregates were observed in TNF-α–treated cremaster venules of SCD mice, requiring neutrophil Mac-1 binding to glycoprotein Ibα (GPIbα) on platelets (23). Interestingly, elevated platelet and leukocyte counts are identified risk factors for acute vaso-occlusive pain crisis (18), and circulating neutrophil-platelet aggregates are significantly elevated in the blood of steady-state SCD patients (25, 26). Despite this recent appreciation of a role for neutrophil-platelet aggregates in systemic vaso-occlusion, the role of these cellular aggregates in pulmonary vaso-occlusion associated with SCD is not known. This study provides proof of principle that specifically targeting platelet P-selectin and neutrophil Mac-1 decreases neutrophil-platelet aggregate formation in SCD patient blood in vitro.

3.2 MATERIALS AND METHODS

3.2.1 Reagents

Recombinant human P-selectin (CD62P)-Fc chimera and recombinant human ICAM-1 (CD54)-Fc chimera were obtained from R&D Systems (Minneapolis, MN). Recombinant human CXCL8/interleukin-8 (IL-8) was obtained from Peprotech Inc. (Rocky Hill, NJ). Alexa Fluor 647 (AF647) conjugated mouse anti-human CD16 mAb (clone 3G8; IgG1κ), fluorescein isothiocyanate (FITC) conjugated mouse anti-human CD49b mAb (clone AK-7; IgG1κ), function blocking NA/LE mouse anti-human CD11b (Mac-1) mAb (clone ICFR44; IgG1κ), purified

NA/LE mouse IgG1κ isotype control (clone 107.3), Brilliant Violet 421 (BV421) mouse anti-human CD62P (P-selectin; clone AK-4), FITC mouse IgG1 κ (clone MOPC-21), phycoerythrin (PE) mouse IgG1 κ (clone MOPC-21), and purified mouse anti-human CD162 (PSGL-1; clone KPL-1) were purchased from BD Biosciences (San Jose, CA). Function blocking mouse anti-human CD62P (P-selectin) mAb (clone G1/G14; IgG1κ) was purchased from Ancell Corp. (Bayport, MN). Toll like receptor-4 (TLR4) inhibitor TAK242 (CLI-095) was purchased from InvivoGen (San Diego, CA) and solubilized in Intralipid (20% emulsion) purchased from Sigma-Aldrich (St. Louis, MO). Gram negative bacterial lipopolysaccharide (LPS) from *Escherichia coli 0111:B4* (*E. coli*) purchased from Sigma-Aldrich. Prostaglandin I2 (PGI2) was purchased from EMD Millipore (Billerica, MA). Cy3 conjugated AffiniPure donkey anti-mouse IgG (H+L) polyclonal (715-165-151**)** was purchased from Jackson Immuno Research Laboratories, Inc (West Grove, PA). Mouse anti-human CD42b mAb (GPIbα; clone VM16d) was purchased from Abcam (San Francisco, CA).

3.2.2 Blood Collection

Fresh blood samples were drawn from 24 non-crisis SCD (23 SS and 1 S/β0 thalassemia) and 8 healthy race-matched control (7AA and 1 AS) subjects at the Adult Sickle Cell Clinic of the University of Pittsburgh Medical Center (see Table 1 for clinical characterization of human subjects). Only nonsmokers who were not on chronic blood transfusion and hydroxyurea were included in this study. Blood was drawn via venipuncture using a 21G vacutainer push-button needle (BD Biosciences) into a 10-ml syringe containing 20U/mL heparin (Henry Schein). The blood-filled syringe was placed on a blood mixer to avoid clotting and used within 2 hours following blood draw. Blood (150 μl) was added to a Microvette 100 potassium EDTA tube

(Sarstedt) and analyzed with the Hemavet HV950 (Drew Scientific) for the assessment of hematocrit, hemoglobin, and blood cell counts in healthy control subjects.

3.2.3 qMFM imaging strategy

qMFM imaging strategy has been described in Chapter 2(60). AF647-conjugated CD16 and FITC-conjugated CD49b monoclonal antibodies were added to 500 μl blood (3:500 CD16 monoclonal antibody; 1:250 CD49b monoclonal antibody) in a 1-ml Eppendorf tube for in situ staining of neutrophils and platelets, respectively. Blood was perfused through a polydimethylsiloxane (PDMS/silicone)–based microfluidic device consisting of 4 identical micro-channels (30 μm high and 500 μm wide) at a physiological wall shear stress of 6 dyn/cm^2(27). A wall shear stress of 6 dyn/cm^2 is within the physiological range of the shear stress observed in arterioles and venules in vivo(27). The sides and roof of each micro-channel were made of silicone, while the bottom was made of glass and coated with a cocktail of recombinant human P-selectin–Fc (2 μg/ml), ICAM-1–Fc(10 μg/ml), and IL-8 (10 μg/ml). The preparation of the adhesive substrate and assembly of the microfluidic device (33, 60) have been described in the Appendix. Platelet-neutrophil interactions in blood-perfused microfluidic channels were visualized using qMFM, a 2-stage imaging strategy that was introduced in Chapter 2 (60). See Appendix A for further details on experimental setup, including coverslip preparation, imaging strategy and analysis.

3.2.4 Experimental design of qMFM studies.

Control and SCD human blood were perfused through microfluidic micro-channels, and footprints of arresting and crawling neutrophils were visualized using qMFM step 1 for 2 minutes. After 2

minutes, platelets nucleating on top of arrested neutrophils were visualized for another 2 minutes using qMFM step 2. The transition from qMFM step 1 to step 2 is shown in Figure 7.

3.2.5 Scanning Electron Microscopy

Blood was perfused through PDMS based microfluidic channels presenting P-selectin, ICAM-1, and IL-8. Neutrophils were allowed to roll, arrest and interact with freely flowing platelets prior to fixation under flow. Coverslips were stored in PBS until processing as described in section A1.9

Scanning Electron Microscopy. Scanning electron micrographs were pseudocolored using Adobe Photoshop as described in A1.10 SEM Pseudocoloring.

3.2.6 Structured Illumination Microscopy

Blood was perfused through PDMS based microfluidic channels presenting P-selectin, ICAM-1, and IL-8. Neutrophils were allowed to roll, arrest and interact with freely flowing platelets prior to fixation under flow. Coverslips were processed as described in the Appendix, see A1.11 Structured illumination microscopy. Brilliant Violet 421 conjugated anti-human CD62P monoclonal antibody or isotype control mouse IgG1κ was added to the blood and cells as a primary antibody. Coverslips were incubated for 45 minutes with Alexa Flour 647-phalloidin to stain for F-actin and a Cy3 conjugated donkey anti-mouse IgG (secondary) to enhance the signal of the anti-CD62P monoclonal antibody.

3.2.7 P-selectin/Mac-1 Ab blocking, GPIbα/PSGL-1 Ab blocking,

Healthy control subject and SCD patient blood was perfused in the microfluidic micro-channels for 2 min, which allowed neutrophils to roll, arrest firmly and then interact with circulating platelets. Once the neutrophils were firmly arrested, platelet-neutrophil interactions were recorded using qMFM for the next 2 min. After 2 min of qMFM observations, the flow was stopped momentarily and Anti-P-selectin, anti-GPIbα, anti-PSGL-1, and/or anti-Mac-1 antibodies (1:100 dilution) or isotype control IgG1 antibody (1:100 dilution) were added to the blood in the reservoir and allowed to flow for 2 minutes. The flow was resumed and the effect on platelet-neutrophil interactions was assessed over the next 2 min. See A1.6 Function Blocking Studies on Platelet-Neutrophil Interactions for more detailed description of experiments.

3.2.8 LPS treatment

Specific concentrations of LPS were added to AA and SCD patient blood following the addition of fluorescent antibodies, FITC conjugated to CD49b and AlexaFlour 647 conjugated to CD16 to stain for platelets and neutrophils, respectively. Blood was incubated with LPS for 10 minutes prior to perfusion through P-selectin, ICAM-1, and IL-8 coated microchannels. Interactions were quantified for total platelet-neutrophil interactions, platelet interactions per neutrophil and lifetime of platelet neutrophil interactions as described in Chapter 2. For more information on treatments refer to A1.7 LPS Treatments.

3.2.9 TLR4 inhibition qMFM studies.

Experiments testing the role of TLR-4 inhibition were done by adding TAK-242+intralipid (50 μg/mL) into the blood following the addition of fluorescent antibodies FITC conjugated to CD49b and AlexaFlour 647 conjugated to CD16 to stain for platelets and neutrophils, respectively and incubating for 5 min. After 5 min, LPS was added to the blood followed by incubation for 10 min at room temperature (22˚C) and perfusion through the micro-channels. To test the effects of the vehicle (intralipid) on platelet-neutrophil interactions, the vehicle was added at the same concentration and procedure as Tak242 studies.

3.2.10 Statistics

The mean number of platelet-neutrophil interactions, mean number of arresting neutrophils, and mean number of platelet-neutrophil interactions per neutrophil were compared between groups using the 2-tailed unpaired Student's t-test along with the Bonferroni correction when appropriate for multiple comparisons. Distributions of the lifetime of platelet-neutrophil interactions under different conditions were compared using the nonparametric Kruskal-Wallis H test. In the dot plots, error bars are presented as mean ± SEM. A P value of less than 0.05 was used to determine the statistical significance.

3.3 RESULTS

3.3.1 Neutrophil-platelet aggregation is higher in human SCD blood under flow.

Healthy control and SCD human blood was collected in heparin (20U/ml) and perfused at a physiological shear stress of 6 dyn/cm^2 (27) through microfluidic micro-channels presenting a combination of P-selectin, ICAM-1, and IL-8. Whole blood was analyzed for blood cell counts and can be seen in Table 1. qMFM was used to visualize neutrophil-platelet aggregation at the level of single cell-cell interactions (60). The magnitude of neutrophil-platelet aggregate formation was assessed based on the ability of free-flowing platelets to interact with arrested neutrophils, which was quantified using 3 parameters: total number of platelet-neutrophil interactions, number of platelets that interact per arrested neutrophil, and the lifetimes of individual interactions of platelets with arrested neutrophils over a 2-minute observation in a FOV of size of ~14,520 μm^2.

Table 1: Clinical Characterization of human Subjects. Data show mean (minimum; maximum; median) except for sex and genotypes. SCD, sickle cell disease; SS, sickle cell anemia; S/β^0, sickle/β^0 thalassemia; AS, sickle cell trait; AA, healthy control; % HbF, % fetal hemoglobin; %HbS, % sickle hemoglobin; NM, not measured. Table published in *Bennewitz MF. Jimenez, MA. et al. JCI Insight 2017.*

	Control	**SCD**
Male/Female	4/2	5/19
Hemoglobin (g/dL)	12.46 (11.2;14.4;12.1)	9.06 (6.6;11.2;9.3)
Hematocrit (%)	41.34 (25.2;50.6;41)	26.39 (18.3;32.6;26.9)
White Blood Cells (k/dL)	4.62 (2.5;8.68;4.43)	9.88 (3;15.72;11.05)
- **% Neutrophils**	NM	55.2 (1.7;77.2; 57.6)
- **Neutrophil Count (k/µL)**	NM	6.89 (1.7;28;6.3)
Platelets (k/µL)	222.06 (134;462;180.5)	328.69 (141;610;333.5)
%HbF	NM	13.95 (2.8;31.6;9.2)
%HbS	NM	58.32 (5.9; 80.9; 64.6)
Genotypes		
- SS	0/6	23/24
- S/β^0	0/6	1/24
- AS	1/6	0/24
- AA	5/6	0/24

When control or SCD human blood was perfused through micro-channels presenting P-selectin, ICAM-1, and IL-8, neutrophils were observed to roll, arrest, crawl, and interact with freely flowing platelets (Figure 12A&B). A snapshot of the same FOV at two different time points 2 minutes apart is shown for control and SCD human blood in Figure 12A&B, respectively. Comparison of Figure 12A with Figure 12B at the time point of 2 minutes reveals that platelet interactions with arrested neutrophils led to the formation of large neutrophil-platelet aggregates, which appeared to be more pronounced in SCD than control human blood. Neutrophil-platelet aggregates in SCD blood were fixed under flow and visualized using scanning electron microscopy (SEM). A pseudo-

colored scanning electron micrograph of SCD patient blood reveal the cellular components of large neutrophil-platelet aggregates (Figure 12C). The aggregates comprise of platelets (green) nucleated on arrested neutrophils (purple) while erythrocytes (pseudo-colored red) can be seen sequestered within these large neutrophil-platelet aggregates leading us to believe the onset of VOC in SCD patients follows the sequential steps of neutrophil rolling and arrest, capture of freely flowing platelets and the trapping of RBC within the aggregates.

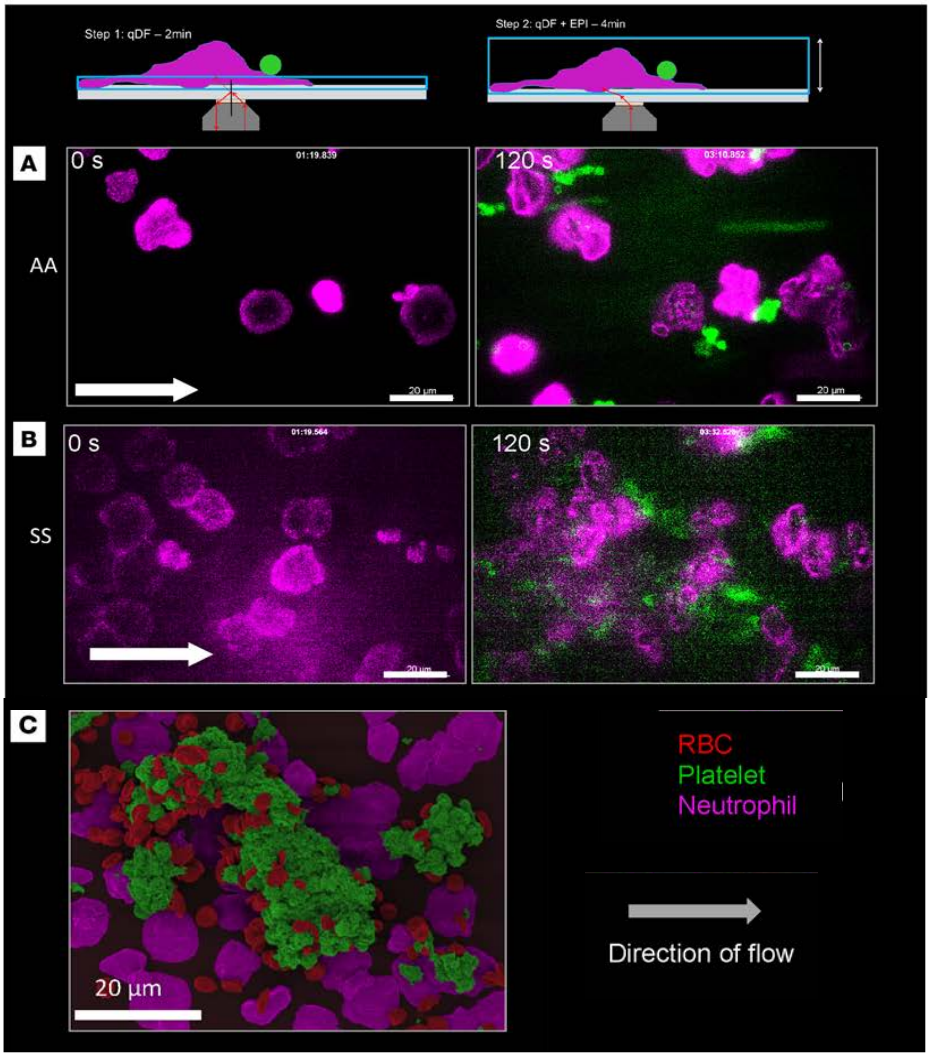

Figure 12: *qMFM reveals neutrophil-platelet aggregation is higher in Sickle Cell Disease (SCD) human blood.* qMFM images of the same FOV at 2 different time points (0 and 120 seconds) showing freely flowing platelets interacting with arrested neutrophils in (A) control and (B) SCD blood. (C) Pseudocolored micrograph of SCD patient blood that was fixed under flow and imaged using Scanning Electron Microscopy. platelets (green), neutrophils (purple), and Erythrocytes (red). Scale bars: 20 µm. Figure published in *Bennewitz MF. Jimenez, MA. et al. JCI Insight 2017*

Quantitative analysis of several time-series of qMFM images revealed that the total number of platelet-neutrophil interactions occurring per minute in a FOV were 2-fold higher in SCD than control human blood (Figure 13A). Similar to what we have reported previously (60), we found that the number of neutrophils arresting per minute in the same FOV was also 2-fold higher in

SCD than control human blood (Figure 13B). To test whether the significantly higher number of platelet-neutrophil interactions was a direct consequence of a higher number of arresting neutrophils, we estimated the number of platelet-neutrophil interactions per arrested neutrophil. As shown in Figure 13C, 1.5-fold more platelets were observed to interact per neutrophil over a 2-minute observation period in SCD compared with control human blood, thus excluding a major role of higher neutrophil numbers in driving increased platelet-neutrophil interactions. Interestingly, when we measured the lifetime of individual platelet-neutrophil interactions and plotted it as a cumulative probability distribution (Figure 13D), the lifetimes were significantly longer in SCD (median lifetime ~14 seconds) than control (median lifetime ~2 seconds), suggesting that neutrophil-platelet aggregate formation under flow is more efficient in SCD than control human blood. These in vitro qMFM studies suggest that neutrophil-platelet interactions were significantly more frequent and of longer duration in non-crisis SCD than control human blood flowing through micro-channels under vascular mimetic shear flow conditions.

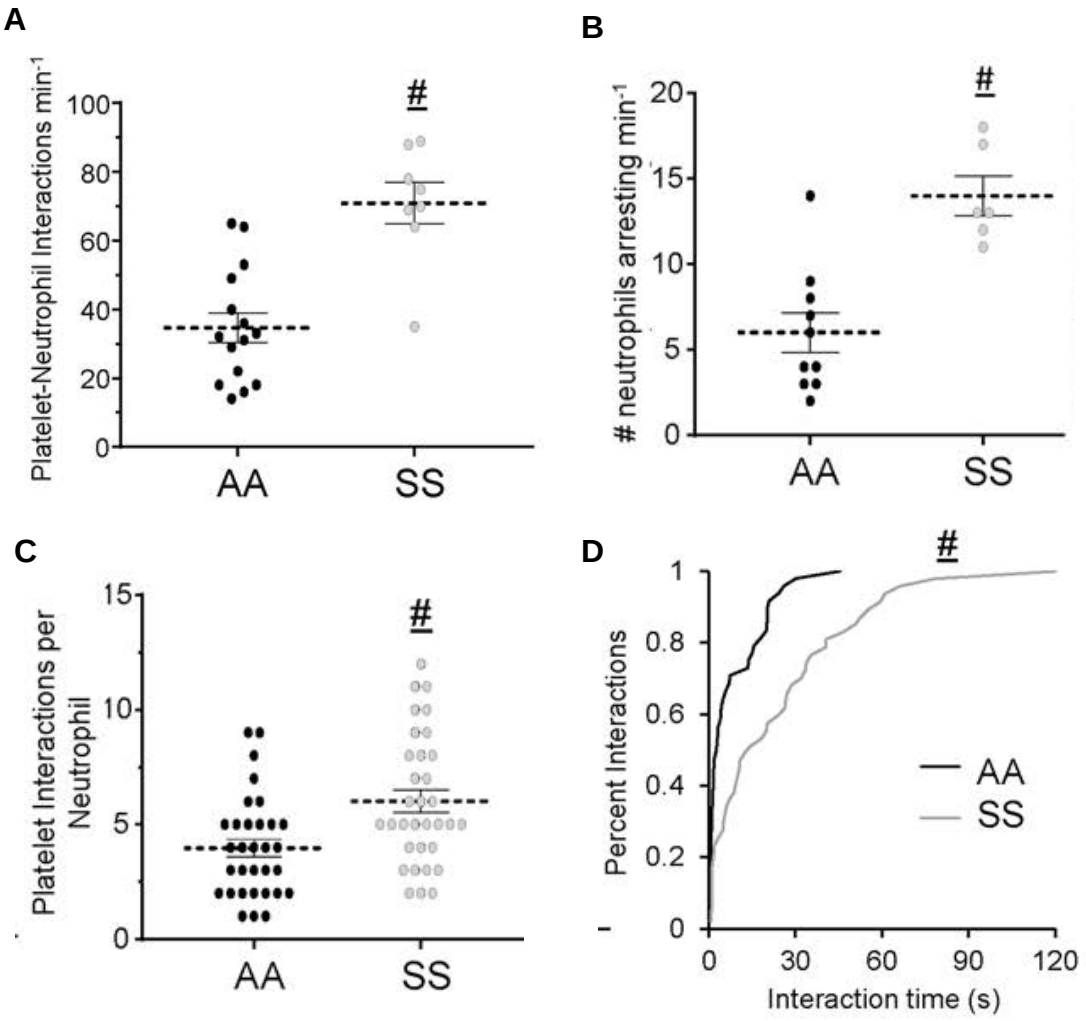

Figure 13: *SCD patients have enhanced platelet-neutrophil interactions.* Interactions were measured as (A) Total platelet-neutrophil interactions per minute (B) Total number of arrested neutrophils per minute (C) Platelet interactions per arrested neutrophil over a 2-minute observation period and (D) Lifetime of platelet-neutrophil interactions shown as a cumulative probability distribution in control and SS patient blood. A-B n= 6 experiments with 3 control and 3 SCD patients. C-D n= 8 experiments with 4 control and 4 SCD patients. Data in represent mean ± SEM; means were compared using Student's *t* test. Distributions in D were compared using the nonparametric Kruskal-Wallis *H* test. Each data point in A and B represents a single FOV. Each data point in C represents a single neutrophil. #$P < 0.05$ when comparing control to SCD. Wall shear stress 6 dyn/cm^2. FOV: ~14,520 μm^2 Figure published in *Bennewitz MF. Jimenez, MA. et al. JCI Insight 2017.*

3.3.2 Neutrophil-platelet aggregation in SCD human blood is platelet P-selectin and neutrophil Mac-1 dependent.

Platelet-neutrophil interactions are known to be primarily mediated by PSGL-1 and Mac-1 (CD11b-CD18) on neutrophils binding to P-selectin and GPIbα on platelets, respectively(23, 61). PSGL-1 is constitutively expressed on neutrophils, and Mac-1 has been shown to be activated in arrested neutrophils (53). Although, GPIbα is constitutively expressed on platelets (61), P-selectin is stored preformed in α-granules and translocated to the membrane for presentation only following activation by platelet agonists both in vivo and in vitro (23). To test whether P-selectin is present on human SCD platelets, neutrophil-platelet aggregates were fixed under flow, stained for P-selectin and F-actin, and subjected to super-resolution fluorescence 3D structured illumination microscopy (SIM). The SIM micrograph shown in Figure 14A reveals that platelets nucleated on top of arrested neutrophils in SCD human blood are positive for P-selectin (blue staining). It also revealed the presence of F-actin (purple) along the outer rim (lamellipodia) of the neutrophil and throughout the platelet membrane. To determine whether P-selectin expression on the surface of platelets in SCD blood facilitates their interaction with arrested neutrophils, qMFM studies were conducted in the presence of a function blocking anti–P-selectin antibody using an experimental approach that selectively blocks platelet P-selectin without compromising P-selectin dependent neutrophil rolling. Platelet P-selectin inhibition led to a significant drop in the ability of freely flowing platelets to nucleate on arrested neutrophils in SCD human blood (Figure 14B). As a next step, we tested the role of Mac-1–GPIbα interactions by conducting qMFM studies in the presence of an anti-Mac-1 function-blocking antibody using an approach that allowed blocking neutrophil Mac-1 without interfering with neutrophil arrest. As shown in Figure 14C, Mac-1 inhibition also led to a significant reduction in platelet-neutrophil interactions in both control and SCD blood.

Remarkably, a combination of P-selectin and Mac-1 function blocking antibodies led to a substantial drop in platelet-neutrophil interactions in both control and SCD human blood. As shown in Figure 14D, platelet-neutrophil interactions following treatment with anti–P-selectin/Mac-1 antibodies were identical in SCD and control human blood. This effect was not the result of an antibody-induced neutrophil detachment from the substrate, as there was no difference in the number of arrested neutrophils before and after anti–P-selectin/Mac-1 antibodies in either control or SCD human blood (Figure 14E). To establish that the anti–P-selectin/Mac-1 antibody induced reduction in total platelet-neutrophil interactions was a direct effect of the inability of individual platelets to bind to arrested neutrophils, we assessed the effect of anti–P-selectin/Mac-1 antibodies on the lifetime of individual platelet-neutrophil interactions (Figure 14F). As anticipated, the anti–P-selectin/Mac-1 antibody treatment reduced the lifetime of platelet-neutrophil interactions in SCD blood to the level observed in control blood, evidenced by the overlap in the lifetime distribution curves of control, control post–anti–P-selectin/Mac-1 antibodies, and SCD post–anti–P-selectin/Mac-1 antibodies (Figure 14F).

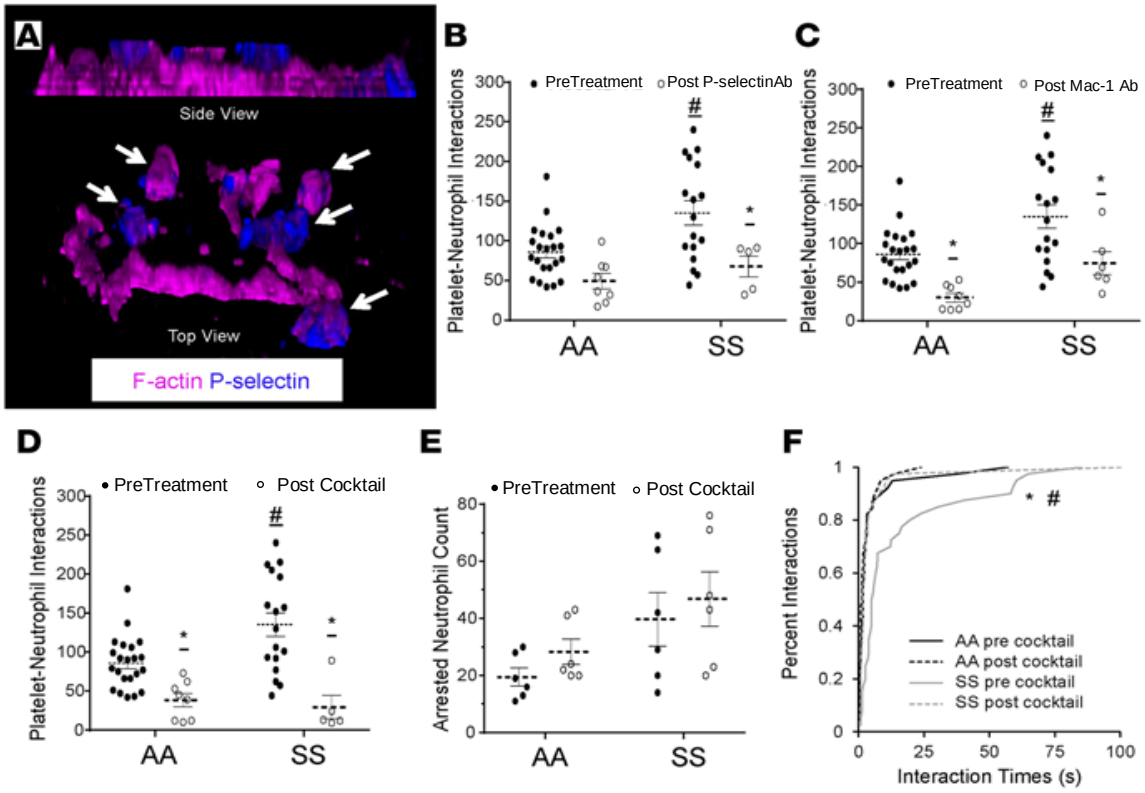

Figure 14: *Neutrophil-platelet aggregation in sickle cell disease (SCD) human blood is platelet P-selectin and neutrophil Mac-1 dependent.* (A) Structured illumination micrograph of platelets nucleated on an arrested neutrophil in SCD blood. F-actin (purple) P-selectin (blue). Platelets are marked with white arrows. (B) Effect of platelet P-selectin inhibition on total platelet interactions with arrested neutrophils. (C) Effect of Mac-1 inhibition on total platelet interactions with arrested neutrophils. Effect of simultaneous inhibition of platelet P-selectin and neutrophil Mac-1 on (D) total platelet interactions with arrested neutrophils, (E) total number of arrested neutrophils and (F) Effect on the lifetime of platelet-neutrophil interactions. B–D n=10 experiments with 4 control and 5 SCD patients; E and F n= 6 experiments with 3 control and 3 SCD patients. Data represent mean ± SEM. Means in B–E were compared using Student's t test with Bonferroni correction. Interaction times in F were compared using the nonparametric Kruskal-Wallis H test. #$p < 0.05$ when comparing control with SCD; * $p < 0.05$ when comparing pre- and post-Ab treatment. Wall shear stress: 6 dyn/cm^2. FOV: ~14,520 μm^2 Figure published in *Bennewitz MF. Jimenez, MA. et al. JCI Insight 2017.*

3.3.3 Low dose of LPS selectively augments neutrophil-platelet aggregation in SCD human blood.

Identical to the findings in SCD mice in vivo, qMFM revealed that pretreatment of SCD human blood with LPS at a concentration of 0.25 μg/ml selectively augmented platelet-neutrophil aggregation in SCD but not control human blood, suggesting that the SCD blood had a higher

sensitivity to LPS. As shown in Figure 15A, pretreatment with an LPS concentration of 0.25 μg/ml was potent enough to cause a significant increase in platelet-neutrophil interactions in SCD human blood. In contrast, LPS at a concentration of 0.25 μg/ml did not result in any increase in platelet-neutrophil interactions in control human blood, but rather a 4-fold higher concentration (1 μg/ml) of LPS was needed to induce a small but significant increase in the total number of platelet-neutrophil interactions in control human blood (Figure 15B). A comparison of platelet-neutrophil interactions in control and SCD blood before and after treatment with 0.25 μg/ml LPS suggests that a concentration of LPS that is ineffective in control blood effectively promulgates neutrophil-platelet aggregation in SCD blood. Pretreatment of SCD human blood with LPS at concentrations greater than 0.25 μg/ml resulted in blood aggregation, thus rendering the blood unfit for qMFM studies. To establish that the increase in neutrophil-platelet interactions in SCD blood following a low dose of LPS was a result of TLR-4 activation, we conducted a separate set of qMFM studies in the presence of a TLR-4 inhibitor. Figure 15C demonstrates that treatment with a TLR-4 antagonist, TAK-242 (50 μg/ml) led to a significant reduction in the number of platelet-neutrophil interactions in LPS-treated SCD blood. Following treatment with TAK-242, the platelet-neutrophil interactions in LPS-treated SCD blood were reduced to a level below that observed in control blood at baseline. The interactions were also slightly reduced following treatment with the vehicle, intralipid, used in the reconstitution of TAK-242 (Figure 15C). Overall, this reduction was small compared to the TAK-242 treatment, suggesting that the reduction in interactions observed following TAK-242 treatment was specific to TLR-4 inhibition (Figure 15C). TAK-242 had no significant effect on the number of arresting neutrophils (Figure 15D), suggesting that the TAK-242–induced reduction in platelet-neutrophil interactions was not a result of neutrophil

detachment, but rather a consequence of the inability of platelets to adhere to neutrophils under vascular mimetic flow.

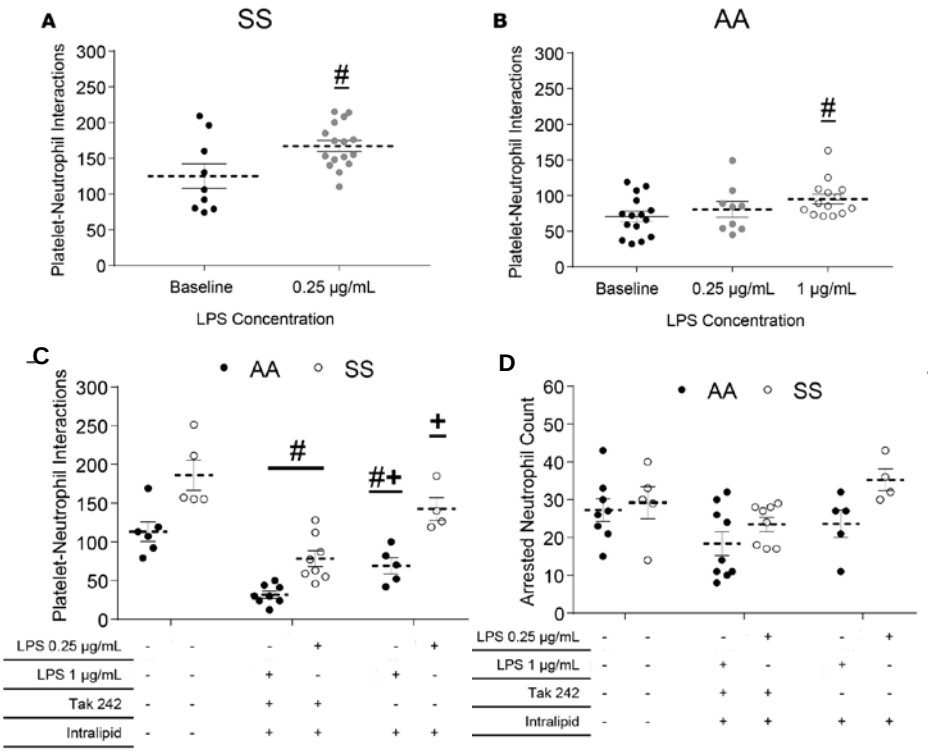

Figure 15: *LPS promotes neutrophil-platelet aggregation in sickle cell disease (SCD) human blood.* Total platelet interactions with arrested neutrophils in (A) SCD whole blood ± 0.25 µg/ml of LPS. n=6 (B) control human blood ± pretreatment with 0.25 and 1 µg/ml LPS. n= 6 with 5 control subjects. Effect of TAK-242 and/or intralipid (vehicle) pretreatment on **(C)** the total number of platelet-neutrophil interactions and **(D)** total number of arrested neutrophils over a 2-minute observation period in 0.25 or 1 µg/ml LPS– treated SCD and control human blood, respectively. N=6 experiments with 3 control and 3 SCD subjects. Data represent mean ± SEM. # p< 0.05 when comparing with baseline; +p< 0.05 when comparing with TAK-242. Means were compared using Student's t test with Bonferroni correction. Wall shear stress: 6 dyn/cm^2. FOV: ~14,520 µm^2. Figure published in *Bennewitz MF. Jimenez, MA. et al. JCI Insight 2017*

3.3.4 LPS-induced neutrophil-platelet aggregation is P-selectin and Mac-1 dependent.

Next, we tested whether simultaneous inhibition of platelet P-selectin and neutrophil Mac-1 ameliorates LPS-triggered platelet-neutrophil interactions in SCD human blood. Control and SCD human blood was preincubated with LPS at the respective potent concentrations of 1 and 0.25

μg/ml, and the efficacy of simultaneous inhibition of platelet P-selectin and neutrophil Mac-1 was determined using the experimental approach described in Chapter 2. Anti–P-selectin/Mac-1 antibodies significantly attenuated neutrophil-platelet aggregate nucleation in SCD blood, evidenced by the substantial reduction in total platelet-neutrophil interactions (Figure 16A) and platelet interactions per neutrophil (Figure 16B). As shown in Figure 16A&B, the platelet-neutrophil interactions after treatment with anti–P-selectin/Mac-1 antibodies were significantly lower and nearly identical in both 1 μg/ml LPS–treated control and 0.25 μg/ml LPS–treated SCD human blood. The reduction in platelet-neutrophil interactions seemed to be a direct effect of the inability of platelets to stay attached to arrested neutrophils under flow. Treatment with a control isotype IgG1 antibody did not inhibit LPS-induced neutrophil-platelet interactions (Figure 16C and D), suggesting that the reduction in interactions achieved after antibody treatment was specific to the inhibition of P-selectin–PSGL-1 and Mac-1–GPIbα binding between freely flowing platelets and arrested neutrophils.

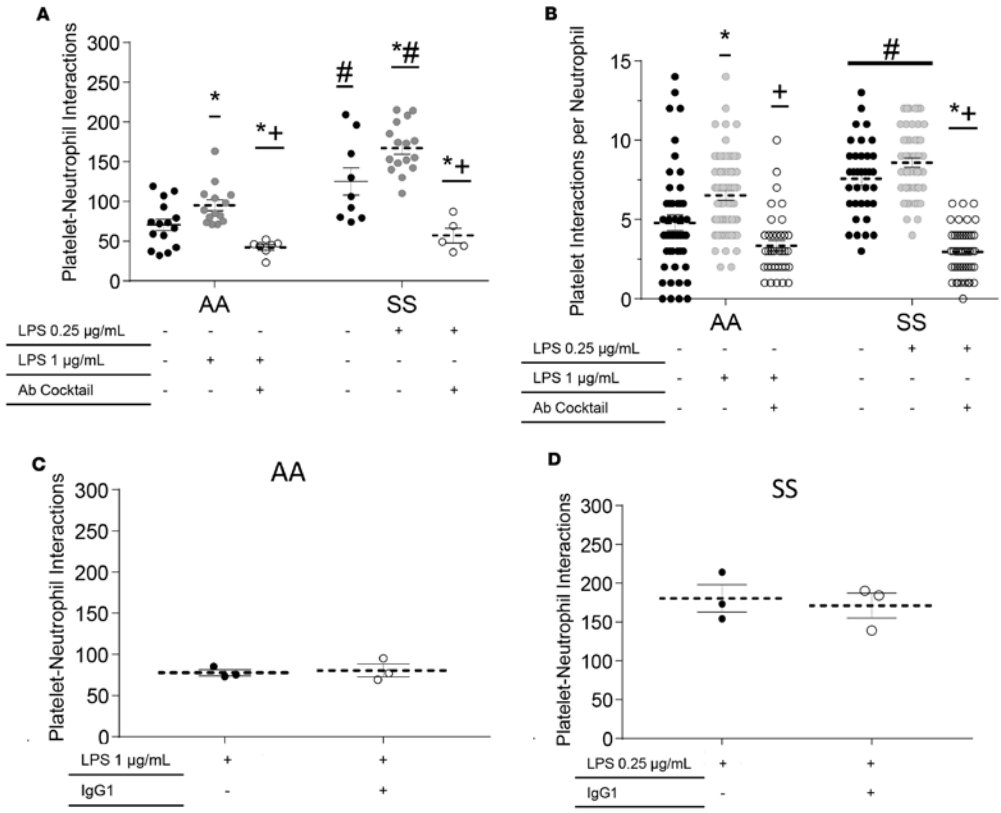

Figure 16: *LPS-induced neutrophil-platelet aggregation is P-selectin and Mac-1 dependent*. Effect of simultaneous inhibition of platelet P-selectin and neutrophil Mac-1 on (A) total platelet interactions with arrested neutrophils and (B) number of platelet interaction events per arrested neutrophil in control and SCD human blood ± pretreatment with LPS (1 and 0.25 µg/ml, respectively). N= 8 (4 control and 4 SCD subjects). * $p< 0.05$ when compared with baseline; # $p< 0.05$ when comparing control with SCD; + $p< 0.05$ when comparing LPS with Ab treatment. No effect of isotype IgG1 control Ab treatment on the total number of platelet-neutrophil interactions in **(C)** 1 µg/ml LPS–treated control and **(D)** 0.25 µg/ml LPS–treated SCD human blood. N= 5 (2 control and 3 SCD subjects). Data represent mean ± SEM. Means were compared using Student's t test with Bonferroni correction for multiple comparisons. Each data point represents a single FOV with multiple FOVs in per experiments. Wall shear stress: 6 dyn/cm^2. FOV: ~14,520 µm^2. Figure published in *Bennewitz MF. Jimenez, MA. et al. JCI Insight 2017.*

3.3.5 PSGL-1 and GPIbα blockade inhibits neutrophil-platelet interactions in LPS treated SCD human blood

Furthermore, anti-PSGL1 (CD162) and anti-GPIbα (CD42b) function-blocking antibodies significantly reduced both the total platelet-neutrophil interactions (Figure 17A & B) and the

number of platelet interactions per neutrophil (Figure 17C & D) in LPS-treated SCD human blood under flow.

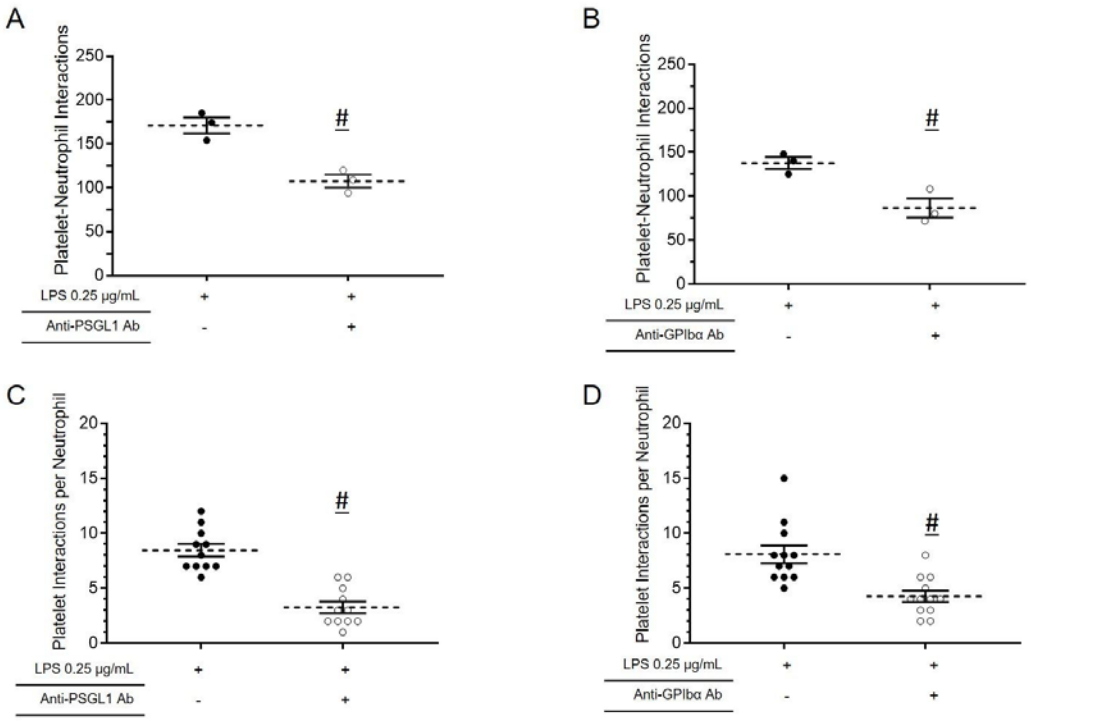

Figure 17: *PSGL-1 and GPIbα blockade inhibits platelet-neutrophil interactions in LPS treated SCD human blood.* Steady state SCD whole human blood was treated with 0.25 µg/ml of LPS and perfused through microfluidic channels with or without addition of blocking antibodies against PSGL-1 **(A, C)** and GPIbα **(B, D)**. Total platelet-neutrophil interactions and platelet interactions per neutrophil were observed over multiple FOVs. N=2 Data represents mean ± SEM. Each data point represents a single FOV and observations were made over multiple FOVs per experiment. Wall shear stress 6 dynes cm^{-2}. FOV (field of view) ~ 14,520 μm^2. # $p<0.05$ when compared to LPS treatment. Figure published in *Bennewitz MF. Jimenez, MA. et al. JCI Insight 2017.*

3.4 DISCUSSION

Epidemiological evidence suggests that systemic vaso-occlusive pain crisis in SCD is often a precursor to acute chest syndrome, a type of acute lung injury (5). The current treatment for acute chest syndrome is primarily supportive, and the molecular mechanism remains largely unknown.

In a recent autopsy study (62), pulmonary histopathology of acute chest syndrome patients revealed occlusion of the pulmonary vasculature with aggregates of platelets or erythrocytes, suggesting that the molecular events surrounding pulmonary vaso-occlusion contribute to lung injury. The study proposes that without specific therapy, typically exchange transfusion and antibiotics, these pulmonary vaso-occlusions can progress to the acute chest syndrome in SCD.

Recent intravital studies have shown that nucleation of platelets on adhered neutrophils during acute inflammation results in the formation of neutrophil-platelet aggregates in both the systemic (22, 23) and pulmonary microcirculation of WT mice (22, 24). Using a whole blood microfluidic in vitro approach (qMFM), it was demonstrated that neutrophil-platelet interactions under vascular mimetic flow conditions are significantly higher in steady-state SCD than control human blood. Similar to what was observed in SCD mice(1), neutrophil-platelet interactions were further augmented in SCD but not control human blood following pretreatment with a small concentration of LPS (0.25 μg/ml). Remarkably, the augmented neutrophil-platelet interactions in SCD human blood were completely attenuated by blocking the interaction of platelet P-selectin and GPIbα with neutrophil PSGL-1 and Mac-1, respectively. In fact, the simultaneous inhibition of platelet P-selectin and neutrophil Mac-1 was potent enough to reduce the magnitude of platelet-neutrophil interactions in SCD human blood to that observed in control human blood. These findings are consistent with several flow cytometry–based studies that have confirmed the presence of circulating preformed neutrophil-platelet aggregates in the blood of steady-state SCD patients (25, 26, 63). This data suggests that the inflammatory milieu in SCD promotes the formation of large neutrophil-platelet aggregates in response to an otherwise innocuous inflammatory stimulus. These aggregates serve to enable pulmonary vaso-occlusion by occluding the arteriolar bottlenecks in the lung(1). The disintegration or inhibition of neutrophil-platelet

aggregates by targeting P-selectin on platelets and Mac-1 on neutrophils leads to resolution of pulmonary vaso-occlusions.

Recent studies have identified a role for TLR4 activation in SCD (2, 64, 65). The mutation in the β-globin gene affects only hemoglobin in erythrocytes (5). Although, intraerythrocytic polymerization of hemoglobin S results in hemolysis and altered rheology, releasing red cell and tissue derived DAMPs and inciting ischemia-reperfusion events, both of which have been proposed to "prime" innate immune signaling pathways (2). A number of erythrocyte-derived DAMPs have been characterized, including hemoglobin, heme, ADP, and uric acid (2). Several recent studies using humanized SCD mice and blood samples from SCD patients have established that cell-free hemoglobin and heme released into the circulation during hemolysis serve to activate neutrophils, platelets, and the endothelium by scavenging NO and activating the TLR4 pathway, respectively (2, 64-67). In a recent study (68), the translocation of bacterial TLR4 ligands from the gut into the blood circulation was shown to promote neutrophil activation in SCD mice, suggesting that the activation of neutrophils by chronic hemolysis primes these cells to activate further when exposed to traces of TLR4 agonists. How hemolysis promotes hypersensitivity of neutrophils and platelets to TLR4 agonists is currently unknown and will be elucidated in future studies. While SCD patients as well as normal healthy humans can develop acute lung injury and pneumonia with severe injury or infection with highly pathogenic bacteria, SCD patients are exquisitely susceptible to acute lung injury when exposed to less severe triggers (59, 69-71).

3.5 CONCLUSION

Although SCD affects millions of people worldwide (72), hydroxyurea (HU) is the only FDA approved drug for the prophylactic treatment of SCD by preventing hemoglobin S polymerization with the induction of fetal hemoglobin expression (3). Despite the high efficacy of HU, disease activity and mortality remain high in patients taking HU, with the life expectancy of SCD patients in the United States still estimated to be 20 years less than that of individuals without the disease (3, 73). It is imperative to identify new treatments to prevent and better manage systemic vaso-occlusive pain crisis, to increase the quality of life for SCD patients(47). Based on this study's findings and the recent work of other investigators, targeting adhesion molecules on platelets and/or neutrophils to prevent or disintegrate neutrophil-platelet aggregates can be a promising therapy for SCD patients, particularly for the prevention of acute chest syndrome in high-risk patients presenting with systemic vaso-occlusive pain crisis. Interestingly, a pan-selectin inhibitor, rivipansel (GMI-1070), has been shown in phase II studies to reduce the time to resolution of systemic vaso-occlusive pain crisis and opioid administration in SCD patients (46). In a separate phase I study, intravenous immunoglobulin (IVIG) was shown to inhibit Mac-1 activation on neutrophils in SCD patient blood (48). An oral P-selectin inhibitor was also shown to improve microvascular blood flow in SCD patients (74), while SelG1, a humanized anti–P-selectin monoclonal antibody, is currently in phase II studies to prevent systemic vaso-occlusive pain crisis in SCD patients (75).

The study findings support testing such blockers in clinical trials and also highlights several key aspects that need to be addressed in designing future therapies to prevent systemic vaso-occlusive pain crisis. First, targeting P-selectin and Mac-1 to prevent neutrophil-platelet

aggregation can be effective in preventing pulmonary vaso-occlusion, suggesting that current agents in clinical trials may be appropriately targeting this pathogenesis. Second, a combination of P-selectin and Mac-1 blockers may be more effective than individual blockers in preventing systemic vaso-occlusive crisis in SCD patients. This also warrants the need for designing small molecule drugs that can simultaneously block both the P-selectin–PSGL-1 and GPIbα–Mac-1 interactions. Third, P-selectin and Mac-1 blockers could be most effective when given prophylactically rather than after vaso-occlusive crisis, or early after admission for vaso-occlusive crisis, perhaps in more severely affected patients with risk factors such as dropping hemoglobin and platelet levels (59, 70). Finally, global inhibition of P-selectin and/or Mac-1 could affect host defense, due to the inability of neutrophils to recruit to sites of inflammation. SCD patients experience leukocytosis even under a steady-state condition (18, 25, 76), and therefore, interference with neutrophil recruitment can cause an elevation in circulating neutrophils. With these potential risks in mind, the targeted delivery of P-selectin or Mac-1 blockers as payloads in liposomes or nanocarriers designed to recruit specifically to the site of vaso-occlusion may represent an alternative approach for targeting vaso-occlusive crisis and pulmonary vaso-occlusion.

4.0 GLYCOPROTEIN IBα INHIBITOR (CCP-224) PREVENTS NEUTROPHIL-PLATELET AGGREGATION IN SICKLE CELL DISEASE

Note: Results discussed in this chapter have been published as Jimenez MA, Novelli EM, Shaw GD, Sundd P. Glycoprotein Ibα inhibitor (CCP-224) prevents neutrophil-platelet aggregation in Sickle Cell Disease. Blood Advances. 2017 1(20), 1712-1716. https://doi.org/10.1182/bloodadvances.2017006742.

4.1 INTRODUCTION

Vaso-occlusion contributes to the onset of acute painful vaso-occlusive crisis (VOC), which is the primary reason for emergency medical care among SCD patients (5, 29). High platelet and leukocyte counts are risk factors for VOC(18) and neutrophil-platelet aggregates are significantly elevated at steady state in the blood circulation of SCD patients (25, 26). Neutrophil-platelet aggregation has also been shown to occur in TNF-α treated cremaster venules of transgenic SCD mice, which was enabled by neutrophil Mac-1 binding to GPIbα on platelets (23). Recently (1), intravital microscopy in transgenic SCD mice showed that large neutrophil-platelet aggregates occlude pulmonary arterioles to promote lung vaso-occlusion in SCD. In the same study (1), quantitative microfluidic fluorescence microscopy (qMFM), an *in vitro* microfluidic based approach (60) discussed in Chapter 2, revealed that the neutrophil-platelet aggregation under vascular mimetic flow was significantly higher in steady state SCD than race matched control human blood, and partially enabled by Mac-1 on neutrophils binding to GPIbα on platelets.

Platelet-neutrophil interactions in SCD human blood were significantly inhibited by function blocking antibodies (Abs) against Mac-1 or GPIbα (1). Taken together, these studies (1, 23, 25) suggest that Mac-1-GPIbα interactions also contribute to neutrophil-platelet aggregation in SCD and GPIbα antagonists can be therapeutically beneficial in preventing VOC. The Mac-1 binding site is situated within the leucine-rich COOH-terminal flanking region of GPIbα (residues 201-268) (77). This region includes a regulatory R-loop (residues 227 to 241), which is also the major binding site for the A1 domain of human von willebrand factor (VWF-A1) (78, 79). OS-1, a cyclic peptide (ACTERMALHNLCGG) has been shown to potently inhibit (K_D 0.74 nM) human platelet-VWF aggregation by stabilizing the R-loop of GPIbα in an alternative configuration that does not support key interactions with the human VWF-A1(78-80). However, OS-1is a selective inhibitor of human but not mouse GPIbα and therefore, it cannot be evaluated by intravital studies in transgenic SCD mice. This study uses qMFM to show that CCP-224, a PEGylated form of the OS-1 peptide, potently inhibits neutrophil-platelet aggregation in SCD human blood flowing through microfluidic channels *in vitro*.

4.2 MATERIALS AND METHODS

4.2.1 Reagents

Recombinant human P-selectin-Fc chimera (P-selectin) and recombinant human ICAM-1-Fc chimera (ICAM-1) were purchased from R&D Systems (Minneapolis, MN). Recombinant human CXCL8/interleukin-8 (IL-8) was purchased from Peprotech Inc. (Rocky Hill, NJ). Alexa Fluor-647 conjugated mouse anti-human CD16 mAb (clone 3G8, mouse IgG1) and FITC conjugated

mouse anti-human CD49b mAb (clone AK-7, mouse IgG1) were purchased from BD Biosciences (San Jose, CA).

4.2.2 Blood Collection and Handling

Blood was drawn via venipuncture in a 10-mL heparinized syringe (20 U/mL Heparin, Henry Schein, Melville, NY) using a 21G needle (BD Biosciences). Fluorescent antibodies against human CD16 (3:500; AlexaFlour 647) and CD49b (1:250; FITC) were added to 500 µl of blood in a 1 ml Eppendorf tube for *in situ* staining of neutrophils and platelets, respectively. Blood was placed on a blood mixer when not in use to reduce coagulation and used within 2 hours of blood draw.

4.2.3 Human Subjects

Blood samples were drawn from 3 non-crisis SCD and 3 control healthy human subjects at the Adult Sickle Cell Clinic of the University of Pittsburgh Medical Center (UPMC) in syringes as per the protocol approved by the University of Pittsburgh Institutional Review Board. All participants gave written informed consent in accordance to the Declaration of Helsinki. Only non-smokers, who did not undergo exchange transfusion within the last 60 days, and diagnosed with sickle cell anemia (SS) were included in the study. Additionally, only those SCD patients who were not experiencing an ongoing VOC were included in the study and referred as steady state patients. The clinical characterization of blood from the human subjects included in the study is shown in Table 2.

Table 2: Clinical Characterization of human subjects. Data represent clinical values based on blood draws. AA, healthy control; F, female; M, male; N, no; NM, not measured; Y, Yes. Table published in *Jimenez, MA. et al. Blood Advances 2017.*

	Control 1	Control 2	Control 3	SCD 1	SCD 2	SCD 3
F/M	M	F	F	F	F	M
Age, y	30	32	35	27	36	47
Hemoglobin, g/dL	13.8	13.2	14.4	8.8	7.1	9.1
Hematocrit, %	38.2	39	45	25.9	20.7	26.2
Neutrophils, %	NM	44.16	57.6	75.3	54.4	41
Neutrophils, $\times 10^9$/L	NM	7.22	4.16	3.9	5.7	2.8
Platelets, $\times 10^9$/L	227	194	104	310	271	394
Genotypes	AA	AA	AA	SS	SS	SS
Race	African American	African American	White	African American	African American	African American
Hydroxyurea	N	N	N	Y	N	Y

4.2.4 CCP-224 and Preparation

CCP-224, a cyclic PEGylated peptide ACTERMALHNLCGGK-Polyethylene glycol (PEG24) polymer with a disulfide bond between Cys2-Cys12 was provided by Quell Pharma Inc., Half Moon Bay, CA. CCP-224 is based on the OS-1 cyclic peptide (ACTERMALHNLCGG), which was derived from a cysteine-constrained phage display library(79, 80). The CCP-224 peptide was synthesized, cysteines were oxidized to form a disulfide bond and PEG polymer was then conjugated via amine chemistry to the unique lysine. CCP-224 was reconstituted in sterile PBS at a concentration of 2 mg/mL and stored at -80ºC. CCP-224 was added to 0.5 mL of blood to achieve a final concentration of 10 µg/mL.

4.2.5 Somatostatin Preparation

Somatostatin-14 (AGCKNFFWKTFTSC) a cyclic peptide with a disulfide bridge between Cys3-Cys14, purchased from AnaSpec Inc. was used as the control peptide. Somatostatin was reconstituted in sterile 1X PBS at a concentration of 2 mg/mL, and was then alloquated and stored at -80ºC until use. Somatostatin was then added to the blood at a concentration of 10 µg/mL.

4.2.6 Methods

Fluorescent antibodies against CD16 and CD49b were added to blood for *in situ* staining of neutrophils and platelets, respectively. Neutrophils were stained with Alexa Fluor 647 anti-human CD16 Ab (purple), and platelets were stained with fluorescein isothiocyanate (FITC) anti-human CD49b Ab (green). Blood was perfused through a polydimethylsiloxane (PDMS/silicone) based microfluidic flow channels with a glass bottom presenting a combination of recombinant human P-selectin, ICAM-1 and IL-8 at a physiological wall shear stress of 6 dyn cm^{-2}. Platelet-neutrophil interactions and aggregation were recorded for 2 min using Quantitative Microfluidic Fluorescence Microscopy (qMFM). The flow was stopped after 2 min of perfusion, VIGS-3 or control peptide (10 µg/mL) was added to the blood and the flow was resumed for another 2 min to assess the effect of VIGS-3 on neutrophil-platelet interactions. qMFM images were recorded by using a Nikon Eclipse Ti inverted microscope equipped with a Zyla-5.5 sCMOS scientific camera and CFI Apochromat TIRF 60× oil objective (numerical aperture: 1.49). All microscope functions and image analyses were conducted by using NIS-Elements software. Refer to Appendix for details on coverslip preparation, imaging and experimental design.

4.2.7 Statistics

Total number of neutrophil-platelet interactions and the number of arrested neutrophils pre- vs post CCP-224 or control peptide treatment were compared using a paired *t*-test. Platelet interactions per arrested neutrophil were compared using Students *t*-test. Lifetime of interactions were compared using the non-parametric Kruskal-Wallis *H*-test. A $p<0.05$ was used to determine significance. Data in Figure 19C and F represents mean ± SEM.

4.3 RESULTS

4.3.1 qMFM reveals the effects of CCP-224 treatment on platelet-neutrophil aggregation in SCD patient blood.

Non-crisis SCD and control human subject blood with or without the addition of CCP-224 or the control peptide was allowed to flow through *in vitro* microfluidic channels presenting a combination of P-selectin, ICAM-1 and IL-8, and neutrophil-platelet interactions were assessed using qMFM(60). Identical to our previous study findings(1, 60), neutrophils were observed to roll, arrest and capture freely flowing platelets leading to the formation of neutrophil-platelet aggregates. As shown in Figure 18A and B, fewer platelets were observed to nucleate on top of arrested neutrophils in the blood of SCD patient 1 (Fig. 18A) and patient 2 (Fig. 18B) following treatment with CCP-224 compared to control peptide treatment. Previously we have shown that the platelet-neutrophil aggregation in qMFM studies can be quantified based on three parameters total platelet-neutrophil interactions per field of view (FOV), total platelet-neutrophil interactions

per arrested neutrophil and the lifetime of platelet-neutrophil interactions(1, 60). These parameters were compared using a pre- and post-treatment paired-sample analyses over several independent experiments done with three control and three SCD subjects.

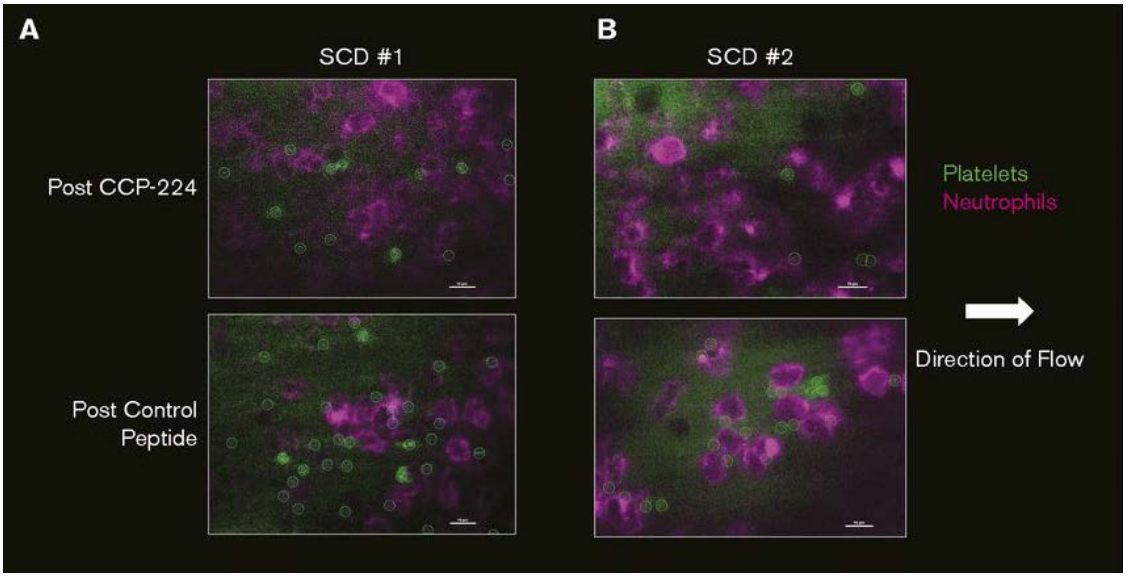

Figure 18: *qMFM allows visualization of CCP-224 inhibition on platelet-neutrophil aggregation in SCD patient blood.* Human blood was perfused through microfluidic channels presenting P-selectin, ICAM-1, and IL-8, and platelet-neutrophil interactions were assessed by using qMFM. qMFM images showing platelets (green circles) interacting with arrested neutrophils (purple) in the blood of SCD patient 1 (A) and patient 2 **(B)** following treatment with 10 µg/mL of CCP-224 (top row) and control peptide (bottom row). Borders of platelets are marked with green circles. The arrow indicates the direction of flow. Scale bars, 20 µm. Wall shear stress= 6 dyn/cm^2. Figure published in *Jimenez, MA. et al. Blood Advances 2017.*

4.3.2 CCP-224 inhibits platelet-neutrophil aggregation in SCD patient blood

Paired analysis revealed that CCP-224 (Fig. 19A) but not the control peptide (Fig. 19B) led to a significant reduction in the total number of platelet-neutrophil interactions in SCD patient blood. Identical to SCD patient blood, CCP-224 also significantly reduced the total number of platelet-neutrophil interactions in healthy control human blood (Fig. 19D). As shown in Figure 19E, control peptide had no effect on platelet-neutrophil interactions in control human subject blood. Treatment

with CCP-224 also led to a significant reduction in the number of platelet interactions per arrested neutrophil in both control (Fig. 19F) and SCD (Fig. 19C) human blood. Platelet-neutrophil aggregation mediated vaso-occlusion is dependent on the ability of platelets to attach to neutrophils under vascular mimetic flow. Assessment of individual interactions (Fig. 19I) revealed that CCP-224 led to a significant reduction in median lifetime (5 s pre vs. 1.7 s post CCP-224) of platelet-neutrophil interactions in SCD human blood. However, the number of arrested neutrophils was unaffected by CCP-224 in both control (Fig. 19G) and SCD (Fig. 19H) human blood, suggesting that the reduction in platelet-neutrophil interactions was not a consequence of neutrophil detachment from the substrate. The OS-1 peptide, which is the non-PEGylated version of CCP-224 is known to stabilize GPIbα in low affinity configuration(78-80). Thus the presence or lack of inhibition with CCP-224 or control peptide, respectively was not primarily caused by the presence or absence of PEG polymer in CCP-224 or the control peptide, respectively. Taken together, the data suggest that the GPIbα antagonist, CCP-224 is a potent inhibitor of neutrophil-platelet aggregation in SCD patient blood under vascular mimetic flow conditions.

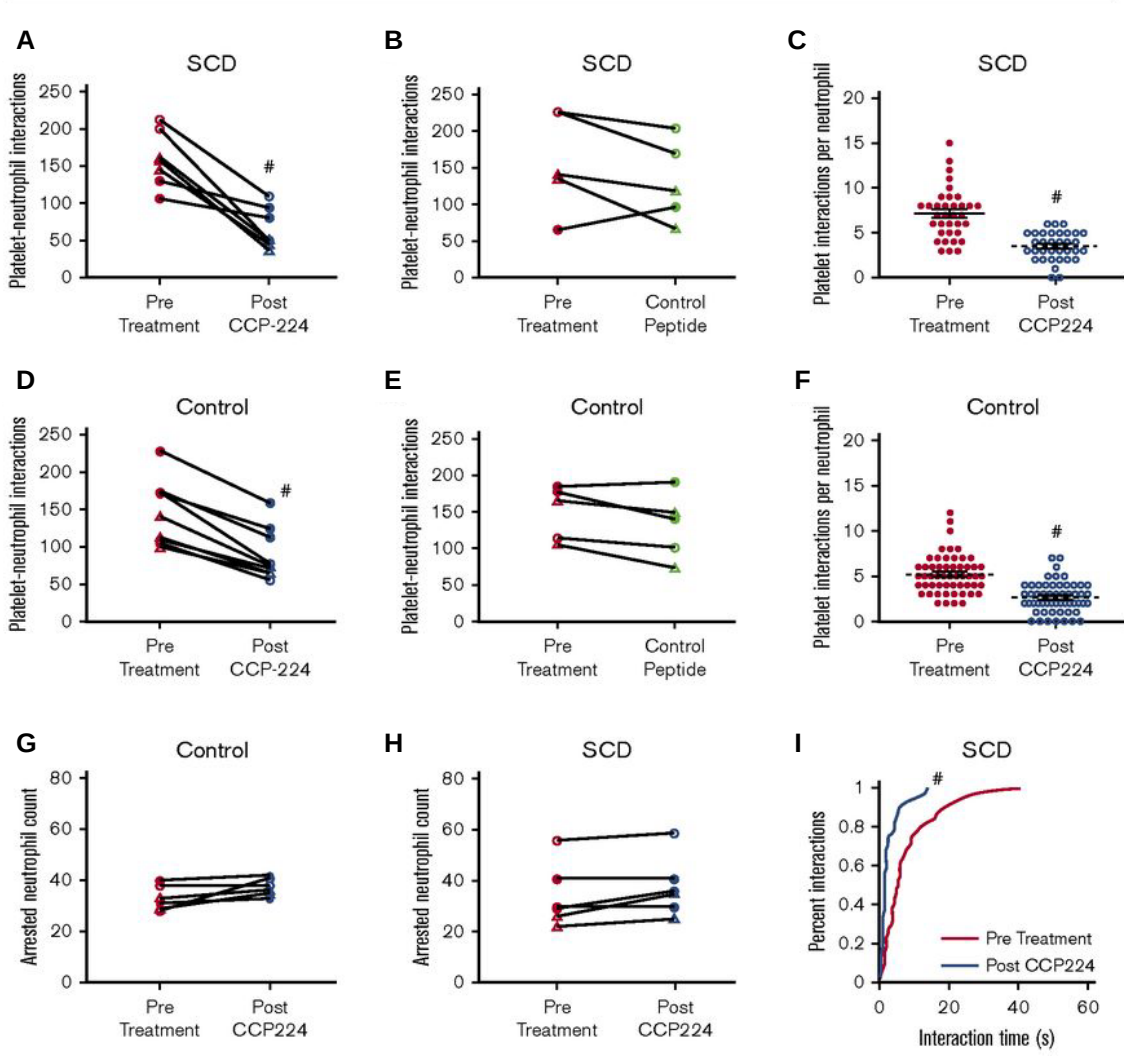

Figure 19: *CCP-224 inhibits platelet-neutrophil aggregation in SCD patient blood*. Pre- and post-treatment paired analyses showing the effect of (A) CCP-224 and (B) control peptide treatment on total platelet-neutrophil interactions and (C) effect of CCP-224 on platelet interactions per arrested neutrophil over a 2-minute observation period in SCD human subject blood. Pre- and post-treatment paired analyses showing the effect of (D) CCP-224 and (E) control peptide on control subject blood and (F) CCP-224 platelet interactions per arrested neutrophil over a 2-minute observation period in healthy control subjects. mean ± SE. (G-H) Paired analyses showing the effect of CCP-224 on the total number of arrested neutrophils in (G) healthy control and (H) SCD human blood. (I) Distribution of the lifetime of platelet-neutrophil interactions pre– and post–CCP-224 treatment in SCD human blood. A-B, D-E and G-H represent paired data from an individual experiment. Blood samples from 3 SCD and 3 control human subjects were used. Closed circles, open circles, and open triangles represent independent experiments performed with subject 1, 2, and 3, respectively in SCD and control subject blood. #p< .05 post- vs pretreatment. Figure published in *Jimenez, MA. et al. Blood Advances 2017.*

4.4 DISCUSSION

Recent studies have identified a role for P-selectin, E-selectin and Mac-1 in mediating vaso-occlusion in transgenic SCD mice *in vivo* (1, 23, 26, 53). These findings have inspired clinical trials designed to test the efficacy of P-selectin (42), E-selectin (46) and Mac-1 (48) blockers in reducing the frequency of VOC in SCD patients. Previous studies (1) and the current findings suggest that the platelet GPIbα is also a potential target for anti-adhesion therapy in SCD.

4.5 CONCLUSION

In a recent clinical trial (42), a P-selectin antibody led to a significant reduction in VOC among SCD patients. Based on the results of the study, a combination therapy using both P-selectin and GPIbα inhibitors could possibly be more potent than the individual inhibitors. CCP-224 also inhibits GPIbα binding to human VWF-A1 (77, 79) and therefore, may increase risk of bleeding complications. However, SCD is associated with elevated plasma levels of hyper-adhesive VWF, which is believed to promote microvascular thrombosis (81). Thus, CCP-224 might also prevent hemostatic complications in SCD by down regulating platelet activation by circulating VWF multimers. These *in vitro* findings support and suggest future clinical studies to test the safety and efficacy of CCP-224 in SCD patients.

5.0 PLATELET-TETHERS ENABLE PLATELET-NEUTROPHIL INTERACTIONS AND SHED IL1β CARRYING EXTRACELLULAR VESICLES TO PROMOTE LUNG VASO-OCCLUSION IN SICKLE CELL DISEASE

Note: The findings described in this chapter are under review in a major peer reviewed journal as: Jimenez MA†, Bennewitz MF†, Brzoska T, Tutuncuoglu E, Jonassaint J, Gutierrez E, Watkins SC, Shiva S, Neal MD, Kato GJ, Gladwin MT, Sundd P. Platelet-tethers enable platelet-neutrophil interactions and shed IL1β carrying extracellular vesicles to promote lung vaso-occlusion in Sickle Cell Disease.

5.1 INTRODUCTION

Sickle Cell Disease (SCD) is a monogenetic disorder that affects over three million people worldwide(5, 82). Sickle Cell Anemia, the most common form of SCD is caused by a homozygous mutation (SS) in the β-globin gene(5, 83). The mutant hemoglobin (HbS) polymerizes upon deoxygenation to form bundles leading to erythrocyte rigidity, dehydration, vaso-occlusion and premature hemolysis(5). Vaso-occlusion and hemolysis are the two dominant pathophysiological events in SCD(2). Intravascular entrapment of erythrocytes and inflammatory cells promote vaso-occlusion and development of acute systemic painful vaso-occlusive crisis, which is the primary reason for emergency medical care among SCD patients(5). Clinical evidence suggests that vaso-occlusive crisis can also progress to acute chest syndrome, a type of acute lung injury and a leading cause of mortality(5, 59, 84). Recently(1), we found that vaso-occlusive crisis in transgenic,

humanized SCD mice led to occlusion of pulmonary arterioles by P-selectin dependent platelet-neutrophil aggregates. Our finding was supported by recent histopathology study, which identified platelet aggregates occluding pulmonary arterioles in acute chest syndrome patients(62). Altogether, these findings suggest that vaso-occlusive crisis promotes pulmonary vaso-occlusion mediated by platelet-neutrophil aggregates in SCD, and the development of acute chest syndrome can be prevented provided targeted therapies to treat pulmonary vaso-occlusion are identified.

Hemolysis promotes an inflammatory milieu in SCD by releasing erythrocyte derived DAMPs(2) that scavenge nitric oxide (NO) and "prime" toll like receptor 4 (TLR4)-dependent innate immune signaling pathways in leukocytes, platelets and the vascular endothelium(85). We recently(1) found that nanogram levels of the TLR4 ligand, bacterial lipopolysaccharide (LPS), selectively promoted P-selectin dependent platelet-neutrophil aggregation in SCD but not in control human blood *in vitro*, and platelet-neutrophil aggregate mediated occlusion of pulmonary arterioles in SCD but not in control mice *in vivo*. These findings are also consistent with the clinical presentation in SCD patients who are susceptible to acute lung injury following exposure to less severe triggers than healthy humans(86). A recent study(68) demonstrated translocation of low levels of bacterial TLR4 ligands from the gut into the blood circulation promoted neutrophil activation and vaso-occlusion in SCD mice. Taken together, these findings suggest that the primed innate immune inflammatory pathways in SCD set a lower threshold for platelet-neutrophil aggregation following exposure to low levels of PAMPs such as TLR4 ligands. However, the innate immune mechanism that promotes such "priming" and catalyzes P-selectin dependent platelet-neutrophil aggregation in SCD remains largely unknown.

Here, we use *in vitro* quantitative microfluidic fluorescence microscopy (qMFM)(87) with SCD human blood to reveal that the inflammatory milieu in SCD promotes TLR4 dependent

activation of the NOD-like receptor family, pyrin domain containing 3 (NLRP3) inflammasome pathway in platelets. We found that the platelet NLRP3-inflammasome activation promotes the formation of P-selectin expressing hair-like membrane tethers and the shedding of interleukin-1β (IL-1β) carrying extracellular vesicles (EVs) by platelets in SCD. Hair-like tethers act like a 'lasso' that allows circulating platelets to interact more efficiently with stationary neutrophils within the vasculature. Platelet EVs activate platelets, neutrophils and other vascular cells in an IL-1β dependent manner to form large platelet-neutrophil aggregates that occlude pulmonary arterioles leading to loss of blood flow in the lung. This study determines a role for platelet tethers in promoting vaso-occlusion in SCD patients, while establishing a role for inflammasome activation in platelet tether formation.

5.2 METHODS

5.2.1 Reagents

Alexa Fluor 647 mouse anti-human CD16 mAb (Clone 3G8), Fluorescein Isothiocyanate (FITC) mouse anti-human CD49b mAb (clone AK-7), Brilliant Violet 421 mouse anti-human CD62P mAb (AK-4), FITC Mouse IgG1κ Isotype control Ab (MOPC21) and Brilliant Violet 421 mouse IgG1κ Isotype control Ab (X40) were purchased from BD Biosciences (San Jose, CA). Gram negative bacterial lipopolysaccharide (LPS) from *Escherichia coli 0111:B4* (*E. coli*) and Bovine Serum Albumin were purchased from Sigma-Aldrich (St. Louis, MO). Tak242 (CLI-095, TLR4 inhibitor) was purchased from InvivoGen (San Diego, CA) and solubilized in Intralipid (20% emulsion) which was purchased from Sigma Aldrich. Recombinant human IL-8 (CXCL8) was

purchased from PeproTech, Inc. (Rocky Hill, NJ). Prostaglandin I2 (PGI2) and cell permeable Caspase-1 Inhibitor-I (YVAD-CHO) were purchased from EMD Millipore (Billerica, MA). Recombinant human P-selectin (CD62P) Fc chimera, and recombinant human ICAM-1 (CD54) Fc chimera were purchased from R&D Systems (Minneapolis, MN). HRP conjugated anti-rabbit IgG1 Ab, HRP conjugated anti-mouse IgG1 Ab, anti-human caspase-1 Ab (rabbit IgG) and anti-human β-actin Ab (rabbit IgG) were purchased from Cell Signaling Technology (Danvers, MA). Erythrocyte lysis buffer was purchased from eBioscience (Santa Clara, CA). Mitotempo was purchased from Enzo Life Sciences (Farmingdale, NY). DC Protein Assay Reagent A, B, and S were purchased from BioRad (Hercules,CA). Bolt LDS sample buffer (4X), Bolt MES SDS running buffer (20x), Bolt transfer buffer (20x), Bolt 4-12% Bis-Tris plus gel, nitrocellulose membrane filter paper sandwich, Novex sharp pre-stained protein standard, iBind Flex solution kit, iBind flex cards, and cy3-conjugated-phalloidin were purchased from Life Technologies (Carlsbad, CA). Hyblot CL autoradiography film was purchased from Denville Scientific, Inc (Holliston, MA). Goat serum, Goat anti-rabbit Cy3 IgG, Goat anti-rabbit Cy5 IgG, Goat anti-mouse Cy3 IgG, and Goat anti-mouse Cy5 IgG were purchased from Jackson Immuno Research Laboratory Inc. (Westgrove, PA). FITC-conjugated anti-human PSGL1 mAb (clone PL2; mouse IgG_1) was purchased from Santa Cruz Technology (Dallas, TX). Mouse anti-human NLRP3/NALP3 mAb (clone Cryo-2; mouse IgG2b) and rabbit anti-human ASC polyclonal Ab (clone AL177) were purchased from AdipoGen Life Science (San Diego, CA). Phosphate buffer saline (without Ca^{2+} and Mg^{2+}) and Super Signal West Pico chemiluminescent substrate were purchased from ThermoFisher Scientific (Rockford IL). Human CD45 depletion kit was purchased from Stem Cell Technologies (Cambridge MA). Biotinylated mouse anti human CD42b mAb (Clone AK2, IgG1) was purchased from BIO-RAD (Hercules, CA).

5.2.2 Blood collection

Healthy race matched control human subjects and non-crisis SCD (SS or S/βº) patient blood was collected via venipuncture in a heparin containing syringe or CPT glass BD Vacutainer tube containing sodium citrate (BD Biosciences, Franklin Lakes, NJ) in accordance with the guidelines set by the Institutional Review Board at the University of Pittsburgh. The procedure for blood draw has been described elsewhere in detail (1). Only non-smokers who were not on chronic transfusion therapy (no transfusion within the last 1 month) were included in the study. Informed written consent was obtained from all the participants in accordance with the Declaration of Helsinki. All blood samples were used within 2 hours of blood draw.

Table 3: Clinical characterization of human subjects. Data shows mean (median; minimum; maximum) except for the gender, genotype and hydroxyurea status. AA, healthy control; AS sickle cell trait; SS, Sickle cell anemia, S/β^0, sickle β^0 thalassemia; %HbF, % fetal hemoglobin; %HbS, % sickle hemoglobin; NM, not measured.

	CONTROL	**SCD**
Female/Male	5/2	9/9
Age	34 (32, 29, 45)	36.7 (32.5;25; 62)
Hemoglobin (g/dL)	13.99 (13.9; 10.3; 16.7)	8.69 (9.2; 5.8; 12.8)
Hematocrit (%)	42.79 (43; 35.7; 49.1)	25.78 (26.4; 17; 37.6)
White Blood Cells (K/µL)	5.44 (5.72; 3.5; 7.28)	10.14 (7.8; 3.9; 27.6)
% Neutrophils	46.5 (49.6; 26.3; 61.5)	51.63 (50.6; 29; 75.3)
Neutrophil Count (K/µL)	2.51 (2.15; 1.47; 3.61)	5.49 (3.9; 1.7; 19.87)
Platelets (K/µL)	160 (153; 110; 243)	329.68 (309; 122; 622)
% HbS	NM	60.98 (60.8; 8.6; 80)
% HbF	NM	17.69 (20; 2.5; 35)
Genotypes		
- AA	6	0
- AS	1	0
- SS	0	15
- S/β^0	0	3
Hydroxyurea (Y/N)	NA	12/6

5.2.3 Quantitative microfluidic fluorescence microscopy (qMFM)

qMFM experimental design, sample preparation and setup has been described in Chapter 2-4 and Appendix A (1, 87, 88). Heparinized whole blood (500µL) from human subjects was transferred into a 1.5 mL Eppendorf (Fisher Scientific) and fluorescent antibodies (Abs) against

CD16 (Alexa Flour 647; 3:500 dilution) and CD49 (FITC; 1:250 dilution) were added to the blood for *in situ* staining of neutrophils and platelets, respectively. Glass coverslips were coated with recombinant human P-selectin (2 µg/mL), ICAM-1 (10 µg/mL) and IL-8 (10 µg/mL) (The following methods are used in the Sundd lab to conduct experiments and analysis. A1.1 Preparation of adhesion molecule presenting substrates for more detailed protocol), and assembled into a polydimethylsiloxane (PDMS) based microfluidic flow chamber with multiple flow channels (500 µm wide x 30 µm high) as described in A1.2 Microfluidic Flow Assay Setup (1, 60). Following the incubation time, blood was perfused through the microfluidic flow channels presenting a combination of P-selectin, ICAM-1 and IL-8, at a physiological(27, 89) wall shear stress of 6 dynes cm-^{2}. Neutrophil-platelet interactions were visualized in several field of views (FOV ~ 14,520 µm^{2}) using qMFM and time series of images were analyzed offline using Nikon NIS-Elements software as described elsewhere (1, 87). As described recently (1, 87, 88), platelet-neutrophil aggregation in microfluidic flow-channels was quantified and compared between treatments using the following three parameters: total platelet-neutrophil interactions per FOV over a 2-minute observation period, total platelet interactions per arrested neutrophil over a 2 minute observation period, and lifetime of individual platelet-neutrophil interactions. See Appendix A1.5 qMFM Data analysis Guidelines, A1.8 Microscope Set up for further details on analysis and microscope setup.

5.2.4 LPS Treatments and Inhibition Studies

In experiments involving LPS treatment, LPS was added to the blood to achieve the desired concentration following the addition of fluorescent antibodies and incubated for 10 minutes at room temperature on a blood mixer. In inhibition studies, fluorescent antibodies were added to the

blood then the inhibitors or antagonists [TAK242 (50 μg/mL), Mitotempo (50 μM) and YVAD-CHO (200μM)] were added 5 minutes prior to the addition of LPS. Blood was then incubated for another 10 minutes prior to perfusion through the PDMS microchannels. In baseline studies done without LPS pretreatment, antagonists or inhibitors were added to the blood following addition of fluorescent Abs, and the blood was incubated for 10 minutes on a blood mixer at room temperature. For more detailed procedures see Appendix A1.6 Function Blocking Studies on Platelet-Neutrophil Interactions and A1.7 LPS Treatments.

5.2.5 Isolation and western blot analysis of human platelets

Blood samples from control and SCD human subjects were drawn in BD CPT Vacutainers containing sodium citrate and centrifuged at 1500g (22ºC) for 10 min. Platelet rich plasma (PRP) was separated, treated with 1 μg/mL Prostaglandin I_2 (PGI_2) to prevent coagulation and incubated with 0.25 μg/ml LPS for 30 min. Samples were then centrifuged at 1500g (22ºC) for 10 min. Platelet poor plasma (PPP) was removed and the platelet pellet was suspended in the recommended buffer for the CD45 depletion kit [1X PBS (-Mg^{2+}, -Ca^{2+}), 2% fetal bovine serum, 1 mM EDTA and 1 μg/mL PGI_2]. Any contaminating leukocytes (CD45+ cells) were removed using human CD45 depletion kit. The purified platelet suspension was centrifuged at 1500g (22ºC) for 5 min and the platelet pellet was resuspended in erythrocyte lysis buffer + 1 μg/mL PGI_2 to remove any contamination from RBC. After a 5 min incubation in lysis buffer, the suspension was centrifuged at 1500g (22ºC) for 5 min, the supernatant was discarded and platelets were resuspended in platelet buffer (20 mM Hepes, 128 mM NaCl, 12 mM bicarbonate, 0.4 mM Na_2PO_2, 5 mM Glucose, 1 mM $MgCl_2$, 2.8 mM KCl, pH 7.4). Platelet suspension was stored at -80ºC until use. Prior to western blot assay, platelet samples were thawed and sonicated to lyse platelets. Protein

concentrations in platelet lysates were measured using BioRad DC Protein Assay. Samples were prepared with 50 µg protein (per well) in Bolt SDS Sample Buffer (4X) and deionized water, to maintain equal sample volume, and heated at 70ºC for 10 minutes. Samples and the Novex Sharp Pre-Stained Protein Standard were loaded into a 12 well Bolt 4-12% Bis-Tris Plus gel and ran in Bolt MES SDS Running Buffer at 200V in an Invitrogen Mini Gel Tank. Proteins were transferred onto a nitrocellulose membrane for 1 hour (10 V) at room temperature. Primary (Rabbit IgG – Caspase-1, β Actin, ASC; Mouse IgG - NLRP3; 1:1000 dilution) and secondary (HRP anti-rabbit IgG, HRP anti-mouse; 1:400) antibody staining and washing were done using the Invitrogen iBind Flex (Thermo Fisher) for 2-3 hours at room temperature. Membranes were washed for 2 minutes in deionized water and protein bands were detected using Super Signal West Pico Chemiluminescent Substrate for 5 minutes. Films were developed using Konica SRX-101A and analyzed using ImageJ.

5.2.6 Scanning electron microscopy of platelet-neutrophil aggregates

Control or SCD human blood with or without treatment with LPS and/or inhibitors was perfused through microfluidic flow channels presenting a combination of P-selectin, ICAM-1 and IL-8 at a shear stress of 6 dyn cm^{-2}. Neutrophils were allowed to arrest and interact with freely flowing platelets for 3 min. After 3 min, the fixative cocktail (4% paraformaldehyde and 2.5% glutaraldehyde) was added to the inlet reservoir and platelet-neutrophil aggregates were fixed under flow by perfusing the fixative through the microfluidic channels. Coverslips were then detached and stored in PBS until processing. Scanning electron microscopy of platelet-neutrophil aggregates was conducted using the strategy described in Appendix A1.9 Scanning Electron Microscopy(1, 87). A minimum of 10 micrographs per treatment group were analyzed using

Adobe Photoshop to estimate the percent platelets with a round or hairy appearance and the cumulative probability distribution of the length of hairy structures was plotted.

5.2.7 Structured illumination microscopy

Control and SCD human blood with or without LPS treatment was perfused through microfluidic flow channels presenting a combination of P-selectin, ICAM-1 and IL-8 at a shear stress of 6 dyn cm^{-2}. Platelet-neutrophil aggregates were fixed under flow, stained for P-selectin and F-actin using BV421 P-selectin Ab and Cy3 phalloidin, respectively, and visualized using super resolution Nikon 3D-Structured Illumination Microscopy (SIM) as in Appendix A1.11 Structured illumination microscopy (1).

5.2.8 Confocal microscopy

Analysis of P-selectin and PSGL-1 expression. Control and SCD human blood, with or without treatment with LPS, was perfused through microfluidic flow channels presenting a combination of P-selectin, ICAM-1 and IL-8 at a shear stress of 6 dyn cm^{-2}. Neutrophil-platelet aggregates were fixed under flow, coverslips were detached and stored in PBS for staining and confocal imaging. The following primary Abs were used for visualizing P-selectin and PSGL-1: BV421 mouse anti-human CD62P Ab (clone AK4) and FITC mouse anti-human PSGL-1 Ab (clone PL2).

NLRP3 and ASC colocalization analysis. SCD and control human blood was collected in BD CPT Vacutainers containing sodium citrate and centrifuged at 1500g (22ºC) for 10 min. PRP was removed and treated with 0.25 µg/mL LPS for 30 minutes. Platelets in PRP were allowed to attach

to glass slides for 1 hour, washed with PBS and then fixed using a fixative cocktail (4% paraformaldehyde and 2.5% glutaraldehyde) for 10 min. Slides were washed to remove excess fixative and stored in PBS for staining and confocal imaging. The following primary Abs were used for NLRP3 and ASC colocalization: mouse anti-human NLRP3 mAb (clone Cryo-2) and rabbit anti-human ASC polyclonal Ab (clone AL177). The following secondary Abs were used: Cy3 conjugated goat anti-rabbit IgG for ASC and Cy5-conjugated goat anti-mouse IgG for NLRP3.

Processing of coverslips for confocal microscopy.. Samples were imaged using Nikon A1R Spectral laser confocal microscope. For further details on coverslip processing see Appendix A1.12 Confocal Microscopy Coverslip .

5.2.9 Strategy for Colocalization Analysis

Two regions of interest (ROI) were selected on each cell included in the analysis to quantify the colocalization of NLRP3 (red) with ASC (green). As a reference, the cell from Figure 24B of a 0.25 μg/ml LPS treated SCD patient platelet is used in this figure. Using Nikon Elements Analysis software, the colocalization function was run on each individual ROI and (B) the intensity of each channel (red and green) were plotted in a graph to calculate the value of Pearson's coefficient. For the analysis shown in Figure 24C, Pearson's coefficient was used to determine the amount of colocalization per cell. Three cells per condition were selected for the analysis with 2 ROI per cell. Data represents the mean of Pearson's coefficient for all cells per condition.

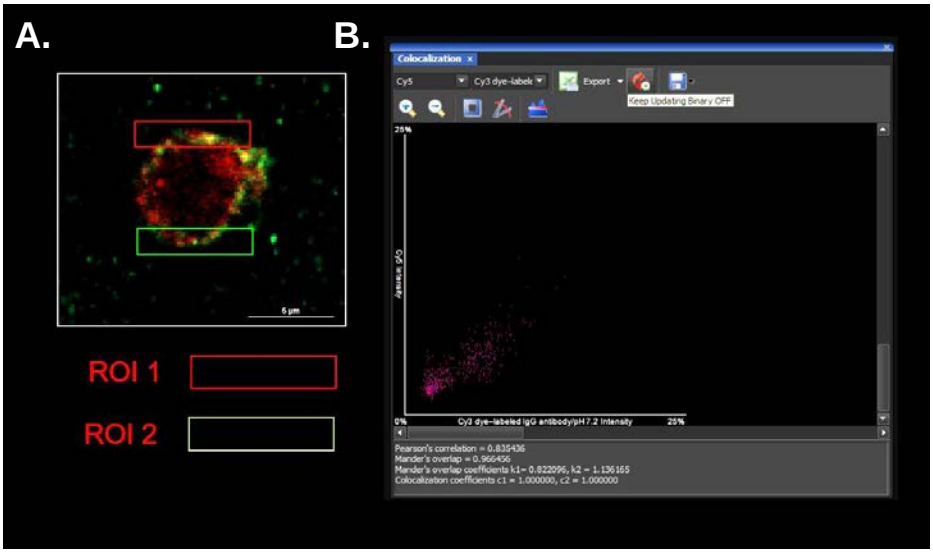

Figure 20: *Strategy for NLRP3 and ASC colocalization analysis.* **(A)** Two regions of interest (ROI) were selected on each cell included in the analysis to quantify the colocalization of NLRP3 (red) with ASC (green). Using Nikon Elements Analysis software, the colocalization function was run on each individual ROI and (B) the intensity of each channel (red and green) were plotted in a graph to calculate the value of Pearson's coefficient.

5.2.10 Statistics

The total platelet-neutrophil interactions, platelet interactions per neutrophil, and Pearson's coefficient for colocalization were compared between groups using the unpaired Student's *t* test with Bonferroni correction when needed. The percent of platelets with a round or hairy appearances were compared between groups using four-fold table analysis with Bonferroni χ^2 statistics. The lifetime of platelet-neutrophil interactions and the length of hairy tethers were compared using the Kruskal Wallis *H*-test. Error bars shown represent mean ± SE. A *p* value less than 0.05 was considered as significant.

5.3 RESULTS

5.3.1 Platelets expressing hair-like membrane tethers promote platelet-neutrophil aggregation in SCD

Race-matched control and SCD human blood were perfused at a physiological shear stress of 6 dyn cm^{-2} (0.6 Pa) (27, 89) through *in vitro* microfluidic flow-channels presenting a combination of P-selectin, ICAM-1 and IL-8, and individual platelet-neutrophil interactions were visualized at high resolution using qMFM. Refer to Table 3 for the clinical characterization of human subjects blood. Similar to what we have reported previously(1), platelet-neutrophil interactions were significantly more numerous and longer in duration in SCD than control human blood. Surprisingly, qMFM revealed for the first time that the platelet-neutrophil interactions in SCD human blood were enabled by hair-like tethers present on the surface of platelets (Figure 21A). Figure 21A shows a freely flowing platelet (green) approaching an arrested neutrophil (purple) in SCD human blood at t = 1 s. As the platelet flows over the arrested neutrophil, it attaches to the neutrophil via a hair-like tether (green; t = 3 to 8 s). The green fluorescence in the hair-like tether indicates the expression of the cell surface marker of platelets (green) but not neutrophils (purple) suggesting that the tether is platelet (green) but not neutrophil (purple) derived. To further validate this finding, platelet-neutrophil aggregates in SCD and control human blood were fixed under flow in microfluidic flow-channels and visualized at high resolution using scanning electron microscopy. Scanning electron micrographs revealed that platelets in SCD human blood (Figure 21B) were indeed ‘hairy’ in appearance, whereas platelets in control human blood were ‘round’ (Figure 21C). As shown in Figure 21B, the ‘hairy’ platelets in SCD human blood were attached to arrested neutrophils through tethers originating from their surface. Quantitative analysis of

scanning electron micrographs (Figure 21D) revealed that platelets were primarily round (~70%) in control but hairy (~80%) in SCD human blood. A small number (~30%) of control human platelets were also observed to have tethers, however, these tethers were significantly shorter than those in SCD human blood (Figure 21E). These findings are the first to identify that platelets in SCD human blood are ‘hairy’ due to the presence of hair-like membrane tethers on their surface, and these tethers enable SCD platelets to interact more efficiently with neutrophils to promote platelet-neutrophil aggregation *in vitro*.

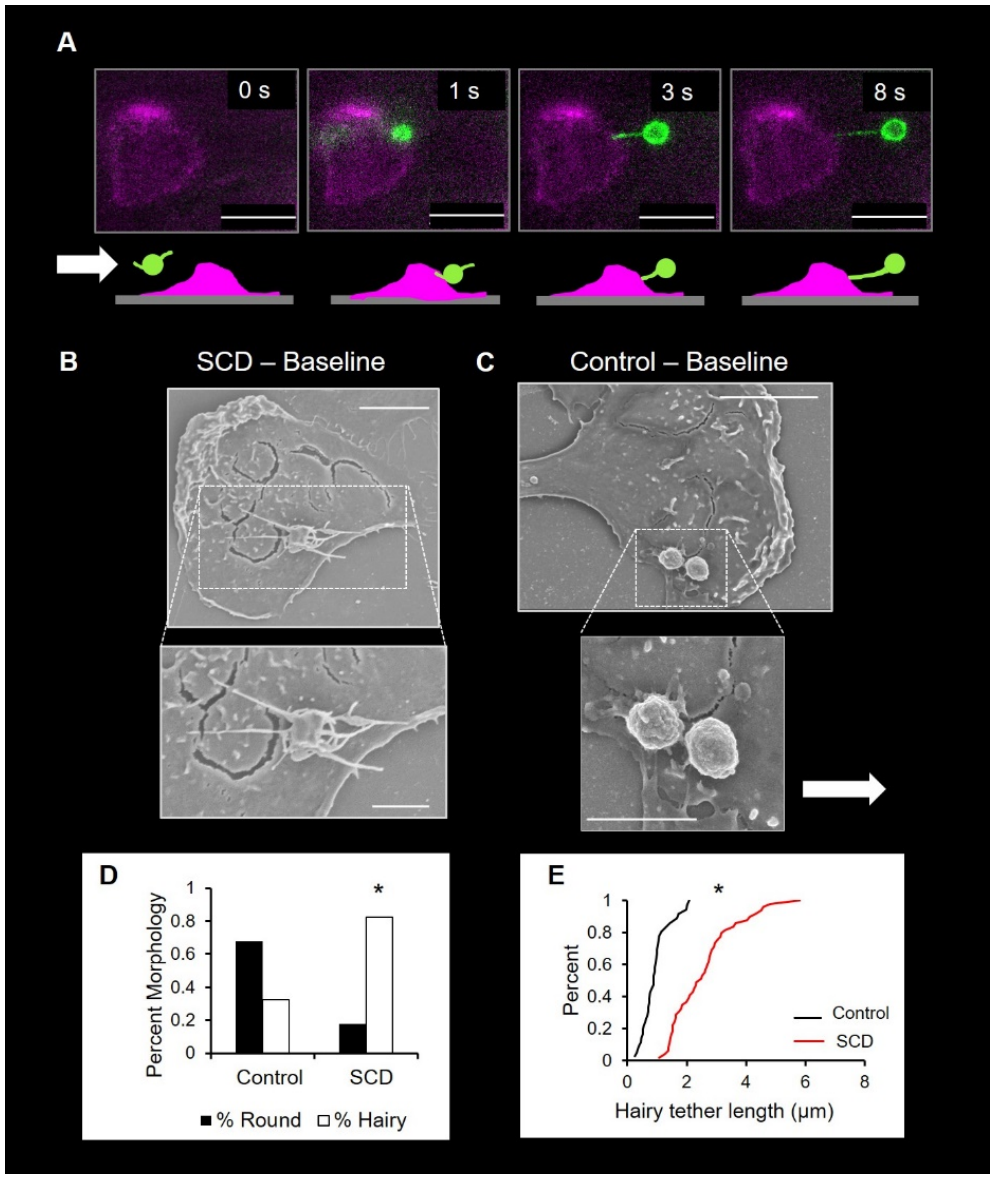

Figure 21: *Hairy platelets promote platelet-neutrophil aggregation in SCD***.** (A) SCD human blood was assessed using quantitative microfluidic fluorescence microscopy (qMFM). At t=0 s, the neutrophil (purple) arrests on the substrate. A freely flowing platelet (Green) attaches to the arrested neutrophil at t=1 s. The platelet is pushed away from the arrested neutrophil by the blood flow at t=3 s and a hair-like tether begins to elongate from platelet surface. At t=8 s the 'hairy' tether continues to elongate, enhancing the lifetime of platelet-neutrophil interaction. The schematic below each qMFM image depicts the side-view of the interaction. Scale bars 10μm. Scanning electron micrographs show platelets nucleated on top of arrested neutrophils in (B) SCD and (C) control human blood. Scale bars 5 μm. Inset- magnified view of region marked by dotted box. Scale bar 2.5 μm. (D) Platelet morphology in control and SCD human blood based on scanning electron micrographs. Percentages compared using Fourfold Table Analysis. (E) Cumulative distribution of platelet tether lengths in control and SCD human blood. The distribution compared using the nonparametric Kruskal-Wallis H test. (B-E) n= 4 experiments (2 control and 2 SCD human subjects). * $p<0.05$ when compared to control. Wall shear stress 6 dyn cm^{-2}. The thick white arrow denotes the direction of blood flow**.**

5.3.2 Platelet derived hair-like tethers present P-selectin to neutrophil PSGL-1 in SCD

Previously(1), it was shown that platelet-neutrophil aggregation in the lung arterioles of SCD mice *in vivo* and SCD human blood flowing through microfluidic flow-channels *in vitro* is partially mediated by platelet P-selectin binding to PSGL-1 on neutrophils. We hypothesized that hair-like platelet tethers may enable platelet-neutrophil interactions by presenting P-selectin to neutrophil PSGL-1. Therefore, platelet-neutrophil aggregates in SCD human blood were fixed under flow, stained for F-actin, PSGL-1 and P-selectin, and visualized using scanning confocal microscopy (Figure 22A-B) and super-resolution structured illumination microscopy (SIM; Figure 22C-D). As shown in Figure 22A and B, F-actin (red) was present in the lamellipodia of arrested neutrophils and in platelets (marked with arrows) that nucleated on top of arrested neutrophils. Identical to our previous findings in Chapter 3(1), P-selectin (blue) was uniformly expressed on the membrane of SCD platelets (Figure 22A and B). We found that platelets were nucleated on arrested neutrophils primarily in areas positive for PSGL-1 (Figure 22A-B), and this preferential localization is evident in the maximum intensity projection images (Figure 22A-B). Due to the poor resolution in the x-y plane, confocal microscopy cannot resolve fine structures such as tethers. To image these structures, we used super-resolution SIM that can resolve structures as small as 100-150 nm. Remarkably, SIM revealed P-selectin (blue) present not only on the platelet surface but also on the hair-like tethers connecting platelets to arrested neutrophils in SCD human blood (Figure 22C and D). Regions marked with ellipses in the maximum intensity projection SIM images (Figure 22C and D) demonstrate that P-selectin (blue) is expressed on platelet hairy tethers, which serve as a bridge between platelets and arrested neutrophils. Staining with isotype control antibodies did not result in any fluorescence suggesting that the blue and green fluorescence in Figure 22 was specific to P-selectin and PSGL-1, respectively. Interestingly, plasma membrane derived tubular structures

known as ‘slings’ or ‘tethers’ have been shown to promote neutrophil rolling on inflamed endothelium(58, 90) and platelet aggregation during thrombosis(91) by shielding the adhesive bonds from the disruptive force of the blood flow(92). However, a similar role for tethers and slings in the vaso-occlusive pathophysiology of SCD is largely unknown. Taken together, our previous and current findings suggest that hair-like membrane tethers on platelets promote platelet-neutrophil aggregation in SCD by presenting P-selectin to neutrophil PSGL-1. Based on the reported role of tethers as force dampeners(27, 58, 90-92), we propose that these platelet derived hair-like tethers contribute to the increased frequency(1) and lifetime(1) of P-selectin-PSGL-1 mediated platelet-neutrophil interactions in SCD.

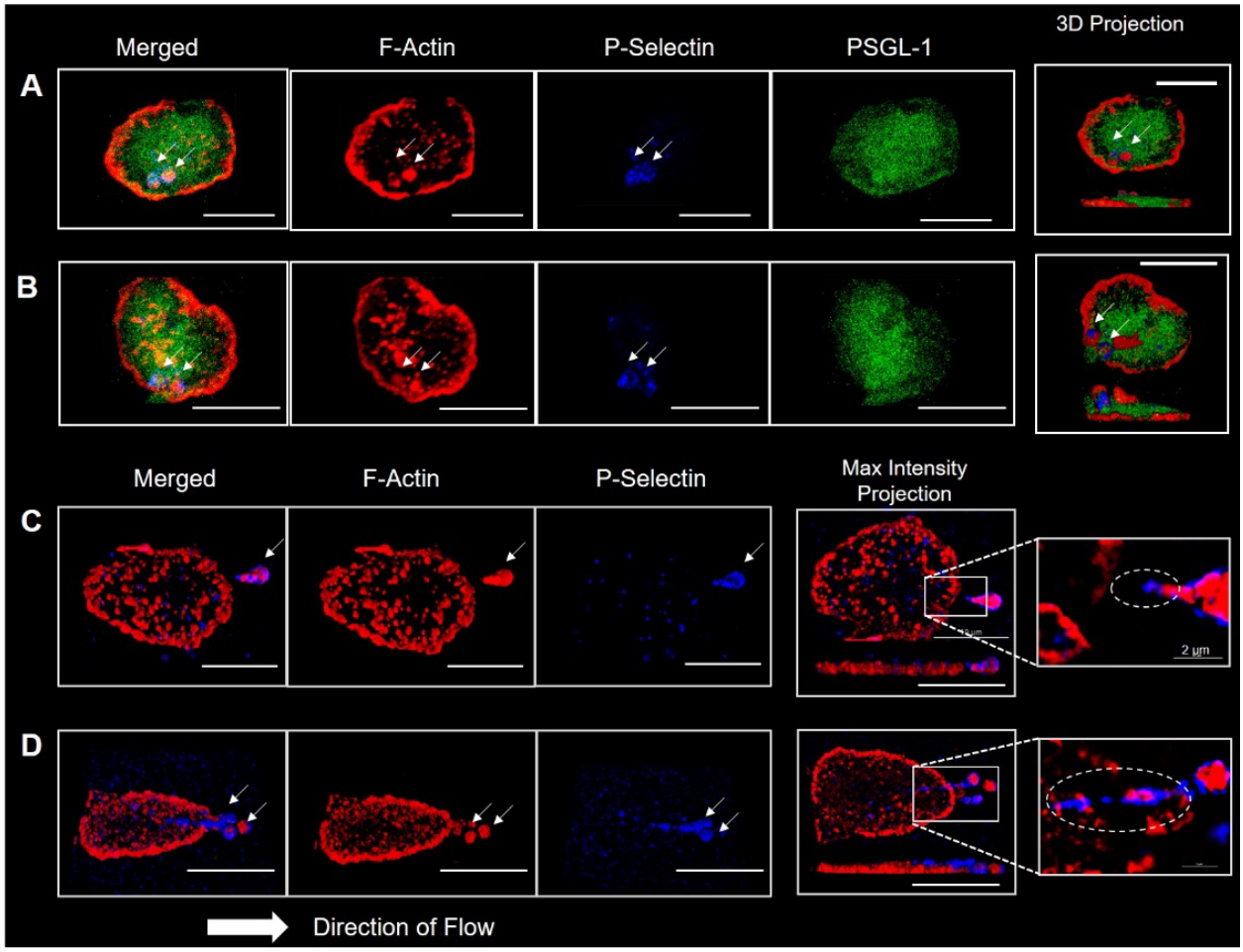

Figure 22: *Hair-like tethers present P-selectin to neutrophil PSGL-1 in SCD patient blood.* (A-B) Confocal microscopy revealed that platelets nucleated on top of an arrested neutrophil in SCD human blood. Arrested neutrophils and platelets were positive for F-actin (red) which can be seen throughout the lamellipodia of the neutrophils and throughout the surface of the platelets. Platelets were positive for P-selectin (blue) while neutrophils expressed PSGL-1 (green). The far-right panel shows the reconstructed 3D confocal image. (C-D) Structured illumination microscopy (SIM) images reveal 'hairy' platelets attached to an arrested neutrophil via sling-like tethers. The arrested neutrophil and platelets were positive for F-actin (red) which was present throughout the lamellipodia of the arrested neutrophil and throughout the platelet (marked with a thin white arrow). P-selectin (blue) was expressed on the platelet surface as well as on the hair-like tethers. Far right panel represents the maximum intensity projections of the 3D SIM image in x-y (top) and y-z plane (bottom). The inset on the right shows a magnified view of the region marked with a white box. The dotted white circle reveals P-selectin (blue) present on hair like tethers (red) that connect platelets to the neutrophil. Wall shear stress 6 dyn cm^{-2} Scale bars 10µm. Thick white arrow denotes direction of blood flow. N= 4 SCD human subjects.

5.3.3 TLR4 activation promotes platelet hair-like tether formation in SCD

Recently(1), we have shown that pretreatment with the TLR4 agonist LPS at a concentration of 1 µg/ml significantly increased the frequency and lifetime of platelet-neutrophil interactions in control human blood flowing through microfluidic flow-channels *in vitro* and this increase was abolished by pretreatment with the TLR4 antagonist TAK242. In the current study, platelet-neutrophil aggregates in control human blood treated with 1 µg/ml LPS ± TAK242 (50 µg/ml) were fixed under flow in microfluidic flow-channels *in vitro* and visualized at high resolution using scanning electron microscopy. Unlike the round platelets in untreated control blood (Figure 21C), platelets in LPS (1 µg/ml) treated control blood were hairy in appearance (Figure 23A) and resembled the platelets in untreated SCD human blood (Figure 21C) suggesting that a LPS (1 µg/ml) dependent increase in platelet-neutrophil interactions was complimentary to an increase in platelet hairiness. Similar to SCD human blood, hair-like tethers originating from the platelet surface served as a bridge, connecting platelets to arrested neutrophils in LPS (1 µg/ml) treated control blood. Quantitative analysis of scanning electron micrographs revealed that the percent hairy platelets (Figure 23D) and length of hairy tethers (Figure 23E) in control human blood were significantly increased by LPS (1 µg/ml) treatment to the levels observed in untreated SCD human blood. TLR4 inhibition with TAK242 abolished the hairiness and rescued the round platelet morphology in LPS (1 µg/ml) treated control blood (Figure 23B). Both the percent 'hairy' platelets (Figure 23D) and the length of hair-like tethers (Figure 23E) were reduced to the levels in untreated control blood suggesting that TLR4 activation promotes hair-like tethers by platelets. Previously(1), we have shown that TLR4 inhibition also abrogated platelet-neutrophil interactions in SCD human blood flowing through microfluidic flow-channels *in vitro*. We hypothesized that this inhibition might also be associated to the loss of hair-like tethers on platelets. To verify,

platelet-neutrophil aggregates in TAK242 treated SCD human blood were fixed under flow in microfluidic channels and visualized using scanning electron microscopy. Remarkably, TLR4 inhibition completely abolished the hairiness of platelets in SCD human blood. Post TLR4 inhibition, SCD human platelets were round (Figure 23C) and the percent hairy platelets (Figure 23F) as well as length of tethers (Figure 23G) were significantly reduced and seemed identical to untreated control blood. These findings suggest that platelet TLR4 activation by the inflammatory *milieu* in SCD promotes the formation of hair-like membrane tethers by platelets.

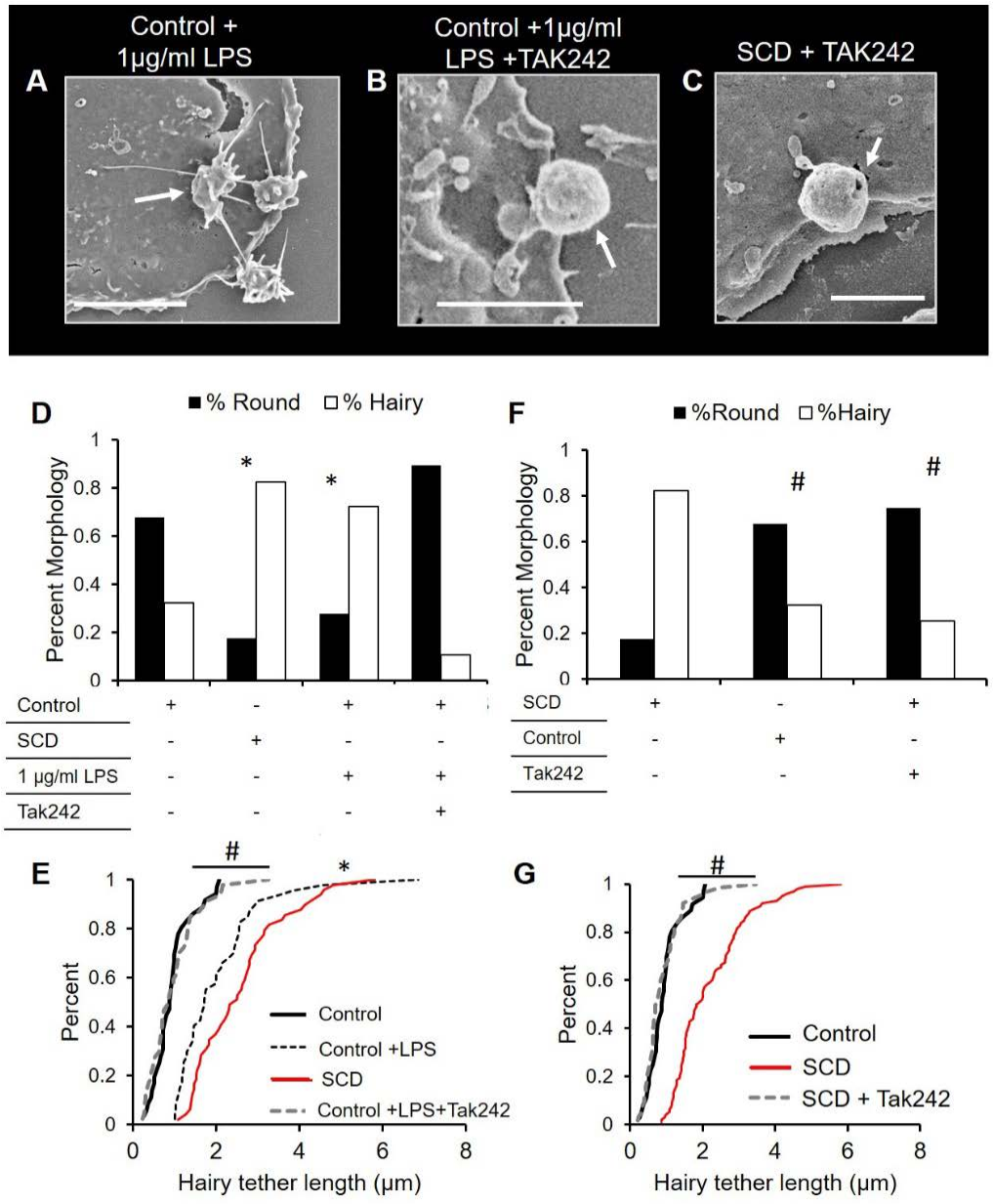

Figure 23: *TLR4 activation promotes platelet hair-like tether formation in SCD.* Platelet-neutrophil aggregates were fixed under flow and visualized using SEM. (A) Treatment with 1 µg/mL LPS led to the formation of hairy tethers on control platelets. TLR4 inhibition with Tak242 (50 µg/mL) led to the disappearance of hairy tethers and rescued the round morphology of platelets in (B) LPS treated control and (C) untreated SCD human blood. Scale bar 5 µm (A) and 2.5 µm (B-C). (D) Percent of round and hairy platelets, and (E) Cumulative probability distribution of tether lengths in control human blood treated with 1 µg/mL LPS treatment ± Tak242. Untreated control and SCD human blood is included for comparison. (F) Platelet morphology and (G) distribution of tether lengths in SCD human blood ± Tak242 treatment. Untreated control human blood is included for comparison. Percentages compared using Fourfold Table Analysis. Distributions in E & G were compared using the nonparametric Kruskal-Wallis *H* test. N=6 experiments done (4 control and 2 SCD human subjects) * $p<0.05$ compared to control. # $p<0.05$ compared to SCD. Wall shear stress 6 dyn cm^{-2}.

5.3.4 Platelet hair-like tether formation in SCD is NLRP3 inflammasome dependent

The NLRP3-inflammasome(93), containing Nucleotide-binding domain, leucine-rich-containing family, pyrin domain-containing 3 (NLRP3), apoptosis-associated speck-like protein containing a caspase recruitment domain (ASC) and caspase-1, was recently discovered to be a functional complex in platelets, which can be activated in response to TLR4 activation by DAMPs or PAMPs leading to the downstream activation of caspase-1(34, 38). Nevertheless, a role for the platelet NLRP3 inflammasome in the vaso-occlusive pathophysiology of SCD remains unknown. Previously(1), we have shown that pretreatment with LPS at a concentration of 0.25 µg/ml was potent enough to significantly increase platelet-neutrophil aggregation in SCD human blood flowing through microfluidic flow-channels *in vitro*, but a four-fold higher concentration of LPS (1 µg/ml) was required to promote aggregation in control human blood. Therefore, platelets were isolated from SCD and control human platelet-rich-plasma (PRP) with or without LPS treatment (0.25 µg/ml). Western blots of platelet lysates confirmed the presence of NLRP3, ASC and Caspase-1 in both control and Sickle Cell Disease human platelets (Figure 24A). Confocal microscopy revealed that NLRP3 (red) and ASC (green) were randomly distributed as punctae with minimal overlap in both untreated and 0.25 µg/ml LPS treated control human platelets (top two rows in Figure 24B). In contrast, both ASC (green) and NLRP3 (red) appeared colocalized around the outer membrane of untreated SCD platelets (red and green overlapping rings in third row of Figure 24B), and completely overlapped in 0.25 µg/ml LPS treated SCD platelets (green and red images are identical in the bottom row of Figure 20B). Based on Pearson's coefficient analysis (Figure 24C), colocalization of NLRP3 with ASC was minimal in untreated control platelets and did not increase with 0.25 µg/ml LPS treatment. However, NLRP3-ASC colocalization was significantly higher in SCD than control human platelets at baseline and further

increased following treatment with 0.25 µg/ml LPS (Figure 24C). These findings suggest that the inflammatory *milieu* in SCD promotes activation of NLRP3-ASC-Caspase-1 inflammasome in platelets and the activation is further enhanced following treatment with a TLR4 agonist (LPS) at a dose which does not induce activation in control human platelets.

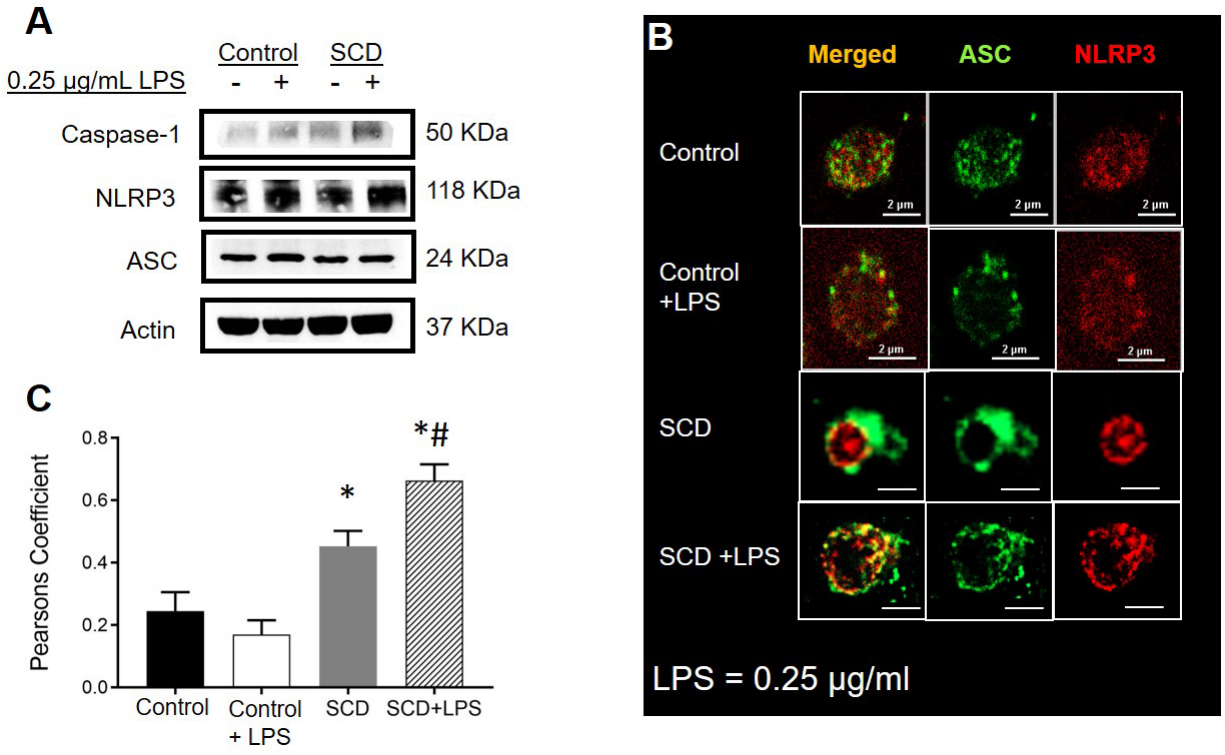

Figure 24: *Platelet hair-like tether formation in SCD is NLRP3-inflammasome dependent.* Platelets were isolated from untreated and LPS (0.25 µg/mL) treated platelet rich plasma (PRP) from SCD and control human. (A) Western blot micrograph showing the presence of NLRP3 (118 KDa), ASC (24 KDa) and Caspase-1 (50 KDa) in both control and SCD platelets. Beta-actin (37 KDa) was used as the house-keeping control. (B) Confocal microscopy images showing the localization of ASC (green) and NLRP3 (red) in control and SCD platelets ± LPS treatment (0.25 µg/ml). Scale bars 2 µm. (C) Analysis of NLRP3 (red) with ASC (green) colocalization in platelets quantified in terms of Pearson's coefficient. Data represents mean ± SE and compared using Student's t-test with Bonferroni correction. *p<0.05 when compared to control. # p<0.05 when compared to SCD.

Interestingly, mitochondrial ROS (mtROS), a potent activator of the NLRP3 inflammasome (93, 94) has been shown to be significantly elevated in platelets of SCD patients(67). Mitotempo a mtROS scavenger(67), and YVAD-CHO, a caspase-1 inhibitor, has been used widely to inhibit NLRP3-inflammasome activation(94, 95). Remarkably, scanning electron micrographs of platelet-

neutrophil aggregates in SCD human blood fixed under vascular mimetic flow *in vitro* revealed that pretreatment with 50 µM Mitotempo (Figure 25A) and 200 µM YVAD-CHO (Figure 25B) led to the disappearance of hair-like tethers from SCD platelets. Following treatment with Mitotempo (Figure 25C) and YVAD-CHO (Figure 25D), SCD platelets were primarily round. The morphology, which was based on the percent round vs hairy platelets, was identical to the untreated control but significantly different from untreated SCD human platelets. As shown earlier, platelets in untreated control human blood were primarily round but became hairy following treatment with 1 µg/ml LPS. We tested whether the platelet hairiness in 1 µg/ml LPS treated control blood was also inflammasome dependent. Indeed, pretreatment with 20 µM Mitotempo (Figure 25A) and 100 µM YVAD-CHO (Figure 25B) rescued the round morphology of platelets in 1 µg/ml LPS treated control human blood. Post Mitotempo and YVAD-CHO treatment, the control platelets were primarily round (Figure 25C and D).

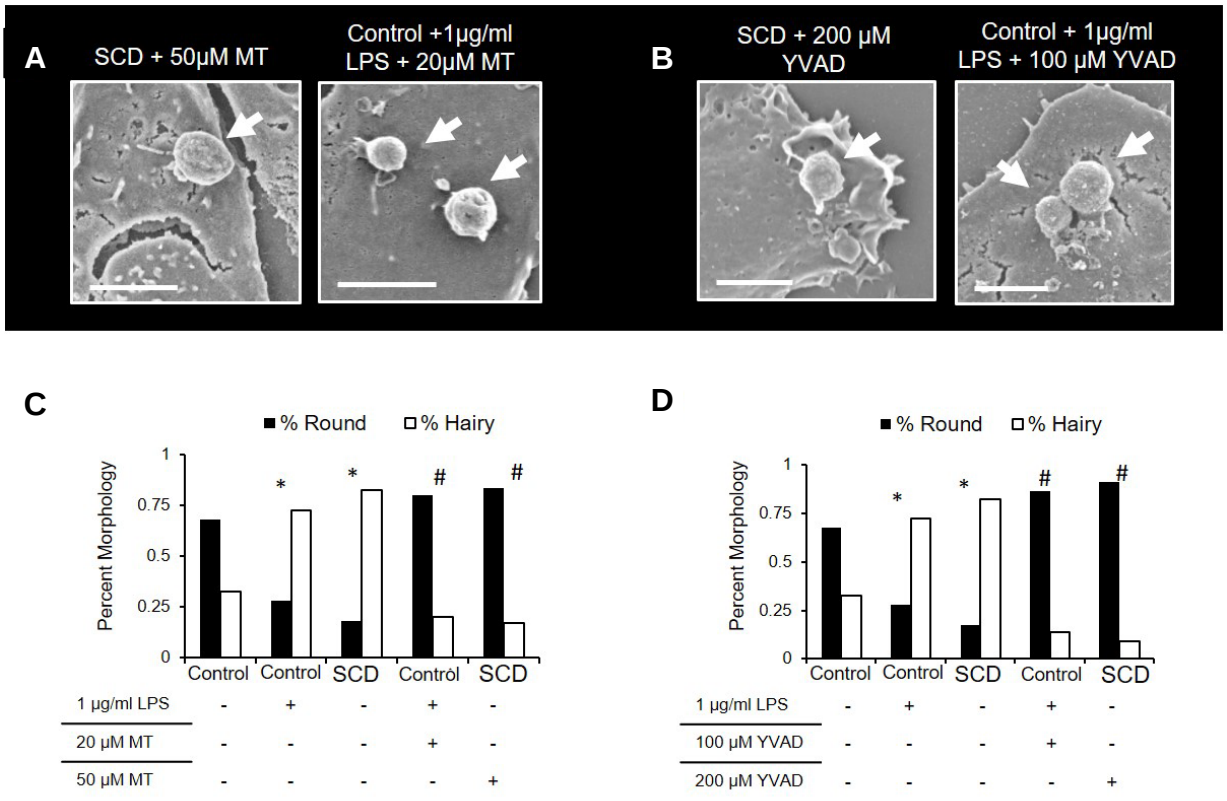

Figure 25: *Scavenging of mtROS and Caspase-1 rescues round platelet morphology.* Scanning electron micrographs showing platelets nucleated on arrested neutrophils in control and SCD human blood fixed under flow. (A) Treatment with mtROS scavenger, Mitotempo, led to the disappearance of platelet tethers in SCD (50μM) and 1μg/ml LPS treated control subject blood (20μM). Similarly (B) Caspase-1 inhibitor YVAD-CHO led to the disappearance of hairy platelet tethers in SCD (200 μM) and LPS treated (1 μg/mL; 100 μM) control human blood. Scale bars – 2.5 μm. Scanning electron micrographs were analyzed to quantify the effect of (C) Mitotempo and (D) YVAD-CHO treatment on platelet morphology in SCD and 1 μg/mL LPS treated control human blood. Compared using Fourfold table analysis. Data for untreated control and SCD human blood included for comparison. * $p<0.05$ when compared to control. # $p<0.05$ when compared to SCD. N=14 with 8 control and 6 SCD human subjects. Wall shear stress 6 dyn cm^{-2}.

Although a small number of platelets in control patient blood were still hairy following treatments, the lengths of these tethers post Mitotempo (Figure 26A) and YVAD-CHO (Figure 26B) were significantly small. As shown in Figures 25C and 25D, hairy tethers were still present on a small number of SCD platelets (17% post Mitotempo and 9% post YVAD-CHO), but the lengths of these tethers in Mitotempo (Figure 26C) and YVAD-CHO (Figure 26D) treated platelets were significantly smaller than those in untreated SCD platelets and not different from the tether lengths in untreated control platelets. Taken together, these results suggest that TLR4-dependent activation

of the platelet NLRP3-inflammasome promotes the generation of hair-like membrane tethers by platelets in SCD.

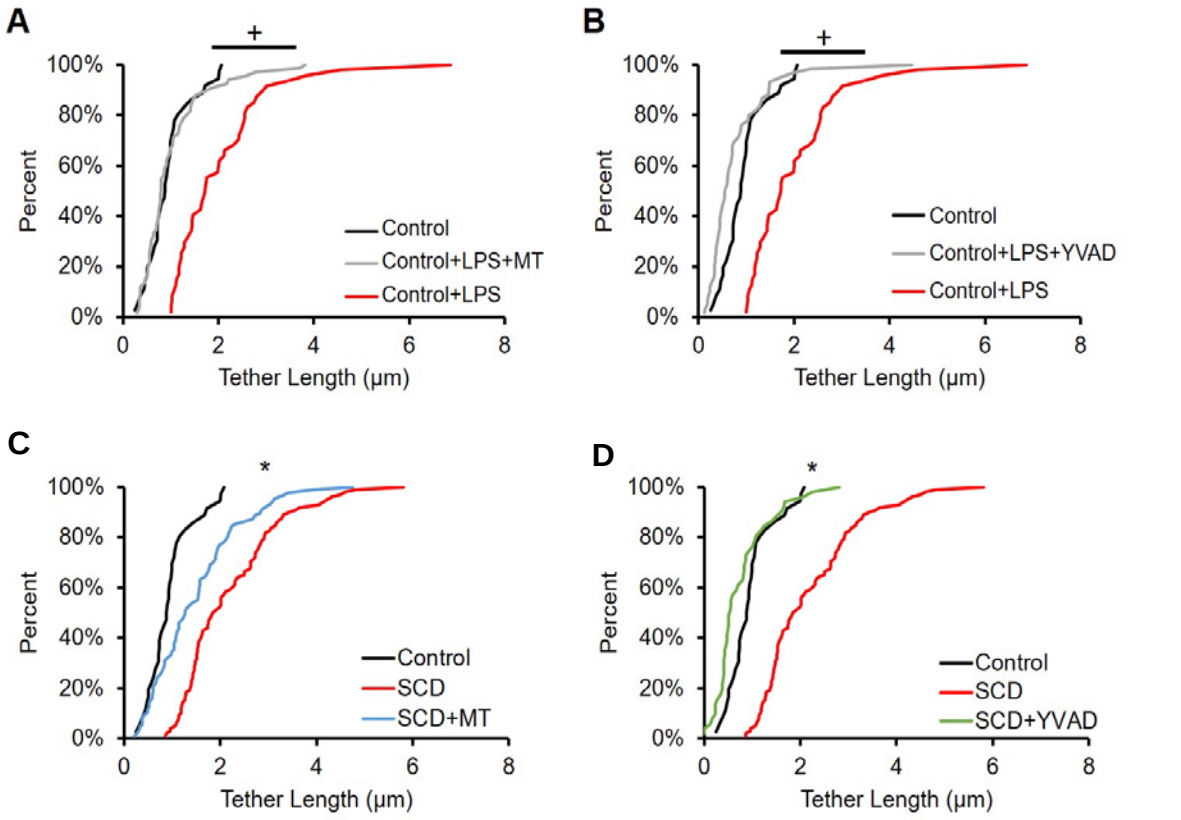

Figure 26: *Scavenging mtROS and inhibiting caspase-1 reduces platelet hairiness.* Control and SCD human blood ± mtROS scavenger Mitotempo or ± caspase-1 inhibitor YVAD were fixed under flow and imaged using Scanning Electron Microscopy. Pretreatment with (A) Mitotempo (20µM) and (B) YVAD-CHO (100µM) significantly reduced the length of platelet tethers in 1 µg/ml LPS treated control blood to the level observed in untreated control blood. N= 8 control human subjects. Pretreatment with (C) Mitotempo (50µM) and (D) YVAD-CHO (200µM) significantly reduced the length of platelet tethers in SCD blood. Following YVAD-CHO treatment, the platelet tether length in SCD blood was reduced to the level observed in untreated control blood. N=8 experiments (2 control and 6 SCD human subjects). Kruskal Wallis *H*- Test was used to measure significance. * $p<0.05$ when compared to SCD. + $p<0.05$ when compared to control + LPS. Shear stress 6 dyn cm^{-2}.

5.3.5 Platelet inflammasome promotes platelet-neutrophil aggregation in SCD

qMFM revealed that inhibiting the NLRP3-inflammasome by either scavenging mtROS or inhibiting caspase-1 abolished TLR4-dependent platelet-neutrophil aggregation in SCD human

blood *in vitro*. SCD and control human blood with or without treatment with 50 μM Mitotempo to scavenge mtROS or 200 μM YVAD-CHO to inhibit caspase-1 was perfused through microfluidic flow-channels presenting a combination of P-selectin, ICAM-1, and IL-8. Identical to our previous report (1), neutrophils were observed to roll, arrest, crawl and interact with freely flowing platelets resulting in significantly more total platelet-neutrophil interactions as well as platelet interactions per arrested neutrophil in untreated SCD than control human blood. Mitotempo significantly reduced the total number of platelet-neutrophil interactions in both untreated control and SCD human blood (Figure 27A). Mitotempo also significantly reduced the number of platelet interactions per arrested neutrophil in SCD human blood (Figure 27B). Following Mitotempo treatment, platelet-neutrophil interactions (Figure 27A) as well as platelet interactions per arrested neutrophil (Figure 27B) were not different between SCD and control human blood. Remarkably, caspase-1 inhibitor YVAD-CHO significantly reduced the total platelet-neutrophil interactions (Figure 27C) and platelet interactions per neutrophil (Figure 27D) in SCD human blood, while having no effect on control human blood.

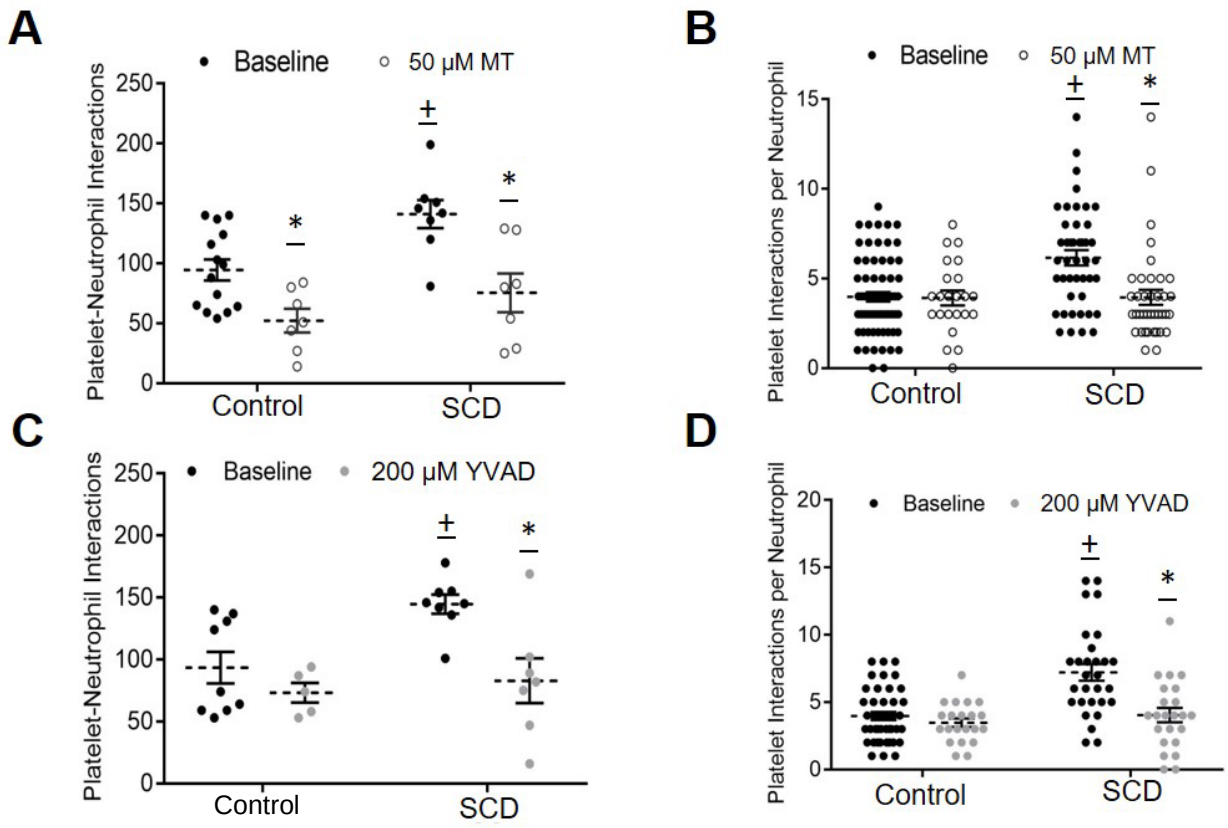

Figure 27: *Scavenging mtROS or inhibiting caspase-1 abolished platelet-neutrophil aggregation in SCD human blood.* Control and SCD human blood, with or without treatment with a mitochondrial ROS scavenger (Mitotempo) or caspase-1 inhibitor (YVAD-CHO) was assessed using qMFM for a 2-min period. Effect of Mitotempo (50μM) treatment on (A) platelet-neutrophil interactions per FOV and (B) platelet interactions per arrested neutrophil in control and SCD human blood. Effect of YVAD-CHO (200 μM) treatment on (C) platelet neutrophil interactions and (D) platelet interactions per arrested neutrophil in control and SCD human blood. Field of view (FOV: ~14,520 μm^2) Wall shear stress 6 dyn cm^{-2}.

Next, SCD and control human blood was treated with 0.25 and 1 μg/ml LPS, respectively, and the effect of Mitotempo as well as YVAD-CHO on platelet-neutrophil aggregation was assessed in microfluidic flow-channels using qMFM. Similar to findings in Chapter 3 (1), 0.25 and 1 μg/ml LPS significantly increased platelet-neutrophil interactions in SCD and control blood, respectively (Figure 28A and 28C). Mitotempo treatment significantly reduced the total number of platelet-neutrophil interactions and the number of platelet interactions per neutrophil in LPS treated control and SCD human blood to the level below that in untreated control and SCD blood (Figure 28A &

B). YVAD-CHO significantly reduced the total platelet-neutrophil interactions in LPS treated SCD human blood (Figure 28C) and platelet interactions per neutrophil in both LPS treated control and SCD human blood (Figure 28D).

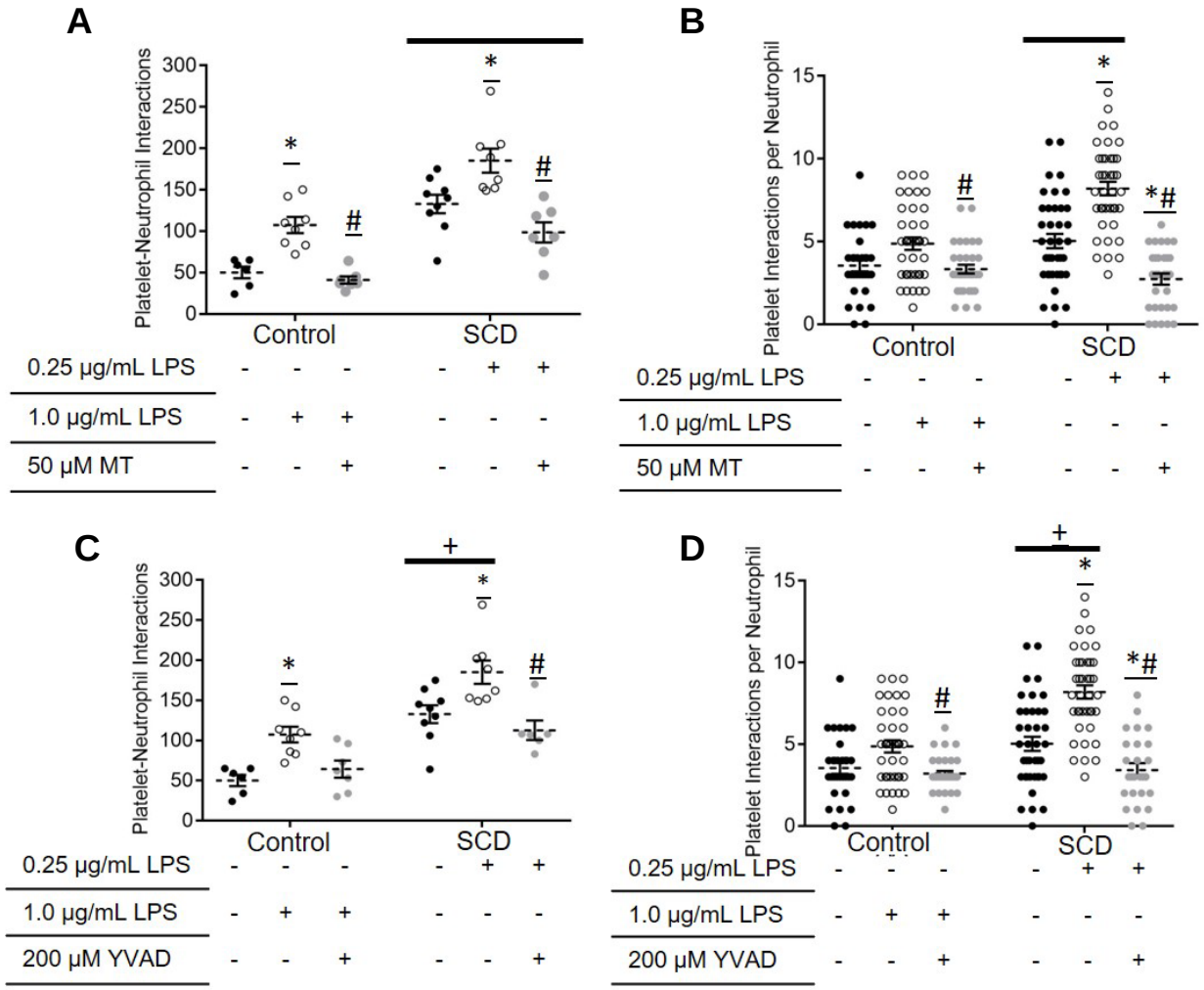

Figure 28: *LPS induced platelet-neutrophil interactions in SCD patient blood are abolished by Scavenging mtROS and inhibiting caspase-1*. Control and SCD human blood, pretreated with 1 µg/mL and 0.25 µg/mL LPS, respectively, with Mitotempo or caspase-1 inhibitor (YVAD-CHO) treatment was assessed using qMFM for a 2-min period. Effect of Mitotempo (50 µM) on (A) platelet-neutrophil interactions per FOV and (B) platelet interactions per arrested neutrophil in control and SCD human blood pretreated with 1 µg/mL and 0.25 µg/ml LPS, respectively. Effect of YVAD-CHO (200 µM) on (C) platelet-neutrophil interactions per FOV and (D) platelet interactions per arrested neutrophil in control and SCD human blood pretreated with 1 µg/ml and 0.25 µg/mL of LPS, respectively. Means compared using Students *t*-test with Bonferroni correction. # $p<0.05$ when compared to LPS. * $p<0.05$ when compared to baseline. + $p<0.05$ when compared to control. (A-B) N= 6 (3 control and 3 SCD human subjects); (C-D) n=8 (4 control and 4 SCD human subjects). Field of view (FOV: ~14,520 μm^2) Wall shear stress 6 dyn cm^{-2}.

Treatment of control (Figure 29A-B) and SCD (Figure 29C-D) human blood with 1 and 0.25 µg/ml LPS, respectively, also led to a significant increase in the lifetime of platelet-neutrophil interactions. This increase was completely abolished following treatment with 50 µM Mitotempo (Figure 29A&C) and 200 µM YVAD-CHO (Figure 29B&D).

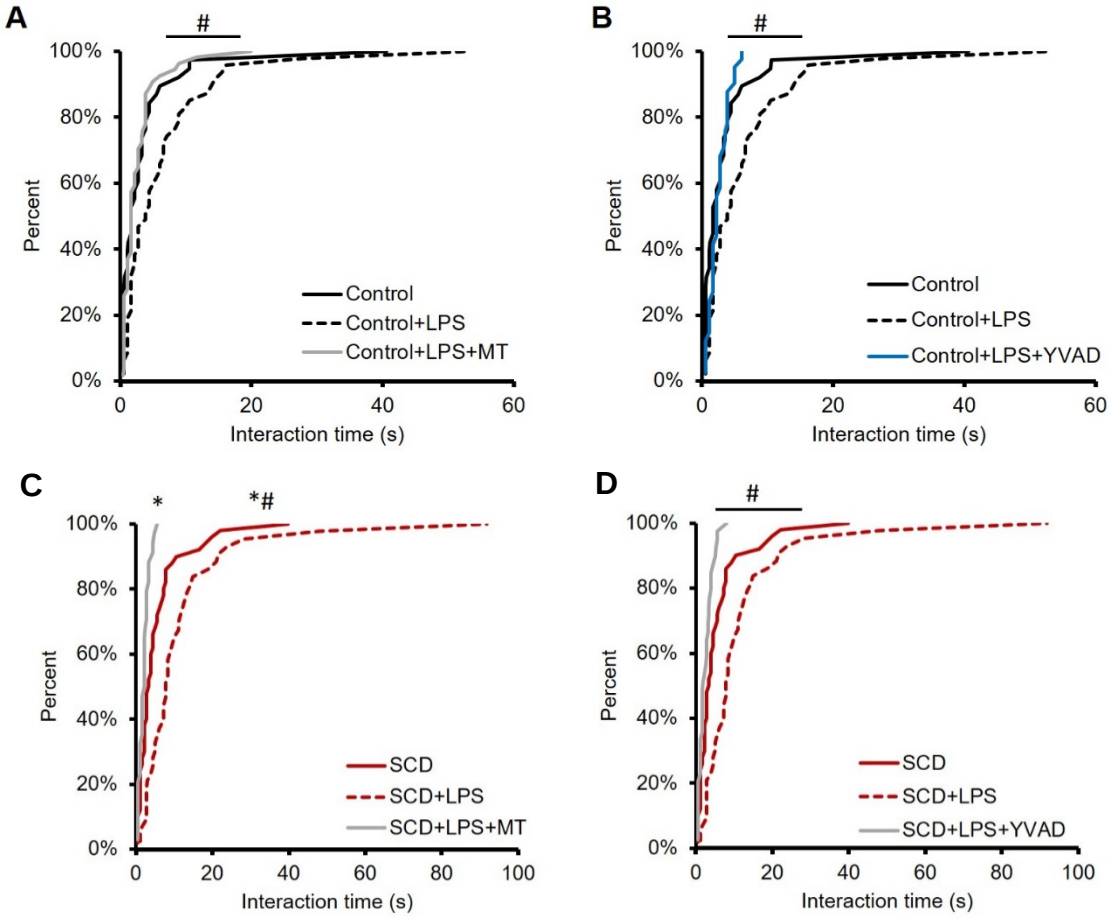

Figure 29: *Scavenging mtROS or inhibiting caspase-1 attenuates lifetime of platelet-neutrophil interactions in LPS treated blood.* The lifetime of platelet-neutrophil interactions was measured in LPS treated control (1 µg/ml) and SCD human blood (0.25 µg/ml) following treatment with mtROS scavenger Mitotempo and YVAD-CHO. Treatment of control human blood with 1 µg/ml LPS significantly increased the lifetime of platelet-neutrophil interactions, which was completely abolished by treatment with (A) Mitotempo (50 µM) and (B) YVAD (200µM). Treatment of SCD human blood with 0.25 µg/ml LPS also significantly increased the lifetime of platelet-neutrophil interactions, which was significantly reduced by (A) Mitotempo (50 µM) and (B) YVAD (200µM) to the level observed in untreated SCD blood. Comparisons made using Kruskal Wallis *H*-test. N=(A) 4 control subjects; (B) 3 control subjects; (C) 3 SCD patients; (D) 4 SCD patients; * $p<0.05$ when compared to SCD baseline. # $p<0.05$ when compared to LPS treatment. Shear stress of 6 dyn cm^{-2}

DMSO was used as a solvent to reconstitute both Mitotempo and YVAD-CHO. Treatment with the vehicle (DMSO) had no effect on the total platelet-neutrophil interactions in SCD human blood (Figure 30).

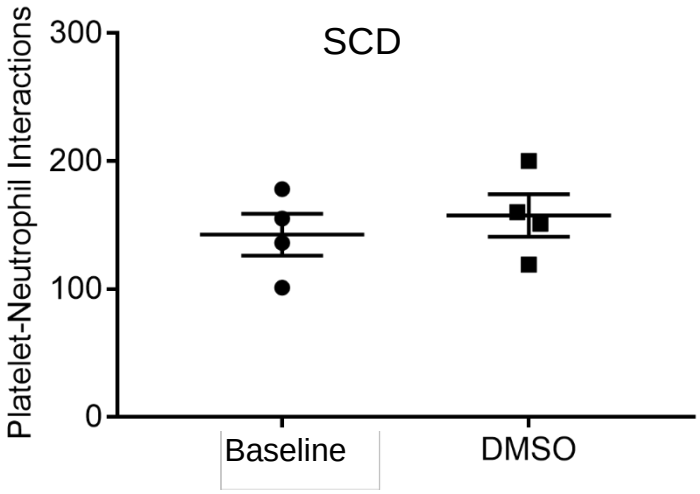

Figure 30: *DMSO does not affect platelet-neutrophil interactions in SCD human blood*. To exclude the possibility that the Mitotempo and YVAD-CHO mediated inhibition of platelet-neutrophil interactions is a contribution of DMSO, SCD human blood with or without treatment with DMSO (vehicle) was perfused through microfluidic flow channels presenting a combination of P-selectin, ICAM-1, and IL-8 at a shear stress of 6 dyn cm-2. Platelet-neutrophil interactions were assessed over a 2-minute time period

5.4 DISCUSSION

Acute chest syndrome is the leading cause of mortality in SCD (70). The current treatment for acute chest syndrome is primarily supportive and the mechanism remains poorly understood (70, 96, 97). Clinical evidence suggests that acute chest syndrome is often a sequela of acute systemic vaso-occlusive crisis (5, 97). Recently, the development of thrombocytopenia was shown to be the reliable predictor of acute chest syndrome in SCD patients hospitalized with vaso-occlusive crisis (84, 97, 98). Also, autopsy (62) and computed tomography (99) studies have identified platelet

aggregates occluding pulmonary arterioles in acute chest syndrome patients. In support of these clinical findings, we recently (1) found that vaso-occlusive crisis in SCD mice triggered by systemic challenge of a few nanograms of TLR4 agonist LPS led to occlusion of pulmonary arterioles by P-selectin dependent platelet-neutrophil aggregates. Altogether, these findings suggest that the inflammatory milieu in SCD promotes platelet-neutrophil aggregate-mediated lung vaso-occlusion, which can progress to acute chest syndrome in the absence of specific therapy, typically exchange transfusion and antibiotics (59, 97). The molecular mechanism that promotes platelet activation and platelet-neutrophil aggregation mediated lung vaso-occlusion in SCD has remained largely unknown. This study is the first to identify that platelet TLR4 and NLRP3-inflammasome activation promotes IL-1β-dependent platelet-neutrophil aggregation mediated vaso-occlusion in SCD.

Here, *in vitro* microfluidic studies (qMFM) with human blood were conducted to reveal for the first time that platelets in SCD are not round but hairy in appearance due to the presence of membrane tethers on their surface. We show that these hair-like membrane tethers presented P-selectin to PSGL-1 on neutrophils and enhanced the lifetime of platelet-neutrophil interactions. TLR4 inhibition abolished platelet hairiness in SCD suggesting that the inflammatory milieu in SCD promotes platelet TLR4 activation, which results in the generation of hair-like tethers by platelets. Although the platelet NLRP3-inflammasome can be activated in response to TLR4 activation by DAMPs or PAMPs to trigger downstream activation of caspase-1(34, 38), a role for the platelet NLRP3-inflammasome in the vaso-occlusive pathophysiology of SCD remains unknown. Using confocal microscopy, we discovered that the NLRP3-ASC-Caspase-1 inflammasome complex was active in untreated SCD but not control human platelets, and activation was amplified only in SCD platelets following treatment with a low concentration of

LPS (0.25 µg/ml) that promotes platelet-neutrophil aggregation only in SCD human blood. Inhibition of the NLRP3-inflammasome by scavenging mtROS or inhibiting caspase-1 completely abolished platelet hairiness as well as platelet-neutrophil aggregation in SCD human blood *in vitro*.

Recent studies in diseases other than SCD have identified that TLR4 and NLRP3-inflammasome dependent caspase-1 activation can promote generation of IL-1β carrying EVs by platelets (34). Interestingly, platelet derived EVs are among the most abundant species of EVs in SCD human blood and their numbers correlate with disease severity (15, 41) but the role of platelet EVs in SCD pathophysiology remains unknown. New unpublished data from our lab shows that NLRP3 inflammasome activation also promotes shedding of IL-1β containing EV's by platelets in SCD human blood, and these platelet EVs may promote platelet-neutrophil aggregation mediated lung vaso-occlusion in SCD by activating the IL-1 receptor on neutrophils, platelets and other vascular cells.

Taken together, our previous (1), current and unpublished findings (Figure 31) suggest that the inflammatory milieu (erythroid DAMPs) in SCD promotes TLR4-dependent activation of the NLRP3-inflammasome in platelets, which is enhanced by the presence of nanogram levels of a TLR4 ligand (PAMPs) such as LPS. Inflammasome activation promotes the generation of hair-like membrane tethers and the generation of IL-1β carrying platelet-derived EVs. Hair-like membrane tethers enable platelets to interact more efficiently with neutrophils within the vasculature, leading to increased P-selectin-PSGL-1 dependent platelet-neutrophil aggregation. Platelet EVs also promote IL-1β dependent activation of neutrophils and platelets to form large aggregates, which promote vaso-occlusion in SCD. The interpretation of our results is associated with the following limitations, which require further investigation by future studies. First, the NLRP3 inflammasome is the only inflammasome complex reported to promote platelet mediated

immune responses (34); however, other inflammasome complexes (100) might also contribute to vaso-occlusion in SCD. Second, IL-1β carrying platelet EVs may activate the IL-1 receptor on platelets by an autocrine loop (34, 101) to further promote generation of platelet EVs. Third, activated platelets trapped within the platelet-neutrophil aggregates may undergo degranulation (102) to locally generate IL-1β carrying EVs. Fourth, IL-1β carrying platelet EVs may also promote vaso-occlusion by activating the vascular endothelium (38).

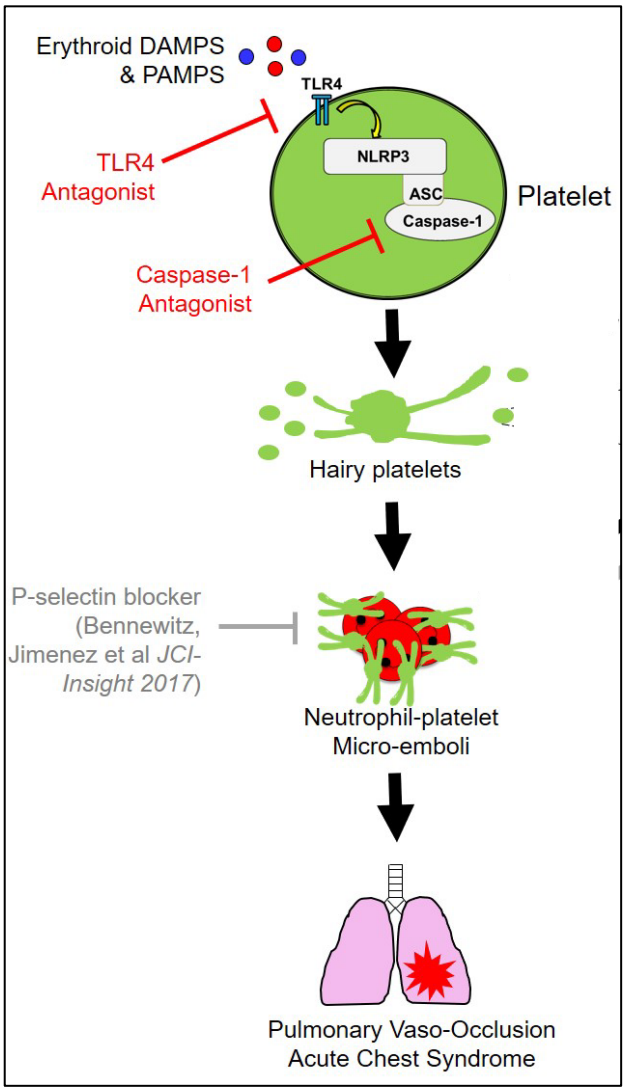

Figure 31:. *TLR4, NLRP3-inflammasome and IL-1β dependent innate immune pathway promotes lung vaso-occlusion in SCD.* The inflammatory milieu in SCD (erythroid DAMPs) primes TLR4-depedent activation of NLRP3-ASC-Caspase-1 inflammasome in platelets, which is enhanced by the presence of TLR4 agonists (PAMPs) at concentrations that are innocuous under healthy conditions. NLRP3 inflammasome promotes (black solid arrow) generation of hair-like membrane tethers and shedding of IL-1β carrying extracellular vesicles (EVs) by platelets, which together promote (black solid arrows) P-selectin and IL-1β dependent platelet-neutrophil aggregation mediated pulmonary vaso-occlusion. Previously (1), we identified that platelet-neutrophil micro-emboli dependent pulmonary vaso-occlusion can be prevented by a P-selectin blocker (gray block line). Here, we show that inhibiting TLR4, NLRP3 effector caspase-1or IL-1β innate immune pathway (red block lines) prevents lung vaso-occlusion in SCD. Although not shown in our current study, IL-1β carrying platelet EVs may activate the IL-1 receptor on platelets by an autocrine loop to further promote generation of platelet EVs (black dotted arrow). Also, activated platelets trapped within the platelet-neutrophil aggregates may undergo degranulation to locally generate IL-1β carrying EVs (gray dotted arrow).

5.5 CONCLUSION

Although SCD results in more than 100,000 deaths every year worldwide (82), hydroxyurea was until 2017 the only FDA approved drug for treatment of SCD that prevents hemoglobin S polymerization by inducing fetal hemoglobin production (3, 5, 97). Despite high efficacy, the disease activity and mortality remain high in patients taking hydroxyurea (3, 97) and there is a growing need to identify new therapies to prevent painful vaso-occlusive crisis and the progression to acute chest syndrome (84, 97). Recently (1), our group discovered that therapeutic blockade of platelet P-selectin prevented lung vaso-occlusion in SCD mice by inhibiting platelet-neutrophil aggregation in the pulmonary arterioles. These findings were validated by the SUSTAIN clinical trial showing a significant reduction in the frequency of painful vaso-occlusive crisis in SCD patients administered P-selectin antibody crizanlizumab (SelG1) (103). Our current data reveals that P-selectin dependent platelet-neutrophil aggregation in SCD is downstream to TLR4/NLRP3-ASC-Caspase-1 activation in platelets and IL-1β mediated activation of neutrophils, platelets and other vascular cells. These findings also imply that therapeutic inhibition of the TLR4, NLRP3, Caspase-1 and IL-1β innate immune pathway can be a promising therapeutic target for SCD patients, particularly to halt the progression of acute chest syndrome in high risk patients presenting with vaso-occlusive pain crisis. Interestingly, IL-1RA (ANAKINRA) and IL-1β blocking Ab (CANAKINUMAB) are already FDA approved as anti-inflammatory biological drugs for the treatment of rheumatoid arthritis (104) and NLRP3-inflammasome-mediated cryopyrin-associated-periodic-syndrome (105), respectively.

Our current findings justify the need for clinical trials to test the safety and efficacy of repurposing these drugs in SCD and also highlight several key aspects that need to be considered

in designing future therapies. Systemic inhibition of the IL-1β dependent innate immune pathway is potentially associated with a risk of immune compromise or off-target effects, which can be detrimental to SCD patients who are susceptible to bacteremia and respiratory infections (71, 106). With these potential risks in mind, targeted delivery of a small dose of these drugs as a payload within biodegradable nanocarriers designed to recruit selectively to the site of platelet-neutrophil aggregation *in vivo* may represent a safer therapy in SCD (107).

Based on epidemiological evidence, 10-20% of SCD patients hospitalized with systemic painful vaso-occlusive crisis develop acute chest syndrome over the course of hospitalization, suggesting that targeted therapies for vaso-occlusion at admission may prevent the development of acute chest syndrome (59). Previously (1), our group discovered that vaso-occlusive crisis in SCD triggers large platelet-neutrophil aggregates in pulmonary arterioles, leading to a loss of blood flow in the lung. Here, we show that the vaso-occlusion is platelet TLR4, NLRP3-inflammasome and IL-1β dependent, and can be prevented and reversed by inhibitors of the inflammasome or IL-1β innate immune pathway.

6.0 FUTURE WORK

The primary focus during this study was on the role of platelets and neutrophils during VOC in Sickle Cell Disease. It would be beneficial to visualize the effects other cells may have on VOC like RBC, monocytes, Natural Killer T Cells, and Natural Killer cells since they have been shown to play a role in VOC (108-110). Additionally, the study tested how LPS treatments affected platelet-neutrophil interactions in SCD patient blood. During hemolysis of RBCs, many proinflammatory stimuli are released into the blood. Future studies testing the role and effects of ADP, heme and/or hemoglobin treatments on interactions of platelets and neutrophils can also help in the understanding of the pathophysiology of vaso-occlusion and mimic a crisis environment. SCD patient blood can be incubated with these stimuli and the effects can be assessed by using qMFM in presence or absence of anti-adhesion or anti-inflammatory drugs.

The NLRP3 inflammasome is the only inflammasome complex reported to date to promote platelet mediated immune responses (34) and the only complex analyzed in this study. Other inflammasome complexes (100) might also contribute to vaso-occlusion in SCD by affecting neutrophils and/or platelets. Additionally, the role of NLRP3 inflammasome activation on neutrophil activity in Sickle Cell Disease has not been studied but could provide a better understanding of neutrophil behavior during VOC and how neutrophil slings(33, 58) may contribute to platelet-neutrophil interactions.

Due to the limitations on patient availability we were unable to include any SCD patients that were in suffering with active VOC prior to treatment. VOC has a major effect on patients and is the leading cause of emergency medical care(3). Using qMFM to study platelet-neutrophil interactions in crisis patients may provide unique insight into the mechanistic changes that exists

in SCD patients at baseline versus crisis. Furthermore, many patients are prescribed HU to reduce HbS sickling and the occurrence of VOC. A study looking at the possible differences between HU and non-HU patients would show the effects the drug may have on cell behavior and cell counts. Using qMFM one could visualize the cells in each patient to determine if there are any changes between the patients.

7.0 CONCLUSION

Vaso-occlusion is the predominant pathophysiology in SCD and responsible for acute vaso-occlusive crisis, which is the leading cause of emergency medical care by SCD patients (6, 9). Vaso-occlusion can lead to acute chest syndrome, pulmonary hypertension, stroke and ischemia reperfusion injury, however, the cellular, molecular, and biophysical mechanisms that drive vaso-occlusion remain incompletely understood. Until 2017, there was only one FDA approved drug to treat SCD, hydroxyurea (3). Although effective at reducing RBC sickling by inducing fetal hemoglobin production (3, 7), which is resistant to sickling, many patients still face severe complications and mortality remains high. Recently, L-glutamine had also been approved by the FDA to reduce the frequency of VOC and length of hospital stays in SCD patients(44). The current study not only developed a novel imaging approach to study the mechanisms of vaso-occlusion but also identified potential targets for therapeutic intervention that can prevent or alleviate vaso-occlusion in Sickle Cell Disease.

Chapter 2 established quantitative microfluidic fluorescence microscopy (qMFM) as a novel fluorescence imaging approach that utilized a PDMS based microfluidic chip to study single cell interactions at high resolution in human blood. Using qMFM, we viewed interactions between platelets and neutrophils and quantified the interactions using three parameters: total platelet-neutrophil interactions, platelet interactions per neutrophil and lifetime of platelet interactions with arrested neutrophils. The use of microfluidic chips that are attached via vacuum to a coverslip provides the versatility to study cellular interactions using a variety of platforms including confocal microscopy, scanning electron microscopy and super resolution structure illumination microscopy. Due to the small amount of blood (100-500 µl) that is required for qMFM studies, it is easy to test

the effects of different antagonists and inhibitors on cell-cell interactions in the same blood sample in real time.

Chapter 3 established a role for platelets and neutrophils in the onset of vaso-occlusion in SCD. Platelet-neutrophil interactions promoted platelet-neutrophil aggregates leading to vaso-occlusion following the sequential steps of neutrophil rolling, activation, arrest, capture of freely flowing platelets leading to platelet-neutrophil aggregates that trap RBC. When analyzed using qMFM, platelets-neutrophil interactions were not only more numerous in SCD patient blood than control human blood but also significantly longer in duration (14s vs. 3s). These interactions were mediated by platelet P-selectin and GPIbα binding to neutrophil PSGL-1 and Mac-1, and were significantly reduced when blood was treated with P-selectin or PSGL-1 and Mac-1 or GPIbα function blocking antibodies. Additionally, a combination of Mac-1 and P-selectin blocking antibodies reduced platelet-neutrophil interactions in SCD blood to a level below that in control human blood at baseline conditions. Treatment with a low dose of LPS significantly enhanced platelet-neutrophil interactions in SCD but not control human blood. These results support the clinical trials in place that are targeting selectins to reduce vaso-occlusion in SCD patients but suggests that using a dual approach of targeting Mac-1 and P-selectin may be more effective.

In Chapter 4, qMFM was used to test the effectiveness of CCP-224, a GPIbα inhibitor, on platelet-neutrophil interactions in SCD patient blood. Similar to what was shown in Chapter 3, inhibition of the interactions between platelet GPIbα and neutrophil Mac-1 significantly reduced the total platelet-neutrophil interactions and platelet interactions per neutrophil in SCD and control human blood. CCP-224 also effectively reduced the lifetime of platelet-neutrophil interactions in SCD patient blood. The effectiveness of CCP-224 suggests that future clinical studies to test the effectiveness and safety of CCP-224 in SCD patients is warranted.

In Chapter 3, it was shown that platelet-neutrophil interactions in SCD patients were not only more numerous but significantly longer than in control human subjects. Chapter 5 described the biophysical and molecular mechanisms that lead to the enhanced platelet-neutrophil interactions in SCD, while providing new targets for therapeutic interventions that could reduce vaso-occlusion in SCD patients. qMFM revealed for the first time that platelets in SCD blood form "hair-like" membrane tethers that promoted platelet-neutrophil interactions by shielding the bonds from the hydrodynamic shear forces of blood. Unlike platelets in SCD blood, control platelets lacked tether formation and were primarily round, unless activated by a large dose (1 μg/ml) of LPS. Structured illumination microscopy revealed that these "hair-like" membrane tethers actively expressed P-selectin throughout the tether, which allowed for interactions with neutrophil PSGL-1. Platelet-derived tether formation was found to be mediated by TLR4 dependent activation of the NLRP3-inflammasome complex. SCD platelets at baseline had a partially activated NLRP3 inflammasome complex, which completely activated following treatment with a low dose of LPS (0.25 μg/ml) that had no effect on control platelets. Mitochondrial ROS production had been shown to activate the NLRP3 inflammasome complex, while Caspase-1 activation lead to the cleavage and release of the proinflammatory cytokine IL1β. Inhibition of TLR4 or NLRP3 inflammasome not only inhibited "hair-like" tether formation in platelets but also significantly reduced the platelet-neutrophil interactions in SCD human blood.

Altogether this study suggests that platelet derived hair-like tethers in SCD patient blood are essential to promoting platelet-neutrophil aggregation that lead to vaso-occlusion. Studies aimed at therapeutically targeting either the physical interactions of platelet P-selectin and GPIbα with neutrophil PSGL-1 and Mac-1, respectively or the NLRP3 inflammasome pathway could be beneficial at alleviating or reducing the occurrence of VOC in SCD patients.

APPENDIX A

SUNDD LAB PROTOCOLS

The following methods are used in the Sundd lab to conduct experiments and analysis.

A1.1 Preparation of adhesion molecule presenting substrates

Rectangular coverslips (No. 1.5, Fisher Scientific) were coated with a cocktail of 2 μg/ml of P-selectin, 10 μg/ml of ICAM-1 and 10 μg/ml of IL-8 followed by incubation at room temperature for 30 min. P-selectin coating concentration of 2 μg/ml has been shown previously to result in a molecular density of ~20 molecules/μm^2, which is comparable to the P-selectin molecular density on cultured endothelial cells(33, 111). Following the incubation, the coverslips were washed once with phosphate buffered saline without Ca2+ and Mg2+ (PBS; MP Biomedicals, Solon, OH) and incubated in 2 ml of blocker casein (Thermo Scientific™, Rockford, IL) until used in assay to block all nonspecific binding sites. During rolling studies only 2 μg/ml of P-selectin were coated onto coverslips, while arrest studies involved P-selectin, ICAM-1, and IL-8.

A1.2 Microfluidic Flow Assay Setup

A PDMS/silicone chip with micro-channels engraved on its surface was gently placed on a glass coverslip either coated with a cocktail of P-selectin, ICAM-1, and IL-8 or cultured with TNF-α treated HMVECs-L or HCAECs and sealed together using vacuum (negative 30 KPa pressure). Prior to blood perfusion, the endothelialized microfluidic devices were filled with a KREBS-HEPES buffer, pH 7.4 (NaCl, KCl, MgSO4, NaHCO3, KH2PO4, Hepes, Glucose and $CaCl_2$) to keep the endothelial monolayer viable. Microfluidic chips attached to adhesion molecules were perfused with 1x PBS. The assembled device has an inlet, an outlet, a vacuum port connected to in-house vacuum supply and four identical micro-channels or perfusion chambers (30 μm high and 500 μm wide) with nearly identical flow rates and wall shear stresses. The wall shear stress was calibrated as a function of the differential pressure between the inlet and outlet reservoir. The differential pressure was set by placing the inlet reservoir next to the device while lowering the outlet reservoir to achieve the physiological wall shear stress (57) of 6 to 10 dyn cm-2. Approximately 500 μL of anticoagulated blood was transferred to a 1.5 mL Eppendorf tube which served as an inlet reservoir while a 10-ml syringe filled with PBS served as the outlet reservoir. The inlet and outlet reservoirs were connected to the inlet and outlet ports of the device using PE10 (ID 0.28 mm, OD 0.61 mm) and TYGON (ID 0.8 mm, OD 2.4 mm) tubing, respectively.

A1.3 Calibration of Wall Shear Stress in Microfluidic Device

The differential pressure across the inlet and outlet of the microfluidic device was set by placing the inlet reservoir on the microscope stage next to the device while lowering the outlet reservoir relative to the inlet reservoir to achieve a difference in height 'Δh'. A 1% suspension of yellow-

green 1 μm Fluoresbrite® microsphere beads in PBS was allowed to flow through the microfluidic device and the center-line velocity of the beads in the micro-channels was estimated by measuring the maximum bead velocity (*v*max) at H/2 (H = 30 μm is the height of the micro-channel) using fluorescence microscopy. Wall shear stress (τ in dyn cm-2) at a chosen differential pressure (Δh) was estimated as $\frac{4\,\eta v max}{H}$, where η is the viscosity of plasma (0.01 dynes cm^{-2}). All the observations were made at a physiological wall shear stress of 6 dyn cm-2 which was achieved with a Δh of 10.6 inches.

A1.4 Microfluidic Adhesion studies

Adhesion specificity was confirmed by either incubating the adhesion molecule or endothelial cells coated cover slips with function blocking Abs against P-selectin (1:500) and E-selectin (1:500) for 10 min at 37˚C/5% CO2 prior to their use in microfluidic assay. In some experiments, function blocking antibodies against Mac-1, LFA-1 and PSGL-1 were added to the blood (1:100) in the inlet reservoir followed by 10 min of incubation with mixing at room temperature prior to use in the microfluidic assay. Finally, the microfluidic device was placed on the heated stage set at 24˚ or 37˚C (Okolab, Ottaviano, Italy) of an inverted microscope and the blood was perfused through the micro-channels at a wall shear stress of 6 to 10 dyn cm-2. Observations were made in the perfusion chambers (30 μm high and 500 μm wide).

A1.5 qMFM Data analysis Guidelines

The following strategy was followed to record observations in adhesion molecule coated micro-channels.

Step-1: Neutrophils were allowed to roll, arrest and crawl for 2 min and observations were recorded in a field of view (FOV~14,520 μm^2) using qDF.

Step-2: After 2 min, the incident angle of the laser was reduced and the platelet-neutrophil interactions were observed in the same FOV for an additional 4 min.

Time series sequences of images were processed and analyzed using NIS-Elements Analysis Advanced Research software (Nikon). Image background was subtracted using the average intensity of a small region of the image background and platelets were identified using the spot detection algorithm available in NIS-Elements. The interacting platelets are marked with white circles. The spot-detection algorithm identifies only those platelets which slowdown to interact with arrested neutrophils and continues to track them until they detach and leave the FOV. Platelets are identified by defining a threshold based on the intensity and size of the bright spots. The final read-out is the number of interactions in a given observation period and the life-time of each interaction. Platelet-Neutrophil interactions were defined as following:

- A freely flowing platelet attaches to an arrested neutrophil → an interaction event.
- A freely flowing platelet aggregate attaches to an arrested neutrophil → an interaction event.
- A rolling neutrophil enters the FOV with a platelet attached to it → an interaction event.
- A platelet or an aggregate of platelets detaches from one neutrophil and attaches to another neutrophil → an interaction event.

A1.6 Function Blocking Studies on Platelet-Neutrophil Interactions

Antibody blocking studies were performed using a strategy that allowed inhibition of platelet-neutrophil interactions without causing detachment of arrested neutrophils. The blood was

perfused in the microfluidic micro-channels for 2 min, which allowed neutrophils to roll, arrest firmly and then interact with circulating platelets. Once the neutrophils were firmly arrested, platelet-neutrophil interactions were recorded using qMFM for the next 2 min. After 2 min of qMFM observations, the flow was stopped momentarily and function blocking was added to the blood in the reservoir. The flow was resumed and the effect on platelet-neutrophil interactions was assessed over the next 2 min.

A1.7 LPS Treatments

LPS treatment was conducted by incubating blood for 10 min with LPS at room temperature (22˚C) following the addition of fluorescent anti-CD16 and anti-CD49b Abs to stain neutrophils and platelets, respectively. Following incubation, blood was perfused through the micro-channels. Platelet-neutrophil interactions were visualized using both steps of qMFM as described in Chapter 2. Function blocking with anti-P-selectin monoclonal antibody, anti-GPIbα monoclonal antibody, anti-PSGL-1 monoclonal antibody (1:100 dilution), and/or anti-Mac-1 monoclonal antibodies or isotype control IgG1 antibody (1:100 dilution) post LPS incubation was performed as described above.

A1.8 Microscope Set up

Experiments were conducted using a Nikon Eclipse-Ti inverted microscope with a TIRF photoactivation unit (NIKON, Melville, NY). The microscope was equipped with a Zyla-5.5 sCMOS scientific camera (5.5 Megapixel resolution; maximum frame rate 100 s-1; ANDOR) and

a motorized Nikon Intensilight CHGFIE fiber illuminator as an epifluorescence source. Lasers were housed in a MLC Monolithic Laser combiner launch (Agilent Technologies) and included 405 nm, 488 nm, 560 nm, and 640 nm wavelength lasers. Observations were made using a CFI Apochromat TIRF 60x oil objective (NA 1.49) or CFI Plan Fluor ELWD 40x air objective (NA 0.60). The laser, camera, filters and other microscope functions were controlled using NIS-Elements software (Nikon) installed on a PC. NIS-Elements allowed sequential capture of green (FITC) and far red channel (Alexa Fluor 647) through a quad-filter by switching between the two lasers at a minimum interval of 10 ms which generated a dual color image every 20 ms.

A1.9 Scanning Electron Microscopy

Freshly collected whole blood was perfused over a rectangular coverslip coated with P-selectin, ICAM-1 and IL-8 in a custom PDMS vacuum chip at a wall shear stress of 6 dyn cm-2. Neutrophils were allowed to roll and arrest on the coverslip and interact with freely flowing platelets. Following a 3-minute perfusion, a cocktail of 16% paraformaldehyde and 2.5% glutaraldehyde was perfused through the micro-channels at the same shear stress (6 dyn cm^{-2}) to fix platelet-neutrophil interactions under flow. Finally, the vacuum was disabled and the coverslips were separated from the PDMS chip. Fixed cover slips were stored in the 1x PBS until used in electron microscopy. Coverslips were cut into small blocks ($8mm^3$) and washed 3 times in 1X PBS for 15 minutes each. Coverslips were then incubated in 1% OsO4 in 0.1 M PBS for 60 minutes, followed by 3 washes in 1X PBS for 15 minutes each. Cells were then dehydrated in graded series of alcohol (in PBS) for 15 minutes each: 30% ethanol, 50% ethanol, 70% ethanol, 90% ethanol, 100% ethanol x 3. Coverslips were then mounted onto studs, sputter coated with gold palladium and visualized using

a Field Emission Scanning Electron Microscope (JEOL JSM 6335F). When not in use coverslips are stored in desiccator.

A1.10 SEM Pseudocoloring

Scanning electron micrographs were pseudo-colored using Adobe Photoshop (Adobe Inc.). Images were duplicated and colored using the color table with corresponding colors to create multiple colorized images. Structures were then selected using the pencil tool and pasted on top of each other to create a multicolor SEM micrograph. Alignment of the structures was done using the move tool in Adobe Photoshop.

A1.11 Structured illumination microscopy

Freshly collected whole blood was perfused over a rectangular coverslip coated with P-selectin, ICAM-1 and IL-8 in a custom PDMS vacuum chip at a wall shear stress of 6 dyn cm^{-2}. Neutrophils were allowed to roll and arrest on the coverslip and interact with freely flowing platelets. Following a 3-minute perfusion, a cocktail of 16% paraformaldehyde and 2.5% glutaraldehyde was perfused through the micro-channels at the same shear stress (6 dyn cm^{-2}) to fix platelet-neutrophil interactions under flow. Finally, the vacuum was disabled and the coverslips were separated from the PDMS chip. Coverslips were washed with PBS (without Ca2+ and Mg2+) and permeabilized with 0.1% Triton X-100 in PBS for 15 minutes. Coverslips were again washed three times with PBS followed by three washes with PBS containing 0.5% BSA. Cells were then blocked with PBS containing 2% BSA for 45 minutes. Incubation with primary antibodies (1:1000 concentration) was conducted for 1 hour at room temperature followed by a wash 5x with PBS containing 0.5%

BSA. Coverslips were incubated with 1:1000 concentration of secondary antibodies and Cy3-Phalloidin for 1 hour at room temperature. Finally, coverslips were washed three times with PBS+0/5% BSA, and 4x with PBS, before being mounted to a glass slide with Gelvatol, and stored at 4ºC in the dark until imaging. Images were processed using NIS-Elements software.

A1.12 Confocal Microscopy Coverslip Processing

Coverslips were removed from PBS and permeabilized with 0.1% Triton-X 100 in PBS for 15 min and washed 5x in PBB (PBS containing 0.5% BSA). Cells were blocked in 20% goat serum for 45 min followed by 5 washes in PBB. Incubation with primary antibodies (1:1000 concentration) was conducted for 1 hour at room temperature. Coverslips were washed 5x in PBB followed by incubation with (1:1000 concentration) of secondary antibodies and Cy3-Phalloidin for 1 hour at room temperature. Samples were washed 3x in PBB followed by 4x in PBS and then mounted to slides using Gelvatol and imaged using Nikon A1R Spectral laser confocal microscope.

APPENDIX B

POLY-DI-METHYL-SILOXANE (PDMS) DEVICE PREPARATION

The following methods are used in the Sundd lab to prepare PDMS based microfluidic chips, coverslips and stoppers.

B1.1 Making microfluidic chips Mold using Silicon Wafer

To create chips using the silicon wafer, clean wafer with isopropanol, dry and coat with TMCS. To coat, place wafer in round dish uncovered and then place the dish in the Tupperware container under the fume hood. Grab a pipette and add ~1 mL of TMCS (chlorotrimethylsilane, 98%) into overturned lid in Tupperware container. Seal lid on Tupperware and allow to sit for 5 minutes. Grab a glass bowl and cover outside of bowl with foil to make imprint of bowl size. Cut extra foil and replace the bowl with the silicon wafer. Press in edges to make a square (be sure to not cover channels).

Mix PDMS in a small container with a ratio of 10:1 for elastomer to curing agent. Use either Sylgard 184 for experimental chips or P-4 when creating a permanent mold of the wafer. Put container on scale and pour in elastomer to desired weight. Zero scale and add curing agent at proper ratio. Place container on mixer for 10 minutes and then pour into 50 mL centrifuge tube. Centrifuge PDMS for 10 min at 300 g at 22C.

Pour PDMS onto wager in the aluminum foil and place in vacuum bowl to remove bubbles. Alternate between vacuum on and off until all bubbles are removed. After checking for any dust or contaminants in PDMS let sit overnight on level surface covered.

B1.3 Making Microfluidic chips using permanent Mold

Clean permanent mold with ethanol and dry with air hose to remove any dust. Mix Sylgard 184 in a small container with a ratio of 10:1 for elastomer to curing agent. Put container on scale and pour in elastomer to desired weight. Zero scale and add curing agent at proper ratio. Place container on mixer for 10 minutes and then pour into 50 mL centrifuge tube. Centrifuge PDMS for 10 min at 300 g at 22C. Pour PDMS into mold and place in vacuum bowl to remove bubbles. Alternate between vacuum on and off until all bubbles are removed. After checking for any dust or contaminants in PDMS let sit overnight on level surface covered. Gently remove wafer from PDMS using forceps and ethanol.

B1.4 Cutting and punching holes in finished chips from mold

Gently remove mold from either the silicon wafer or permanent mold. Take box cutting blade and carefully remove extra PDMS along outer edge of mold. Then carefully cut out each microfluidic chip without cutting into the vacuum channel. Chips should be rectangular based on shape of mold. Once cut clean each chip with ethanol and dry with air hose. Take duct tape and clean top and bottom of the chip to remove all dust. Store chips in clean dish until use.

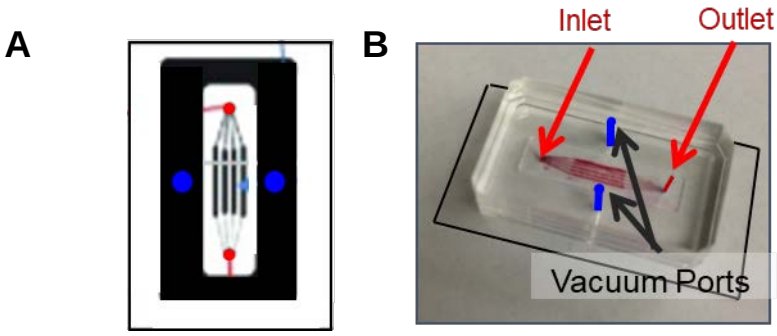

Figure 32: Schematic for punching holes in microfluidic chips. (A) overhead schematic of the microfluidic chip design. Red dots represent the inlet and outlet areas. Blue dots represent the area for the vacuum ports. (B) Image of completed microfluidic chip attached to a coverslip (outlined in black). Red arrows denote the inlet and outlet ports. Blue holes and lines denote the vacuum ports.

Take chips and place on mirror under a microscope. Grab a yellow tip needle (20 gauge) and punch holes for the inlet and outlet (Figure 32 red circles). Line up the hole with the small circle at the ends of the chip. Next grab a green tip needle (14 gauge) with the metal bottom to punch vacuum ports. Punch a hole on each side of the channels in the vacuum area (Figure 28, blue circles). Clean chips with ethanol and tape to remove all dust. Chips are ready to be used but need to be hydrophilic for experiments.

B1.5 Making Chips Hydrophilic

PDMS chips are hydrophobic following curing process and must be made hydrophilic to use in microfluidic experiments. To being prepare solution of Hepes Buffer and mPEG-SIL. Add 20 µL of Hepes Buffer to 980 µL of deionized water in a 1.5 mL Eppendorf. Weigh out 0.01 g mPEG-SIL and combine the two solutions, mixing thoroughly. Turn on Plasma Preen Reactor and grab a clean dish. Take 1 cleaned microfluidic chip, place on clean dish and plasma treat for 12s. Remove dish and add 50 µL of the solution onto the channels making sure the channels are completely covered. Set chip aside and repeat with remaining chips. Incubate chips for 1 hour with solution.

Following incubation rinse chip with water and then deionized water before drying. Clean with duct tape and set chips aside.

B1.6 Cleaning Microfluidic Chips

Use 1000 mL beaker with stir bar and add 0.01 N HCl in deionized water (800 mL DI water + 800 µL HCl). Place beaker on stirrer and heat to maximum heat with low level of spinning. Let run for 20 minutes or until boiling. Make sure chips do not touch bottom of the beaker or they will melt. Let cool and rinse with water and deionized water. Clean with duct tape and store in clean dish until use.

B1.7 Preparing PDMS coating wells

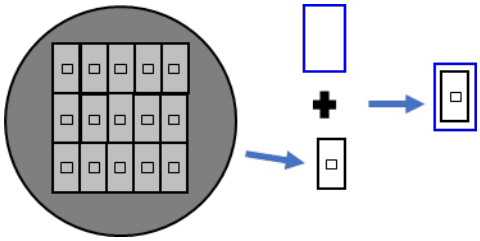

Figure 33: Schematic of Silicon wafer with PDMS layer. Each silicon wafer contains 15 rectangles. Using sharp razor individual rectangles are cut out and removed from wafer (black rectangle). Rectangular coverslips (blue) are cleaned with methanol and dried with air before being placed on the PDMS layer as shown in the far right.

Prepare Sylgard 184 PDMS as described above. Turn Spin coater on and allow time to warm up. Clean wafer with isopropanol and dry with air. Place Clean wafer on plate in spin coater. Pour half dollar size of mixed PDMS on wafer and place cover on spin coater. Run recipe 1 (5s ramp, 30s dwell – RPM 600). Remove coated part and place in plastic dish covered in oven for 30 minutes. Layer is now ready for use. Clean rectangular coverslips using methanol and dry with air (blue

rectangle). Cut out individual rectangles (black grey outlines) layers and place on mirror. Clean both sides of PDMS layer with tape and place on white paper. Gently place clean rectangular coverslip on top of PDMS layer. Turn coverslip over and remove any air bubbles using forceps. Once complete place coverslips in oven overnight to seal PDMS layer to wafer. Coverslips are ready for use.

B1.8 Making Connectors and round stoppers for microfluidic setup

Connectors and round stoppers utilize a soft PDMS **(**XP565**)** at a 10:1 ratio for elastomer to curing agent. Measure out the elastomer on scale until desired amount met. Add equal ratio of curing agent to the elastomer. Place container on mixer and mix for 1-2 minutes. Quickly pour into dish (large for connectors; small for round stoppers. Place in Plasma Preen reactor to use the vacuum to remove the bubbles. Plasma preen should only be used for vacuum. Alternate power of vacuum until all bubbles are removed. Soft PDMS will cure quickly so this must be done fast.

Connectors: Once PDMS is cured it can be used for microfluidics. To make connectors cut out small squares with the razor. Punch a hole through the middle with the yellow tip (30 gauge) needle. Connector is ready for use.

Stoppers: Round stoppers (Figure 34) are punched with a metal round puncher to fit on the top of a 1.5 mL Eppendorf. Next grab the yellow tip (30 gauge) needle and punch a hole through the stopper. Remove inner PDMS from the needle and carefully thread PE10 tubing through the needle tip. Bottom should be about 1.5 inches while the top of the stopper tubing should be cut to ~5inches in length. Remove yellow tip needle and grab green tip (17 gauge) needle. Punch hole next

Figure 34: Round stopper

to tubing and remove inner PDMS from the needle. Remove needle and carefully push through green tip needle tip with brown tubing through the hole.

BIBLIOGRAPHY

1. Bennewitz MF, Jimenez MA, Vats R, Tutuncuoglu E, Jonassaint J, Kato GJ, Gladwin MT, Sundd P. Lung vaso-occlusion in sickle cell disease mediated by arteriolar neutrophil-platelet microemboli. JCI Insight. 2017;2(1):e89761. doi: 10.1172/jci.insight.89761. PubMed PMID: 28097236.

2. Gladwin MT, Ofori-Acquah SF. Erythroid DAMPs drive inflammation in SCD. Blood. 2014;123(24):3689-90. doi: 10.1182/blood-2014-03-563874. PubMed PMID: 24926069; PMCID: 4055918.

3. Manwani D, Frenette PS. Vaso-occlusion in sickle cell disease: pathophysiology and novel targeted therapies. Blood. 2013;122(24):3892-8. doi: 10.1182/blood-2013-05-498311. PubMed PMID: 24052549; PMCID: 3854110.

4. Piel FB, Patil AP, Howes RE, Nyangiri OA, Gething PW, Dewi M, Temperley WH, Williams TN, Weatherall DJ, Hay SI. Global epidemiology of sickle haemoglobin in neonates: a contemporary geostatistical model-based map and population estimates. Lancet. 2013;381(9861):142-51. Epub 2012/10/30. doi: 10.1016/s0140-6736(12)61229-x. PubMed PMID: 23103089; PMCID: PMC3547249.

5. Rees DC, Williams TN, Gladwin MT. Sickle-cell disease. Lancet. 2010;376(9757):2018-31. doi: 10.1016/S0140-6736(10)61029-X. PubMed PMID: 21131035.

6. Gladwin MT, Sachdev V. Cardiovascular abnormalities in sickle cell disease. Journal of the American College of Cardiology. 2012;59(13):1123-33. doi: 10.1016/j.jacc.2011.10.900. PubMed PMID: 22440212; PMCID: 3881188.

7. Finnegan EM, Turhan A, Golan DE, Barabino GA. Adherent leukocytes capture sickle erythrocytes in an in vitro flow model of vaso-occlusion. Am J Hematol. 2007;82(4):266-75. doi: 10.1002/ajh.20819. PubMed PMID: 17094094.

8. Wun T, Styles L, DeCastro L, Telen MJ, Kuypers F, Cheung A, Kramer W, Flanner H, Rhee S, Magnani JL, Thackray H. Phase 1 study of the E-selectin inhibitor GMI 1070 in patients with sickle cell anemia. PloS one. 2014;9(7):e101301. Epub 2014/07/06. doi: 10.1371/journal.pone.0101301. PubMed PMID: 24988449; PMCID: PMC4079300.

9. Barabino GA, Platt MO, Kaul DK. Sickle cell biomechanics. Annual review of biomedical engineering. 2010;12:345-67. doi: 10.1146/annurev-bioeng-070909-105339. PubMed PMID: 20455701.

10. Piel FB, Steinberg MH, Rees DC. Sickle Cell Disease. N Engl J Med. 2017;376(16):1561-73. Epub 2017/04/20. doi: 10.1056/NEJMra1510865. PubMed PMID: 28423290.

11. Global Burden of Disease Study C. Global, regional, and national incidence, prevalence, and years lived with disability for 301 acute and chronic diseases and injuries in 188 countries, 1990-2013: a systematic analysis for the Global Burden of Disease Study 2013. Lancet. 2015;386(9995):743-800. doi: 10.1016/S0140-6736(15)60692-4. PubMed PMID: 26063472; PMCID: PMC4561509.

12. Kaul DK, Finnegan E, Barabino GA. Sickle red cell-endothelium interactions. Microcirculation. 2009;16(1):97-111. doi: 10.1080/10739680802279394. PubMed PMID: 18720225; PMCID: 3059190.

13. Helms CC, Marvel M, Zhao W, Stahle M, Vest R, Kato GJ, Lee JS, Christ G, Gladwin MT, Hantgan RR, Kim-Shapiro DB. Mechanisms of hemolysis-associated platelet activation. J Thromb Haemost. 2013;11(12):2148-54. doi: Doi 10.1111/Jth.12422. PubMed PMID: WOS:000328003900009.

14. Holtzclaw JD, Jack D, Aguayo SM, Eckman JR, Roman J, Hsu LL. Enhanced pulmonary and systemic response to endotoxin in transgenic sickle mice. American journal of respiratory and critical care medicine. 2004;169(6):687-95. doi: 10.1164/rccm.200302-224OC. PubMed PMID: 14684557.

15. Tantawy AA, Adly AA, Ismail EA, Habeeb NM, Farouk A. Circulating platelet and erythrocyte microparticles in young children and adolescents with sickle cell disease: Relation to cardiovascular complications. Platelets. 2013;24(8):605-14. doi: 10.3109/09537104.2012.749397. PubMed PMID: 23249216.

16. Kauf TL, Coates TD, Huazhi L, Mody-Patel N, Hartzema AG. The cost of health care for children and adults with sickle cell disease. Am J Hematol. 2009;84(6):323-7. Epub 2009/04/10. doi: 10.1002/ajh.21408. PubMed PMID: 19358302.

17. Chang J, Patton JT, Sarkar A, Ernst B, Magnani JL, Frenette PS. GMI-1070, a novel pan-selectin antagonist, reverses acute vascular occlusions in sickle cell mice. Blood. 2010;116(10):1779-86. Epub 2010/05/29. doi: 10.1182/blood-2009-12-260513. PubMed PMID: 20508165; PMCID: Pmc2947397.

18. Curtis SA, Danda N, Etzion Z, Cohen HW, Billett HH. Elevated Steady State WBC and Platelet Counts Are Associated with Frequent Emergency Room Use in Adults with Sickle Cell Anemia. PLoS One. 2015;10(8):e0133116. doi: 10.1371/journal.pone.0133116. PubMed PMID: 26248283; PMCID: 4527736.

19. Kolaczkowska E, Kubes P. Neutrophil recruitment and function in health and inflammation. Nature reviews Immunology. 2013;13(3):159-75. doi: 10.1038/nri3399. PubMed PMID: 23435331.

20. Hall JE. Guyton and Hall textbook of medical physiology [still image]. Philadelphia, PA: Elsevier,; 2016.

21. Mankan AK, Dau T, Jenne D, Hornung V. The NLRP3/ASC/Caspase-1 axis regulates IL-1beta processing in neutrophils. Eur J Immunol. 2012;42(3):710-5. doi: 10.1002/eji.201141921. PubMed PMID: 22213227.

22. Sreeramkumar V, Adrover JM, Ballesteros I, Cuartero MI, Rossaint J, Bilbao I, Nacher M, Pitaval C, Radovanovic I, Fukui Y, McEver RP, Filippi MD, Lizasoain I, Ruiz-Cabello J, Zarbock A, Moro MA, Hidalgo A. Neutrophils scan for activated platelets to initiate inflammation. Science. 2014;346(6214):1234-8. doi: 10.1126/science.1256478. PubMed PMID: 25477463; PMCID: PMC4280847.

23. Li J, Kim K, Hahm E, Molokie R, Hay N, Gordeuk VR, Du X, Cho J. Neutrophil AKT2 regulates heterotypic cell-cell interactions during vascular inflammation. J Clin Invest. 2014;124(4):1483-96. doi: 10.1172/JCI72305. PubMed PMID: 24642468; PMCID: 3973084.

24. Ortiz-Munoz G, Mallavia B, Bins A, Headley M, Krummel MF, Looney MR. Aspirin-triggered 15-epi-lipoxin A4 regulates neutrophil-platelet aggregation and attenuates acute lung injury in mice. Blood. 2014;124(17):2625-34. Epub 2014/08/22. doi: 10.1182/blood-2014-03-562876. PubMed PMID: 25143486; PMCID: PMC4208278.

25. Dominical VM, Samsel L, Nichols JS, Costa FF, McCoy JP, Jr., Conran N, Kato GJ. Prominent role of platelets in the formation of circulating neutrophil-red cell heterocellular aggregates in sickle cell anemia. Haematologica. 2014;99(11):e214-7. doi: 10.3324/haematol.2014.108555. PubMed PMID: 25420284; PMCID: 4222482.

26. Polanowska-Grabowska R, Wallace K, Field JJ, Chen L, Marshall MA, Figler R, Gear AR, Linden J. P-selectin-mediated platelet-neutrophil aggregate formation activates neutrophils in mouse and human sickle cell disease. Arterioscler Thromb Vasc Biol. 2010;30(12):2392-9. doi: 10.1161/ATVBAHA.110.211615. PubMed PMID: 21071696; PMCID: 3058044.

27. Sundd P, Pospieszalska MK, Cheung LS, Konstantopoulos K, Ley K. Biomechanics of leukocyte rolling. Biorheology. 2011;48(1):1-35. doi: 10.3233/BIR-2011-0579. PubMed PMID: 21515934; PMCID: 3103268.

28. Sundd P, Pospieszalska MK, Ley K. Neutrophil rolling at high shear: flattening, catch bond behavior, tethers and slings. Molecular immunology. 2013;55(1):59-69. doi: 10.1016/j.molimm.2012.10.025. PubMed PMID: 23141302; PMCID: 3601566.

29. Zhang D, Xu C, Manwani D, Frenette PS. Neutrophils, platelets, and inflammatory pathways at the nexus of sickle cell disease pathophysiology. Blood. 2016;127(7):801-9. doi: 10.1182/blood-2015-09-618538. PubMed PMID: 26758915; PMCID: PMC4760086.

30. Sundd P, Gutierrez E, Petrich BG, Ginsberg MH, Groisman A, Ley K. Live cell imaging of paxillin in rolling neutrophils by dual-color quantitative dynamic footprinting. Microcirculation. 2011;18(5):361-72. doi: 10.1111/j.1549-8719.2011.00090.x. PubMed PMID: 21418380; PMCID: 3123727.

31. McEver RP, Zhu C. Rolling cell adhesion. Annual review of cell and developmental biology. 2010;26:363-96. doi: 10.1146/annurev.cellbio.042308.113238. PubMed PMID: 19575676; PMCID: 3557855.

32. Montes RA, Eckman JR, Hsu LL, Wick TM. Sickle erythrocyte adherence to endothelium at low shear: role of shear stress in propagation of vaso-occlusion. Am J Hematol. 2002;70(3):216-27. doi: 10.1002/ajh.10145. PubMed PMID: 12111767.

33. Sundd P, Gutierrez E, Pospieszalska MK, Zhang H, Groisman A, Ley K. Quantitative dynamic footprinting microscopy reveals mechanisms of neutrophil rolling. Nature methods. 2010;7(10):821-4. doi: 10.1038/nmeth.1508. PubMed PMID: 20871617; PMCID: 2967732.

34. Hottz ED, Monteiro AP, Bozza FA, Bozza PT. Inflammasome in platelets: allying coagulation and inflammation in infectious and sterile diseases? Mediators Inflamm. 2015;2015:435783. doi: 10.1155/2015/435783. PubMed PMID: 25814789; PMCID: PMC4357129.

35. Dutra FF, Bozza MT. Heme on innate immunity and inflammation. Front Pharmacol. 2014;5:115. doi: 10.3389/fphar.2014.00115. PubMed PMID: 24904418; PMCID: PMC4035012.

36. Sutterwala FS, Haasken S, Cassel SL. Mechanism of NLRP3 inflammasome activation. Ann N Y Acad Sci. 2014;1319:82-95. doi: 10.1111/nyas.12458. PubMed PMID: 24840700; PMCID: PMC4074217.

37. Guo H, Callaway JB, Ting JP. Inflammasomes: mechanism of action, role in disease, and therapeutics. Nat Med. 2015;21(7):677-87. doi: 10.1038/nm.3893. PubMed PMID: 26121197; PMCID: PMC4519035.

38. Hottz ED, Lopes JF, Freitas C, Valls-de-Souza R, Oliveira MF, Bozza MT, Da Poian AT, Weyrich AS, Zimmerman GA, Bozza FA, Bozza PT. Platelets mediate increased endothelium permeability in dengue through NLRP3-inflammasome activation. Blood. 2013;122(20):3405-14. doi: 10.1182/blood-2013-05-504449. PubMed PMID: 24009231; PMCID: PMC3829114.

39. Shashkin PN, Brown GT, Ghosh A, Marathe GK, McIntyre TM. Lipopolysaccharide is a direct agonist for platelet RNA splicing. J Immunol. 2008;181(5):3495-502. PubMed PMID: 18714022; PMCID: PMC2551315.

40. Brown GT, McIntyre TM. Lipopolysaccharide signaling without a nucleus: kinase cascades stimulate platelet shedding of proinflammatory IL-1beta-rich microparticles. J Immunol. 2011;186(9):5489-96. doi: 10.4049/jimmunol.1001623. PubMed PMID: 21430222; PMCID: PMC3100655.

41. Tomer A, Harker LA, Kasey S, Eckman JR. Thrombogenesis in sickle cell disease. J Lab Clin Med. 2001;137(6):398-407. doi: 10.1067/mlc.2001.115450. PubMed PMID: 11385360.

42. Ataga KI, Kutlar A, Kanter J, Liles D, Cancado R, Friedrisch J, Guthrie TH, Knight-Madden J, Alvarez OA, Gordeuk VR, Gualandro S, Colella MP, Smith WR, Rollins SA, Stocker JW, Rother RP. Crizanlizumab for the Prevention of Pain Crises in Sickle Cell Disease. N Engl J Med. 2016. doi: 10.1056/NEJMoa1611770. PubMed PMID: 27959701.

43. Ware RE, de Montalembert M, Tshilolo L, Abboud MR. Sickle cell disease. Lancet. 2017;390(10091):311-23. Epub 2017/02/06. doi: 10.1016/s0140-6736(17)30193-9. PubMed PMID: 28159390.

44. Wilmore DW. Food and Drug Administration Approval of Glutamine for Sickle Cell Disease: Success and Precautions in Glutamine Research. JPEN Journal of parenteral and enteral nutrition. 2017;41(6):912-7. Epub 2017/09/01. doi: 10.1177/0148607117727271. PubMed PMID: 28858569.

45. Tammara BK, Plotka A, Shafer FE, Readett DRJ, Riley S, Korth-Bradley JM. Lack of Effect of Rivipansel on QTc Interval in Healthy Adult African American Male Subjects. Journal of clinical pharmacology. 2017;57(10):1315-21. Epub 2017/05/17. doi: 10.1002/jcph.924. PubMed PMID: 28510346.

46. Telen MJ, Wun T, McCavit TL, De Castro LM, Krishnamurti L, Lanzkron S, Hsu LL, Smith WR, Rhee S, Magnani JL, Thackray H. Randomized phase 2 study of GMI-1070 in SCD: reduction in time to resolution of vaso-occlusive events and decreased opioid use. Blood. 2015;125(17):2656-64. Epub 2015/03/04. doi: 10.1182/blood-2014-06-583351. PubMed PMID: 25733584; PMCID: PMC4408290.

47. Telen MJ. Beyond hydroxyurea: new and old drugs in the pipeline for sickle cell disease. Blood. 2016;127(7):810-9. doi: 10.1182/blood-2015-09-618553. PubMed PMID: 26758919; PMCID: PMC4760087.

48. Manwani D, Chen G, Carullo V, Serban S, Olowokure O, Jang J, Huggins M, Cohen HW, Billett H, Atweh GF, Frenette PS, Shi PA. Single-dose intravenous gammaglobulin can stabilize neutrophil Mac-1 activation in sickle cell pain crisis. Am J Hematol. 2015;90(5):381-5. Epub 2015/01/24. doi: 10.1002/ajh.23956. PubMed PMID: 25616042; PMCID: PMC4409477.

49. Conran N, Rees DC. Prasugrel hydrochloride for the treatment of sickle cell disease. Expert Opin Investig Drugs. 2017;26(7):865-72. doi: 10.1080/13543784.2017.1335710. PubMed PMID: 28562105.

50. Dominical VM, Vital DM, O'Dowd F, Saad ST, Costa FF, Conran N. In vitro microfluidic model for the study of vaso-occlusive processes. Exp Hematol. 2015;43(3):223-8. doi: 10.1016/j.exphem.2014.10.015. PubMed PMID: 25461252.

51. Wood DK, Soriano A, Mahadevan L, Higgins JM, Bhatia SN. A biophysical indicator of vaso-occlusive risk in sickle cell disease. Science translational medicine. 2012;4(123):123ra26. doi: 10.1126/scitranslmed.3002738. PubMed PMID: 22378926; PMCID: 3633235.

52. Tsai M, Kita A, Leach J, Rounsevell R, Huang JN, Moake J, Ware RE, Fletcher DA, Lam WA. In vitro modeling of the microvascular occlusion and thrombosis that occur in hematologic diseases using microfluidic technology. J Clin Invest. 2012;122(1):408-18. doi: 10.1172/JCI58753. PubMed PMID: 22156199; PMCID: 3248292.

53. Hidalgo A, Chang J, Jang JE, Peired AJ, Chiang EY, Frenette PS. Heterotypic interactions enabled by polarized neutrophil microdomains mediate thromboinflammatory injury. Nat Med. 2009;15(4):384-91. doi: 10.1038/nm.1939. PubMed PMID: 19305412; PMCID: 2772164.

54. Jenne CN, Wong CH, Petri B, Kubes P. The use of spinning-disk confocal microscopy for the intravital analysis of platelet dynamics in response to systemic and local inflammation. PloS one. 2011;6(9):e25109. Epub 2011/09/29. doi: 10.1371/journal.pone.0025109. PubMed PMID: 21949865; PMCID: PMC3176312.

55. Yipp BG, Petri B, Salina D, Jenne CN, Scott BN, Zbytnuik LD, Pittman K, Asaduzzaman M, Wu K, Meijndert HC, Malawista SE, de Boisfleury Chevance A, Zhang K, Conly J, Kubes P. Infection-induced NETosis is a dynamic process involving neutrophil multitasking in vivo. Nat Med. 2012;18(9):1386-93. Epub 2012/08/28. doi: 10.1038/nm.2847. PubMed PMID: 22922410; PMCID: PMC4529131.

56. Sundd P, Ley K. Quantitative dynamic footprinting microscopy. Immunology and cell biology. 2013;91(4):311-20. doi: 10.1038/icb.2012.84. PubMed PMID: 23478358.

57. Damiano ER, Westheider J, Tozeren A, Ley K. Variation in the velocity, deformation, and adhesion energy density of leukocytes rolling within venules. Circ Res. 1996;79(6):1122-30. PubMed PMID: 8943950.

58. Sundd P, Gutierrez E, Koltsova EK, Kuwano Y, Fukuda S, Pospieszalska MK, Groisman A, Ley K. 'Slings' enable neutrophil rolling at high shear. Nature. 2012;488(7411):399-403. doi: 10.1038/nature11248. PubMed PMID: 22763437; PMCID: 3433404.

59. Miller AC, Gladwin MT. Pulmonary complications of sickle cell disease. American journal of respiratory and critical care medicine. 2012;185(11):1154-65. doi: 10.1164/rccm.201111-2082CI. PubMed PMID: 22447965; PMCID: 3373067.

60. Jimenez MA, Tutuncuoglu E, Barge S, Novelli EM, Sundd P. Quantitative microfluidic fluorescence microscopy to study vaso-occlusion in Sickle Cell Disease. Haematologica. 2015. doi: 10.3324/haematol.2015.126631. PubMed PMID: 25975836.

61. Koltsova EK, Sundd P, Zarpellon A, Ouyang H, Mikulski Z, Zampolli A, Ruggeri ZM, Ley K. Genetic deletion of platelet glycoprotein Ib alpha but not its extracellular domain protects from atherosclerosis. Thromb Haemost. 2014;112(6):1252-63. Epub 2014/08/12. doi: 10.1160/th14-02-0130. PubMed PMID: 25104056; PMCID: PMC4429870.

62. Anea CB, Lyon M, Lee IA, Gonzales JN, Adeyemi A, Falls G, Kutlar A, Brittain JE. Pulmonary platelet thrombi and vascular pathology in acute chest syndrome in patients

with sickle cell disease. Am J Hematol. 2016;91(2):173-8. doi: 10.1002/ajh.24224. PubMed PMID: 26492581; PMCID: PMC4724297.

63. Frelinger AL, 3rd, Jakubowski JA, Brooks JK, Carmichael SL, Berny-Lang MA, Barnard MR, Heeney MM, Michelson AD. Platelet activation and inhibition in sickle cell disease (pains) study. Platelets. 2014;25(1):27-35. doi: 10.3109/09537104.2013.770136. PubMed PMID: 23469943.

64. Belcher JD, Chen C, Nguyen J, Milbauer L, Abdulla F, Alayash AI, Smith A, Nath KA, Hebbel RP, Vercellotti GM. Heme triggers TLR4 signaling leading to endothelial cell activation and vaso-occlusion in murine sickle cell disease. Blood. 2014;123(3):377-90. doi: 10.1182/blood-2013-04-495887. PubMed PMID: 24277079; PMCID: 3894494.

65. Ghosh S, Adisa OA, Chappa P, Tan F, Jackson KA, Archer DR, Ofori-Acquah SF. Extracellular hemin crisis triggers acute chest syndrome in sickle mice. J Clin Invest. 2013;123(11):4809-20. doi: 10.1172/JCI64578. PubMed PMID: 24084741; PMCID: 3809772.

66. Chen G, Zhang D, Fuchs TA, Manwani D, Wagner DD, Frenette PS. Heme-induced neutrophil extracellular traps contribute to the pathogenesis of sickle cell disease. Blood. 2014;123(24):3818-27. doi: 10.1182/blood-2013-10-529982. PubMed PMID: 24620350; PMCID: PMC4055928.

67. Cardenes N, Corey C, Geary L, Jain S, Zharikov S, Barge S, Novelli EM, Shiva S. Platelet bioenergetic screen in sickle cell patients reveals mitochondrial complex V inhibition, which contributes to platelet activation. Blood. 2014;123(18):2864-72. doi: 10.1182/blood-2013-09-529420. PubMed PMID: 24677541; PMCID: PMC4007612.

68. Zhang D, Chen G, Manwani D, Mortha A, Xu C, Faith JJ, Burk RD, Kunisaki Y, Jang JE, Scheiermann C, Merad M, Frenette PS. Neutrophil ageing is regulated by the microbiome. Nature. 2015;525(7570):528-32. doi: 10.1038/nature15367. PubMed PMID: 26374999; PMCID: PMC4712631.

69. Gladwin MT, Vichinsky E. Pulmonary complications of sickle cell disease. N Engl J Med. 2008;359(21):2254-65. doi: 10.1056/NEJMra0804411. PubMed PMID: 19020327.

70. Vichinsky EP, Neumayr LD, Earles AN, Williams R, Lennette ET, Dean D, Nickerson B, Orringer E, McKie V, Bellevue R, Daeschner C, Manci EA. Causes and outcomes of the acute chest syndrome in sickle cell disease. National Acute Chest Syndrome Study Group. N Engl J Med. 2000;342(25):1855-65. doi: 10.1056/NEJM200006223422502. PubMed PMID: 10861320.

71. Strouse JJ, Reller ME, Bundy DG, Amoako M, Cancio M, Han RN, Valsamakis A, Casella JF. Severe pandemic H1N1 and seasonal influenza in children and young adults with sickle cell disease. Blood. 2010;116(18):3431-4. doi: 10.1182/blood-2010-05-282194. PubMed PMID: 20656929; PMCID: PMC2981471.

72. Global, regional, and national age-sex specific all-cause and cause-specific mortality for 240 causes of death, 1990-2013: a systematic analysis for the Global Burden of Disease Study 2013. Lancet. 2015;385(9963):117-71. Epub 2014/12/23. doi: 10.1016/s0140-6736(14)61682-2. PubMed PMID: 25530442; PMCID: PMC4340604.

73. Elmariah H, Garrett ME, De Castro LM, Jonassaint JC, Ataga KI, Eckman JR, Ashley-Koch AE, Telen MJ. Factors associated with survival in a contemporary adult sickle cell disease cohort. Am J Hematol. 2014;89(5):530-5. doi: 10.1002/ajh.23683. PubMed PMID: 24478166; PMCID: PMC3988218.

74. Kutlar A, Ataga KI, McMahon L, Howard J, Galacteros F, Hagar W, Vichinsky E, Cheung AT, Matsui N, Embury SH. A potent oral P-selectin blocking agent improves microcirculatory blood flow and a marker of endothelial cell injury in patients with sickle cell disease. Am J Hematol. 2012;87(5):536-9. doi: 10.1002/ajh.23147. PubMed PMID: 22488107.

75. Mandarino D, Kawar Z, Alvarez R, Falconer D, Rollins SA, Rother RP. Placebo-Controlled, Double-Blind, First-In-Human, Ascending Single Dose and Multiple Dose, Healthy Subject Study Of Intravenous-Administered SelG1, a Humanized Anti-P-Selectin Antibody In Development For Sickle Cell Disease. Blood. 2013;122(21):970-.

76. Miller ST, Sleeper LA, Pegelow CH, Enos LE, Wang WC, Weiner SJ, Wethers DL, Smith J, Kinney TR. Prediction of adverse outcomes in children with sickle cell disease. N Engl J Med. 2000;342(2):83-9. doi: 10.1056/NEJM200001133420203. PubMed PMID: 10631276.

77. Simon DI, Chen Z, Xu H, Li CQ, Dong J, McIntire LV, Ballantyne CM, Zhang L, Furman MI, Berndt MC, Lopez JA. Platelet glycoprotein ibalpha is a counterreceptor for the leukocyte integrin Mac-1 (CD11b/CD18). J Exp Med. 2000;192(2):193-204. PubMed PMID: 10899906; PMCID: PMC2193258.

78. McEwan PA, Andrews RK, Emsley J. Glycoprotein Ibalpha inhibitor complex structure reveals a combined steric and allosteric mechanism of von Willebrand factor antagonism. Blood. 2009;114(23):4883-5. doi: 10.1182/blood-2009-05-224170. PubMed PMID: 19726719.

79. Chen J, Zhou H, Diacovo A, Zheng XL, Emsley J, Diacovo TG. Exploiting the kinetic interplay between GPIbalpha-VWF binding interfaces to regulate hemostasis and thrombosis. Blood. 2014;124(25):3799-807. doi: 10.1182/blood-2014-04-569392. PubMed PMID: 25293780; PMCID: PMC4263987.

80. Benard SA, Smith TM, Cunningham K, Jacob J, DeSilva T, Lin L, Shaw GD, Kriz R, Kelleher KS. Identification of peptide antagonists to glycoprotein Ibalpha that selectively inhibit von Willebrand factor dependent platelet aggregation. Biochemistry. 2008;47(16):4674-82. doi: 10.1021/bi702428q. PubMed PMID: 18363340.

81. Chen J, Hobbs WE, Le J, Lenting PJ, de Groot PG, Lopez JA. The rate of hemolysis in sickle cell disease correlates with the quantity of active von Willebrand factor in the

plasma. Blood. 2011;117(13):3680-3. Epub 2011/02/09. doi: 10.1182/blood-2010-08-302539. PubMed PMID: 21300978; PMCID: PMC3072883.

82. Mortality GBD, Causes of Death C. Global, regional, and national age-sex specific all-cause and cause-specific mortality for 240 causes of death, 1990-2013: a systematic analysis for the Global Burden of Disease Study 2013. Lancet. 2015;385(9963):117-71. doi: 10.1016/S0140-6736(14)61682-2. PubMed PMID: 25530442; PMCID: 4340604.

83. Frenette PS, Atweh GF. Sickle cell disease: old discoveries, new concepts, and future promise. J Clin Invest. 2007;117(4):850-8. doi: 10.1172/JCI30920. PubMed PMID: 17404610; PMCID: PMC1838946.

84. Chaturvedi S, Ghafuri DL, Glassberg J, Kassim AA, Rodeghier M, DeBaun MR. Rapidly progressive acute chest syndrome in individuals with sickle cell anemia: a distinct acute chest syndrome phenotype. Am J Hematol. 2016;91(12):1185-90. doi: 10.1002/ajh.24539. PubMed PMID: 27543812.

85. Kato GJ, Steinberg MH, Gladwin MT. Intravascular hemolysis and the pathophysiology of sickle cell disease. J Clin Invest. 2017;127(3):750-60. Epub 2017/03/02. doi: 10.1172/jci89741. PubMed PMID: 28248201; PMCID: PMC5330745.

86. !!! INVALID CITATION !!! (59, 69-71).

87. Jimenez MA, Tutuncuoglu E, Barge S, Novelli EM, Sundd P. Quantitative microfluidic fluorescence microscopy to study vaso-occlusion in sickle cell disease. Haematologica. 2015;100(10):e390-3. doi: 10.3324/haematol.2015.126631. PubMed PMID: 25975836; PMCID: 4591772.

88. Jimenez MA, Novelli EM, Shaw GD, Sundd P. Glycoprotein Ib alpha inhibitor (CCP-224) prevents neutrophil-platelet aggregation in sickle cell disease. Blood Adv. 2017;1(20):1712-6. doi: 10.1182/bloodadvances.2017006742. PubMed PMID: WOS:000410489200011.

89. Damiano ER, Westheider J, Tozeren A, Ley K. Variation in the velocity, deformation, and adhesion energy density of leukocytes rolling within venules. Circ Res. 1996;79(6):1122-30. PubMed PMID: 8943950.

90. Sundd P, Gutierrez E, Pospieszalska MK, Zhang H, Groisman A, Ley K. Quantitative dynamic footprinting microscopy reveals mechanisms of neutrophil rolling. Nature Methods. 2010;7(10):821-4. Epub 2010/09/28. doi: 10.1038/nmeth.1508. PubMed PMID: 20871617; PMCID: 2967732.

91. Nesbitt WS, Westein E, Tovar-Lopez FJ, Tolouei E, Mitchell A, Fu J, Carberry J, Fouras A, Jackson SP. A shear gradient-dependent platelet aggregation mechanism drives thrombus formation. Nat Med. 2009;15(6):665-73. doi: 10.1038/nm.1955. PubMed PMID: 19465929.

92. Sundd P, Pospieszalska MK, Ley K. Neutrophil rolling at high shear: Flattening, catch bond behavior, tethers and slings. Mol Immunol. 2012. Epub 2012/11/13. doi: 10.1016/j.molimm.2012.10.025. PubMed PMID: 23141302.

93. Elliott EI, Sutterwala FS. Initiation and perpetuation of NLRP3 inflammasome activation and assembly. Immunol Rev. 2015;265(1):35-52. doi: 10.1111/imr.12286. PubMed PMID: 25879282; PMCID: PMC4400874.

94. Nakahira K, Haspel JA, Rathinam VA, Lee SJ, Dolinay T, Lam HC, Englert JA, Rabinovitch M, Cernadas M, Kim HP, Fitzgerald KA, Ryter SW, Choi AM. Autophagy proteins regulate innate immune responses by inhibiting the release of mitochondrial DNA mediated by the NALP3 inflammasome. Nat Immunol. 2011;12(3):222-30. doi: 10.1038/ni.1980. PubMed PMID: 21151103; PMCID: PMC3079381.

95. Sokolovska A, Becker CE, Ip WK, Rathinam VA, Brudner M, Paquette N, Tanne A, Vanaja SK, Moore KJ, Fitzgerald KA, Lacy-Hulbert A, Stuart LM. Activation of caspase-1 by the NLRP3 inflammasome regulates the NADPH oxidase NOX2 to control phagosome function. Nat Immunol. 2013;14(6):543-53. doi: 10.1038/ni.2595. PubMed PMID: 23644505; PMCID: PMC3708594.

96. Vichinsky EP, Styles LA, Colangelo LH, Wright EC, Castro O, Nickerson B. Acute chest syndrome in sickle cell disease: clinical presentation and course. Cooperative Study of Sickle Cell Disease. Blood. 1997;89(5):1787-92. PubMed PMID: 9057664.

97. Novelli EM, Gladwin MT. Crises in Sickle Cell Disease. Chest. 2016;149(4):1082-93. doi: 10.1016/j.chest.2015.12.016. PubMed PMID: 26836899.

98. Alhandalous CH, Han J, Hsu L, Gowhari M, Hassan J, Molokie R, Abbasi TA, Gordeuk VR. Platelets decline during Vaso-occlusive crisis as a predictor of acute chest syndrome in sickle cell disease. Am J Hematol. 2015;90(12):E228-9. doi: 10.1002/ajh.24214. PubMed PMID: 26453077.

99. Mekontso Dessap A, Deux JF, Abidi N, Lavenu-Bombled C, Melica G, Renaud B, Godeau B, Adnot S, Brochard L, Brun-Buisson C, Galacteros F, Rahmouni A, Habibi A, Maitre B. Pulmonary artery thrombosis during acute chest syndrome in sickle cell disease. American journal of respiratory and critical care medicine. 2011;184(9):1022-9. doi: 10.1164/rccm.201105-0783OC. PubMed PMID: 21836136.

100. Man SM, Kanneganti TD. Regulation of inflammasome activation. Immunol Rev. 2015;265(1):6-21. doi: 10.1111/imr.12296. PubMed PMID: 25879280; PMCID: PMC4400844.

101. Brown GT, Narayanan P, Li W, Silverstein RL, McIntyre TM. Lipopolysaccharide stimulates platelets through an IL-1beta autocrine loop. J Immunol. 2013;191(10):5196-203. doi: 10.4049/jimmunol.1300354. PubMed PMID: 24081990; PMCID: PMC3818355.

102. Eckly A, Rinckel JY, Proamer F, Ulas N, Joshi S, Whiteheart SW, Gachet C. Respective contributions of single and compound granule fusion to secretion by activated platelets.

Blood. 2016;128(21):2538-49. doi: 10.1182/blood-2016-03-705681. PubMed PMID: 27625359.

103. Ataga KI, Kutlar A, Kanter J, Liles D, Cancado R, Friedrisch J, Guthrie TH, Knight-Madden J, Alvarez OA, Gordeuk VR, Gualandro S, Colella MP, Smith WR, Rollins SA, Stocker JW, Rother RP. Crizanlizumab for the Prevention of Pain Crises in Sickle Cell Disease. N Engl J Med. 2017;376(5):429-39. Epub 2016/12/14. doi: 10.1056/NEJMoa1611770. PubMed PMID: 27959701; PMCID: PMC5481200.

104. Fleischmann RM, Tesser J, Schiff MH, Schechtman J, Burmester GR, Bennett R, Modafferi D, Zhou L, Bell D, Appleton B. Safety of extended treatment with anakinra in patients with rheumatoid arthritis. Ann Rheum Dis. 2006;65(8):1006-12. doi: 10.1136/ard.2005.048371. PubMed PMID: 16396977; PMCID: PMC1798263.

105. Lachmann HJ, Kone-Paut I, Kuemmerle-Deschner JB, Leslie KS, Hachulla E, Quartier P, Gitton X, Widmer A, Patel N, Hawkins PN, Canakinumab in CSG. Use of canakinumab in the cryopyrin-associated periodic syndrome. The New England journal of medicine. 2009;360(23):2416-25. doi: 10.1056/NEJMoa0810787. PubMed PMID: 19494217.

106. Ballas SK, Lieff S, Benjamin LJ, Dampier CD, Heeney MM, Hoppe C, Johnson CS, Rogers ZR, Smith-Whitley K, Wang WC, Telen MJ, Investigators CSCC. Definitions of the phenotypic manifestations of sickle cell disease. Am J Hematol. 2010;85(1):6-13. doi: 10.1002/ajh.21550. PubMed PMID: 19902523.

107. Pawlowski CL, Li W, Sun M, Ravichandran K, Hickman D, Kos C, Kaur G, Sen Gupta A. Platelet microparticle-inspired clot-responsive nanomedicine for targeted fibrinolysis. Biomaterials. 2017;128:94-108. doi: 10.1016/j.biomaterials.2017.03.012. PubMed PMID: 28314136.

108. Wallace KL, Linden J. Adenosine A2A receptors induced on iNKT and NK cells reduce pulmonary inflammation and injury in mice with sickle cell disease. Blood. 2010;116(23):5010-20. doi: 10.1182/blood-2010-06-290643. PubMed PMID: 20798237; PMCID: PMC3012594.

109. Chantrathammachart P, Mackman N, Sparkenbaugh E, Wang JG, Parise LV, Kirchhofer D, Key NS, Pawlinski R. Tissue factor promotes activation of coagulation and inflammation in a mouse model of sickle cell disease. Blood. 2012;120(3):636-46. doi: 10.1182/blood-2012-04-424143. PubMed PMID: 22661702; PMCID: PMC3401215.

110. Zennadi R. MEK inhibitors, novel anti-adhesive molecules, reduce sickle red blood cell adhesion in vitro and in vivo, and vasoocclusion in vivo. PloS one. 2014;9(10):e110306. doi: 10.1371/journal.pone.0110306. PubMed PMID: 25330306; PMCID: PMC4203776.

111. Hattori R, Hamilton KK, Fugate RD, McEver RP, Sims PJ. Stimulated secretion of endothelial von Willebrand factor is accompanied by rapid redistribution to the cell surface of the intracellular granule membrane protein GMP-140. J Biol Chem. 1989;264(14):7768-71. PubMed PMID: 2470733.